Cosmic structure from phase transitions

Delivorias, Nikitas Alex

Cosmic Structure from Phase Transitions

Nikitas Alex Delivorias
Department of Physics
University of Durham

A thesis submitted to the University of Durham
for the degree of Doctor of Philosophy
March 1997

I declare that no material in this thesis has been submitted for a degree at this or any other University.

Acknowledgements

I would like to express my thanks and gratitude to my supervisor Peter Collins for his guidance, support and encouragement throughout this project.

I would also like to acknowledge the help I received from R. Fong and T. Shanks who suggested valuable reading material and to Mike Pennington for encouragement. The research reported in this thesis owes a great deal to previous uncompleted work on the same subject by David Pentney.

I am grateful to Adnan Bashir, Ghadir Abu-Leil, Ayse Kirilersu and especially Elena Boglione for help and support with the numerical aspects of this work and to all the friends I made in England who made my stay here so enjoyable.

I am grateful to the 'Alexander S. Onassis' Public Benefit Foundation for financing this research and to Durham University for helping with the cost of attending a conference in Italy.

My warmest gratitude and love goes to my family for their continuing support without which this project would have never been completed.

Nikitas Alex Delivorias

A thesis submitted to the University of Durham
for the degree of Doctor of Philosophy
March 1997

Cosmic Structure from Phase Transitions

Abstract

Motivated by recent observations suggesting that structures in the Universe appear to be concentrated on the walls of bubbles that surround giant voids, we examine the possibility that the observed structure may have resulted from a first order phase transition that occured after inflation and which proceeded by quantum tunnelling and the formation of bubbles of true vacuum.

Since we lack a fundamental theory of particle physics that would define the scalar field responsible for the second phase change and predict the scale of the resulting structures, we instead examine two similar parametrised forms for the potential motivated by the standard Higgs model, and attempt to determine values of the parameters that can reproduce the kind of structures that are observed through bubble wall collisions. The method deployed is quite general and can be applied to any phase transition that occured after inflation. It is found that although the shape of the required potential and its coupling can be determined, the epoch of the proposed second phase transition is in general not specified by the observed structures.

The full verification or otherwise of our proposal will require not only a more detailed consideration of its predictions for the large scale structure of the Universe and its compatibility with the cosmic microwave background radiation but also the embedding of our ideas in a credible theory of particle physics beyond the Standard Model.

Contents

Chapter 1

Introduction

Nature posseses four fundamental interactions – gravitational, electromagnetic and the strong and weak nuclear forces – that seem to account for all physical processes and structures found in the Universe. The ultimate, so far unsuccessful, goal of modern science is to find a unified field theory that can bring all these interactions into a single unified picture. Even though such a 'theory of everything' is still far from being constructed, during the past 50 years there have emerged two 'standard models' of physics that describe the macroscopic and microscopic properties of matter.

The standard model of cosmology, popularly known as the Big Bang, has developed from Einstein's equation of General Relativity for a homogeneous and isotropic Universe and seems to describe succesfully its evolution for all times after the first hundredth of a second after its creation. In studying the bulk properties of the Universe it is gravity that dominates and the effects of the other three interactions can safely be neglected.

When studying the properties of elementary particles, on the other hand, at low energies, it is gravity, the weakest of the interactions, that can be ignored. Field theories of the remaining interactions provide the standard model of particle physics. The fact that three different couplings are needed suggests that this

standard model of particle physics is still incomplete and Grand Unified Theories ($GUTS$) have been developed that unify the strong with the electroweak interactions at an energy scale $M_x \approx 10^{14} GeV$. Even though there are still problems to be answered, most notably the 'hierarchy' problem, i.e. the difficulty in understanding why the symmetry breaking scale of GUT theories is so vastly different from that of electroweak symmetry breaking, GUT theories have enabled scientists for the first time to speculate about the very early Universe at times of the order of $10^{-35} s$ or so. It has become increasingly clear that the very early Universe can provide a unique laboratory for testing new ideas from particle physics. Attempts to unify all the known interactions, including gravity, have led to even more speculative ideas such as those found in sypersymmetry ($SUSY$) theories or superstrings, which takes us to the Planck energy scale and times as early as $10^{-44} s$.

Even though a satisfactory theory of everything is far from being constructed, the fact that we are able to discuss questions relating to the very early Universe is a remarkable success of modern scientific research.

The inflationary universe scenario was first introduced in 1981 in an attempt to solve some of the long–standing problems of the Big Bang theory and to find a mechanism that can suppress the overproduction of the superheavy topological deffects that are predicted to arise whenever a GUT theory undergoes spontaneous symmetry breaking (SSB).

Inflation arises naturally from Einstein's equation since the uniform 'vacuum energy density' generated during the SSB of a particle physics theory is equivalent to an effective cosmological constant and if it becomes dominant it can cause the size of the Universe to increase exponentially. Unfortunately, the lack of a fundamental theory of particle physics leaves the nature of the scalar field that

causes this inflation undetermined and it has become known as the 'inflaton' field. Numerous attempts have been made to construct a successful inflationary model, but, none is particularly compelling. Despite this, the theoretical prejudice in favour of inflation is very strong and it is hoped that eventually the scalar field that drives inflation will be found to arise naturally from the fundamental theory of particle physics.

Two of the other outstanding problems facing modern cosmology concern the nature of the dark matter and the problem of structure formation. With the adoption of inflationary theories which require that $\Omega = 1$ (see, however, chapters 2 and 4) most of the material content of the Universe must be non–baryonic in origin. The continuing search for viable dark matter candidates is an exciting example of the close interconnection between cosmology and particle physics.

Structure formation is widely considered to have resulted from the growth of small density inhomogeneities in the early Universe that were ampified via the Jean's mechanism and collapsed to produce the structure now observed. Recent observations, however, suggesting that galaxies lie predominantly on the surfaces of bubble-like structures that surround giant voids, indicate that this may not be the whole story. Attempts to explain these new observations include explosive galaxy formation and the introduction of cosmic strings as the seeds from which galaxies have evolved.

In our research we have examined a different possibility, namely that these structures have resulted from a first order phase transition that occured after inflation and which proceeded by quantum tunnelling, resulting in the nucleation of bubbles of true vacuum which eventually coalesced to form sheets of matter surrounding giant voids. To this end, we have examined two similar forms of the scalar field potential and tried to determine the parameters which describe them,

including the energy scale which fixes the epoch of the second phase transition, by demanding that the mass, radius and thickness of typical shells produced by the bubble collisions match those which we observe.

We start in chapters 2 and 3 with reviews of the standard model of cosmology and inflation, followed in chapter 4 with a discussion of the formation of structure, of the wide variety of models which have been proposed to explain it and the constraints imposed on all such models from the CMBR. Then, in chapter 5, by following Coleman's work we will derive the standard equation for the rate of tunnelling of the true vacuum bubbles using the path integral formulation. In chapter 6 we introduce the general form of potentials that can produce a first order phase transition and examine how bubble collisions can give rise to shells of matter. At the end of this chapter we derive general equations describing the shell parameters, that are further developed in chapter 7 to include their explicit dependence on the potential parameters. The results of comparing our outputs with the structures actually observed are presented in chapter 7 with our conclusions reserved for chapter 8.

Chapter 2

Standard Cosmology

The key idea of the standard model of cosmology is that the Universe began with an awesome explosion popularly known as the Big Bang. The force of this explosion pushed the developing material content of the Universe outwards in all directions, the rate of expansion being gradually slowed down by the force of gravity. We give here a necessarily brief account of the main features of Big Bang cosmology and derive the standard results which we will need throughout this thesis. We conclude this chapter with a brief exposition of the main successes of the model to be followed, in the next chapter, by a discussion of its failures and how an attempt to solve them leads naturally to the idea of inflation. In these two chapters we will draw heavily from standard texts on cosmology such as those of Collins, Martin and Squires (1989), Kolb and Turner (1990) and Weinberg (1972).

2.1 The Hot Big Bang

The standard model of Cosmology is based on a number of assumptions, the most important of which are the following:

- The fundamental laws of physics do not change with time.

- The effects of gravitation are correctly described by Einstein's theory of General Relativity.
- The Universe on very large scales is homogeneous and isotropic.
- The early Universe is filled with an expanding, extremely hot gas of elementary particles in thermal equilibrium.
- The geometry of space-time is described by the Robertson-Walker (RW) metric.

The line element corresponding the RW metric is given by

$$ds^2 = c^2dt^2 - R^2(t)\left[\frac{dr^2}{1-kr^2} + r^2(d\theta^2 + \sin^2\theta d\phi^2)\right], \quad k = 0, \pm 1 \tag{2.1}$$

where $R(t)$ is the time-dependent scale factor and r, θ, ϕ are comoving polar coordinates, while the parameter k is introduced to represent the sign of the curvature. Based on these assumptions we can look for solutions to Einstein's equation,

$$\mathcal{R}_{\mu\nu} - \frac{1}{2}\mathcal{R}g_{\mu\nu} + \frac{\Lambda}{c^2}g_{\mu\nu} = \frac{8\pi G}{c^4}T_{\mu\nu}, \tag{2.2}$$

by treating all matter and radiation in the Universe as a uniform perfect fluid of energy density ρ and presure P. $\mathcal{R}_{\mu\nu}$ and $\mathcal{R}$ are the Ricci tensor and curvature scalar respectively, $g_{\mu\nu}$ is the RW metric tensor and Λ is the cosmological constant. For co-moving observers the energy-momentum tensor $T_{\mu\nu}$ has only diagonal non-vanishing elements

$$\begin{aligned} T_{00} &= \rho c^2 \\ T_{ii} &= P g_{ii}, \quad i = 1, 2, 3 \end{aligned}$$

and on substituting these back to Einstein's equation, together with the corresponding non-vanishing components of the metric tensor, we obtain

$$H^2 \equiv \left(\frac{\dot{R}}{R}\right)^2 = \frac{8\pi G\rho}{3} - \frac{kc^2}{R^2} + \frac{\Lambda}{3} \tag{2.3}$$

$$\frac{\ddot{R}}{R} = -\frac{4\pi G}{3}\left(\rho + \frac{3P}{c^2}\right) + \frac{\Lambda}{3} \tag{2.4}$$

$$\dot{\rho} + \frac{3\dot{R}}{R}\left(\rho - \frac{P}{c^2}\right) = 0 \tag{2.5}$$

where H is the Hubble 'constant' to be defined below. We shall see shortly that observational bounds on the deceleration parameter require $\Lambda = 0$ today or, at least, that it be very small on the Planck scale. In the absence of Λ (2.3) and (2.4) are known as Friedman's equations. In the rest of this chapter we will assume that $\Lambda = 0$ but we will have to say more on this point when we consider inflation. We should, also, keep in mind that cosmological models have been proposed whereby as much as 80% of the critical density of the Universe is accounted for by a cosmological constant (Efstathiou, Sutherland and Maddox (1990)).

The first of these equations can be seen of as a conservation of energy equation and can be derived from Newtonian principles with k representing the sign of the total energy. Equation (2.4) is a deceleration equation reflecting the fact that in Standard Cosmology the rate of the expansion of the Universe slows down because of the universal gravitational attraction between all forms of matter (we will see, however, that in inflationary cosmologies we can have accelerated expansion and it is this fact that solves most of the long–standing problems of the Big Bang). The last equation derives from the more compact form

$$\frac{d}{dt}(\rho R^3 c^2) = -P\frac{d}{dt}(R^3), \tag{2.6}$$

which is a statement of the first law of thermodynamics, namely that the rate of change in the energy of a system equals (the negative of) the pressure times

the change in volume or, $dE = -PdV$. Any two of Friedman's equations are sufficient to describe the evolution of the Universe provided that an equation of state $P(\rho)$ for the material content of the Universe is specified. Before we go into this, however, we will define some quantities important for our cosmological considerations.

Hubble's parameter:

This is the 'constant' of proportionality that appears in Hubble's relation, $\dot{R} = HR$, which describes the fact that galaxies are receding from each other with velocities proportional to their distance apart. As can be seen from (2.3) H is not a constant but varies slowly with time as the Universe evolves. Hubble's parameter is currently estimated to be

$$H_0 = 100 h_0 kms^{-1} Mpc^{-1}, \quad \frac{1}{2} < h_0 < 1$$

where h_0 is introduced to account for the observational uncertainties (hereafter a subscript '0' will denote the present value of any quantity unless otherwise specified).

redshift:

The redshift z of a source is defined as the ratio of the detected wavelength to the emitted wavelength and is related to the scale factor by

$$1 + z \equiv \frac{\lambda_0}{\lambda} = \frac{R(t_0)}{R(t)}.$$

The deceleration parameter:

A dimensionless measurement of the expansion rate of the Universe is given in terms of the deceleration parameter defined by

$$q \equiv -\frac{R\ddot{R}}{\dot{R}^2} = \frac{4\pi G\rho}{3H^2},$$

or, in terms of the curvature k by

$$q = \frac{1}{2}\left[1 + \frac{kc^2}{R^2H^2}\right],$$

and so q is larger or smaller than $\frac{1}{2}$ depending on whether the curvature of the Universe is positive or negative. At the moment observations suggest that $-1 < q_0 < 2$ so the sign of k is still unknown. Also, the cosmological constant is bounded by $\Lambda \leq 3H^2 \sim 10^{-122}{t_p}^{-2}$ (Collins, Martin, Squires (1989)).

The critical density:

This is the energy density of a flat ($k = 0,\ q = 1/2$) Universe given by (cf. (2.3))

$$\rho_c = \frac{3{H_0}^2}{8\pi G} \simeq 2{h_0}^2 \times 10^{-29} gmcm^{-3}.$$

Ω-parameter:

The Ω-parameter relates the energy density of the Universe to its critical energy density through the dimensionles ratio

$$\Omega \equiv \frac{\rho}{\rho_c} = 1 + \frac{kc^2}{R^2H^2} = 2q.$$

According to the value assumed by Ω (or equivalently k or q) the Universe is said to be either open, or closed or flat. The three different types of universe are summarised in table (2.1) and in figure (2.1) we show the corresponding variations of the scale factor with time. Note, also, that if $\Lambda \neq 0$, low-density universes are spatially flat if $\Lambda_0 = 3(1-\Omega_0){H_0}^2$ and can thus be compatible with inflation (Peebles (1984)). Hence, it has been suggested that the successes of the CDM model based on a spatially flat Universe with scale-invariant adiabatic fluctuations can be sustained even if $\Omega_0 \approx 0.2$ since the rest of the critical energy density of the Universe can be accounted for by the positive cosmological constant (Efstathiou, Sutherland and Maddox (1990)).

TYPE OF UNIVERSE	RATIO OF ENERGY DENSITY TO CRITICAL DENSITY (Ω)	SPATIAL GEOMETRY	VOLUME	TEMPORAL EVOLUTION
CLOSED	>1	POSITIVE CURVATURE (SPHERICAL)	FINITE	EXPANDS AND RECOLLAPSES
OPEN	<1	NEGATIVE CURVATURE (HYPERBOLIC)	INFINITE	EXPANDS FOREVER
FLAT	1	ZERO CURVATURE (EUCLIDEAN)	INFINITE	EXPANDS FOREVER, BUT EXPANSION RATE APPROACHES ZERO

Table 2.1: The geometry of the Universe (Guth and Steinhardt (1984)).

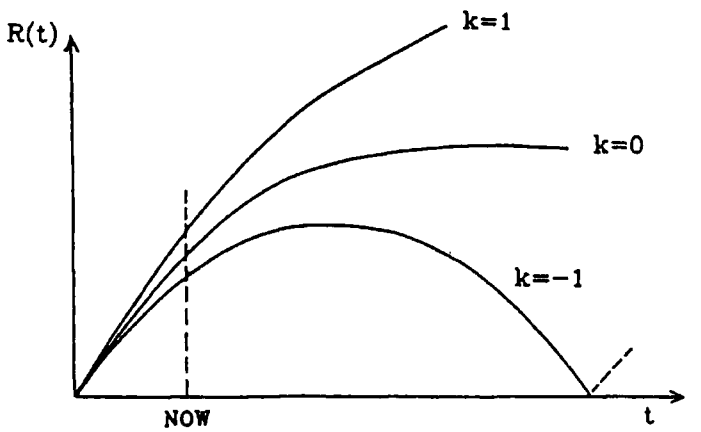

Figure 2.1: Variation of the scale factor with time for the three types of universe.

As we stressed before, knowing the equation of state for the material content of the Universe, Friedman's equations enable us to study its evolution at any later time. For our purposes we shall adopt (Barrow (1988))

$$P = (\gamma - 1)\rho c^2, \quad \gamma = constant. \tag{2.7}$$

This constant is of fundamental importance in cosmology because it not only specifies the equations of state for the radiation and the matter dominated epochs for which the values are $\gamma = 4/3$ and $\gamma = 1$ respectively, but, equally important, with $\gamma = 0$ we have the equation of state required for inflation.

For example, when the Universe was a fully ionised plasma of relativistic particles in thermal equilibrium, the so-called radiation-dominated era, then

$$P = \frac{1}{3}\rho_r c^2, \quad \rho_r = \sigma T^4, \tag{2.8}$$

$\sigma = \pi^2 {k_B}^4/15\hbar^3 c^5$ being the radiation density constant and T being the temperature. Using Friedman's equations it can be shown that

$$\begin{aligned} \rho_r &\propto R^{-4} \\ R &\propto t^{1/2}. \end{aligned}$$

On the other hand, because matter today is extremely nonrelativistic as dust or clumped in astronomical bodies, the equation of state for a matter-dominated universe can be approximated by

$$P = 0$$

in which case

$$\begin{aligned} \rho_m &\propto R^{-3} \\ R &\propto t^{2/3}. \end{aligned}$$

Although the matter density today greatly exceeds that of radiation,

$$\begin{aligned}\rho_r &\sim 4.71 \times 10^{-34} gm/cm^3(1+z)^4 \\ \rho_m &\sim 1.88 \times 10^{-29}\Omega_0 h_0{}^2 gm/cm^3(1+z)^3\end{aligned}$$

this was not always the case. We have seen that the radiation density falls of more rapidly with time which suggests that at some time in the past it must have exceeded that of matter. Thus, there was a time t_{eq}, when $R = R_{eq}$ and $z = z_{eq}$, when the energy densities of matter and radiation were equal

$$\rho_m = \rho_r \Longrightarrow 1 + z_{eq} \approx 4 \times 10^4 \Omega_0 h_0{}^2 \tag{2.9}$$

and hence

$$\begin{aligned}1 + z_{eq} &= \frac{R_0}{R_{eq}} = \left(\frac{t_0}{t_{eq}}\right)^{2/3} \\ &\Longrightarrow \quad t_{eq} \approx 2.5 \times 10^{10} h_0{}^{-4} \Omega_0{}^{-3/2} sec,\end{aligned}$$

where t_0 is the present age of the Universe. So, from t_{eq} onwards the equation of state is accurately approximated by $P = 0$ and it describes a dust or matter-dominated Universe. Before this there was the radiation-dominated era, from the moment of creation up to t_{eq}, during which time the curvature of the Universe was negligible. Solving the $k = 0$ Friedman's equations for the radiation-dominated Universe we obtain

$$R(t) \propto t^{1/2}, \quad \rho_r = \frac{3}{32\pi G t^2}, \quad H = \frac{1}{2t}. \tag{2.10}$$

2.2 Equilibrium Thermodynamics

Conditions in the early Universe are expected mostly to be very close to thermodynamic equilibrium, the main reason being that at such high densities and temperatures the rates of interaction between particle species are fast compared

to the expansion rate of the Universe. The criterion to determine which particles remain in thermal equilibrium at a given temperature is

$$\Gamma = \langle n\sigma v \rangle \gg H \sim \frac{1}{2t} \tag{2.11}$$

where n is the number density of particles, σ is their reaction crossection and v their velocity. Initially, when n and v are large, particles are in equilibrium but, as the temperature drops, the energy of a given particle will fall below its production threshold, σ will reduce and eventually vanish, whereupon these particles will drop out of equilibrium and decouple from the surrounding plasma.

In the ideal gas approximation the total number density of particles in thermal equilibrium with momenta between p and $p + dp$ is

$$dn = \frac{g_*}{2\pi^2\hbar^3} \frac{p^2 dp}{(e^{E/kT} \pm 1)} \tag{2.12}$$

where $E = (p^2c^2 + m^2c^4)^{1/2}$ is the energy, g_* is the total number of relativistic degrees of freedom at temperature T given by

$$g_* = \sum_{bosons} g_b + \frac{7}{8} \sum_{fermions} g_f, \tag{2.13}$$

g_b and g_f being the number of degrees of freedom for bosons and fermions respectively and where the $\pm$ sign accounts for the difference in boson and fermion statistics. Thus, for photons, or for any relativistic particles with $kT \gg mc^2$

$$n = \int_0^\infty \frac{dn}{dp} dp = \frac{g_*}{2\pi^2\hbar^3} \int_0^\infty \frac{p^2 dp}{(e^{pc/kT} \pm 1)}. \tag{2.14}$$

Similarly the energy density is

$$\rho c^2 = \int_0^\infty E \frac{dn}{dp} dp = \frac{g_*}{2\pi^2\hbar^3} \int_0^\infty \frac{Ep^2 dp}{(e^{pc/kT} \pm 1)}. \tag{2.15}$$

Thus, at high temperatures ($kT > mc^2$) or, at any temperature for massless particles, the number density and energy density of particle species are given by

$$\rho_b = \frac{g_b}{2}\rho_\gamma, \quad n_b = \frac{g_b}{2} n_\gamma$$

kT less than	Particles in Equilibrium	g_*
1eV	γ	2
$m_e c^2$	γ, e^+, e^-	11/2
$m_\mu c^2$	γ, ν_e, ν_μ, e^+, e^-	43/4
$m_\pi c^2$	$+\mu^+$, μ^-	57/4
Λ_C	$+\pi^+$, π^-, π^0	69/4
$m_s c^2$	γ, ν_e, ν_μ, ν_τ, $e^\pm$, $\mu^\pm$, u, $\overline{u}$, d, $\overline{d}$, g	205/4
$m_c c^2$	$+$s, $\overline{s}$	247/4
$m_\tau c^2$	$+$c, $\overline{c}$	289/4
$m_b c^2$	$+\tau$, $\overline{\tau}$	303/4
$m_t c^2$	$+$b, $\overline{b}$	345/4
$M_W c^2$	$+$t, $\overline{t}$	387/4
$> M_W c^2$	$+W^+$, W^-, Z	423/4

Table 2.2: Variation of the effective degrees of freedom with temperature (Collins, Martin and Squires (1989)).

$$\rho_f = \frac{7}{16} g_f \rho_\gamma, \quad n_f = \frac{3}{8} g_b n_\gamma$$

where ρ_γ and n_γ are the photon energy density and number density respectively given by

$$\rho_\gamma c^2 = \alpha T^4 \tag{2.16}$$

$$n_\gamma = \frac{2\zeta(3)}{\pi^2}\left(\frac{kT}{c\hbar}\right)^3 \tag{2.17}$$

where $\alpha = \pi^2 k^4/(15c^3\hbar^3)$ is the Stefan–Boltzmann constant. Hence, the total energy density at high temperature is given by

$$\rho c^2 = \frac{1}{2} g_* \alpha T^4. \tag{2.18}$$

The value of g_* will change as the Universe cools (see table (2.2)) and different species go out of equilibrium. A relation showing the variation of temperature with g_* and t can be derived by combining (2.10) with (2.18) viz.

$$T = \left(\frac{45c^5\hbar^3}{16\pi^3 G g_* k^4}\right)^{1/4} t^{-1/2}. \tag{2.19}$$

2.3 Successes of the Big Bang

2.3.1 Expansion from a Hot Big Bang

The first major success of the Big Bang model of cosmology was the discovery by Hubble in 1929 that galaxies are moving away from each other. The second piece of evidence that pointed towards a hot Big Bang came later when the cosmic microwave background radiation ($CMBR$) was first detected by Penzias and Wilson in 1965. The $CMBR$ is the relic radiation from the earliest moments in the history of the Universe when radiation and matter were in equilibrium and when processes like, for example,

$$\gamma + H \longleftrightarrow e^- + p$$

where common. The ionisation potential of hydrogen is $13.6eV$ corresponding to a photon temperature $T_H = 1.6 \times 10^5 K$. As the Universe expands the photon temperature drops and at temperatures well below T_H there are few photons energetic enough to be reabsorbed by H atoms and so matter will become transparent to radiation. This decoupling occurs at $T_d \simeq 3 \times 10^3 K$. After decoupling the temperature of the radiation continues to drop and is redshifted by the expansion of the Universe towards the microwave part of the spectrum. The $CMBR$ is received uniformly from all directions in the sky and (apart from a small dipole anisotropy due to the earth's motion relative to the cosmic rest frame) has almost the same effective temperature, $T_0 \approx 2.735 \pm 0.06K$, to a high degree of accuracy (Smoot *et al.* (1991)). Assuming that matter has dominated the dynamics of the Universe since decoupling, since $T \sim t^{-2/3}$, we can estimate the decoupling time as follows.

$$\frac{T_0}{T_d} = \left(\frac{t_d}{t_0}\right)^{2/3} \Longrightarrow t_d \simeq 5 \times 10^{12} sec. \tag{2.20}$$

It is apparently a coincidence that $t_{eq} \approx t_d$.

2.3.2 Nucleosynthesis

Nucleosynthesis is the study of the formation of the light elements. The main idea is that at high temperatures ($T \gg 10^{10}K$) nuclear particle interactions occur reversibly and thermal equilibrium is achieved through reactions like

$$\begin{aligned} e^+ + e^- &\longleftrightarrow \nu_i + \overline{\nu}_i \\ p + e^- &\longleftrightarrow n + \nu_e \\ n + e^+ &\longleftrightarrow p + +\overline{\nu}_e \\ n &\longleftrightarrow p + e^- + \overline{\nu}_e. \end{aligned}$$

As the temperature gradually lowers and becomes of order $10^{10}K$ these interactions become too slow to compete with the expansion of the Universe and the neutrinos decouple. At temperatures $T < \mathcal{O}(10^{10}K)$ equilibrium ceases and the n/p ratio 'freezes out' and then decreases slowly due to neutron decay until the onset of nucleosynthesis. At even lower temperatures electron-positron pairs start to annihilate and at about 10^9K they vanish transfering their energies to the photons. At this point reactions of the form

$$p + n \longrightarrow {}^2H + \gamma$$

also occur but the vast excess of photons over nucleons ensures that the inverse reaction also proceeds destroying ${}^2H$ almost as fast as it is produced. As the Universe expands further and cools fewer photons are capable of destroying deuterium and its abundance begins to increase. Subsequently tritium and helium begin to form through reactions such as

$$\begin{aligned} p + n &\longrightarrow {}^2H + \gamma \\ {}^2H + n &\longrightarrow {}^3H + \gamma \end{aligned}$$

$$^2H + p \longrightarrow {}^3He + \gamma$$

$$^3H + p \longrightarrow {}^4He + \gamma$$

$$^3He + n \longrightarrow {}^4He + \gamma$$

The fact that no stable nuclei with atomic numbers $A = 5$ and $A = 8$ exist ensures that there is little further nucleosynthesis (however some trace amounts of ^7Li and ^7Be are also produced). Finally at temperatures $T \leq 5 \times 10^8 K$ Coulomb barriers ensure that nuclei cannot come sufficiently close together and nucleosynthesis is effectively terminated.

We will not examine Big Bang Nucleosynthesis (BBN) in more detail except to note the factors that affect the relative abundances of the light elements (more complete surveys of BBN can be found in Boesgaard *et al* (1985), Bernstein *et al* (1989),Walker *et al* (1991)). The primordial abundance of helium depends on the n/p ratio at freeze out which is in turn determined by the competition between the weak interaction rate and the expansion rate. Thus (Hoyle, Tayler (1964)) if there exist more light particles (for example a fourth neutrino), g_* will be larger leading to a faster expansion and hence an earlier freeze out of the weak interactions leaving behind more n and hence a larger helium abundance. The predicted abundances of ^2H, ^3He and ^7Li on the other hand depend only on the baryon to photon ratio, the larger the nucleon abundance the more rapidly ^2H and ^3He are destroyed leaving behind more ^4He. In figure (2.2) we show the predictions for the primordial abundances of the light elements which demonstrate that, in the context of the Big Bang, BBN requires that

$$N_\nu = 3 \pm 1$$

$$\eta = 4 - 7 \times 10^{-10}$$

in remarkable agreement with observations.

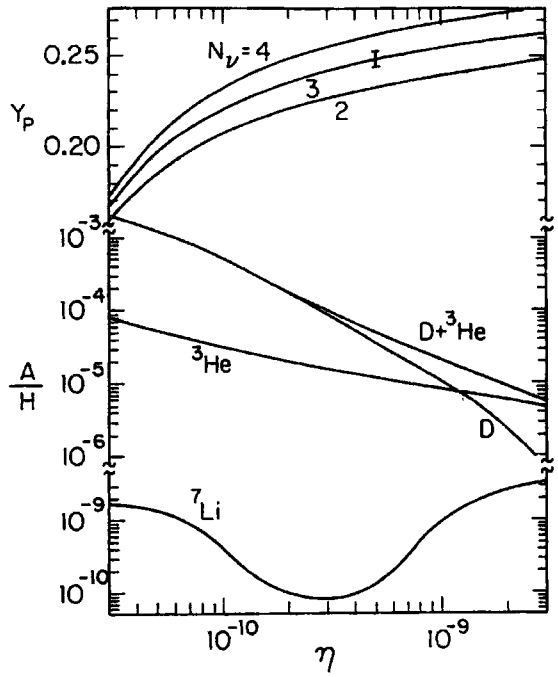

Figure 2.2: Predictions of the primordial abundances of the light elements where Y_p denotes the primordial mass fraction of ^4He (Kolb and Turner (1990)).

In the next chapter we shall see that there are a number of unsatisfactory features wich indicate that the Big Bang is probably not the whole story. We will conclude this chapter by presenting the main events in the history of the Universe.

2.4 Main Events in the History of the Universe

The Big Bang model of cosmology seems to give a very successful description of the evolution of the Universe from about the first hundredth of a second after its creation when BBN began up to now. With the invention of the Grand Unified Theories ($GUTS$) and supersymmetry ($SUSY$) that arose from attempts to explain the properties of elementary particles at very high energy scales cosmologists were able to explore the hypothetical history of the Universe as far back as $10^{-35} sec$ after the Big Bang when it had an effective temperature of about

$10^{15}GeV$. Our present knowledge of physics is insufficient to study the history of the Universe at even earlier times. Quantum gravity effects must be taken into account and the theory of General Relativity will have to be suplemented by a proper quantum theory of gravity which so far does not exist. Thus to describe the earliest moments in the history of the Universe, $t \leq 10^{-44}s$, as we approach the initial singularity at $t \to 0$, we require a fundamentally different approach involving new ideas such as those found in superstrings perhaps. This, however, need only be done on scales set by the so-called 'Planck units' which define the energy, mass, length and time in terms of G as follows:

$$\begin{aligned} E_P &= \left(\frac{\hbar c^5}{G}\right)^{1/2} \approx 1.2 \times 10^{19} GeV \\ M_P &= \left(\frac{\hbar c}{G}\right)^{1/2} \approx 2.1 \times 10^{-8} kg \\ l_P &= \left(\frac{\hbar G}{c^3}\right)^{1/2} \approx 16 \times 10^{-35} m \\ t_P &= \left(\frac{\hbar G}{c^5}\right)^{1/2} \approx 5.4 \times 10^{-44} s. \end{aligned}$$

As the Universe cools it is believed to have undergone a number of phase transitions within the context of GUT or $SUSY$ theories because of the spontaneous breakdown of the relevant symmetries at their characteristic energy scale, i.e. approximately $10^{15}GeV$ for $GUTS$ and anywhere between 10^{11} and $10^{3}GeV$ for $SUSY$ respectively. Inflation is believed to have resulted from a phase transition of this kind although the inflaton field that is responsible is not known. After that, a phase transition which breaks the electroweak symmetry of the standard model of particle physics is thought to have occured at about $250GeV$. At energies around $100 - 300MeV$ the quark-hadron phase transition occured, followed by the epoch of nucleosynthesis at around $t \approx 1s$ which we mentioned earlier. Much later, at $t \approx 10^{11}sec$, matter began to dominate the dynamics of the Uni-

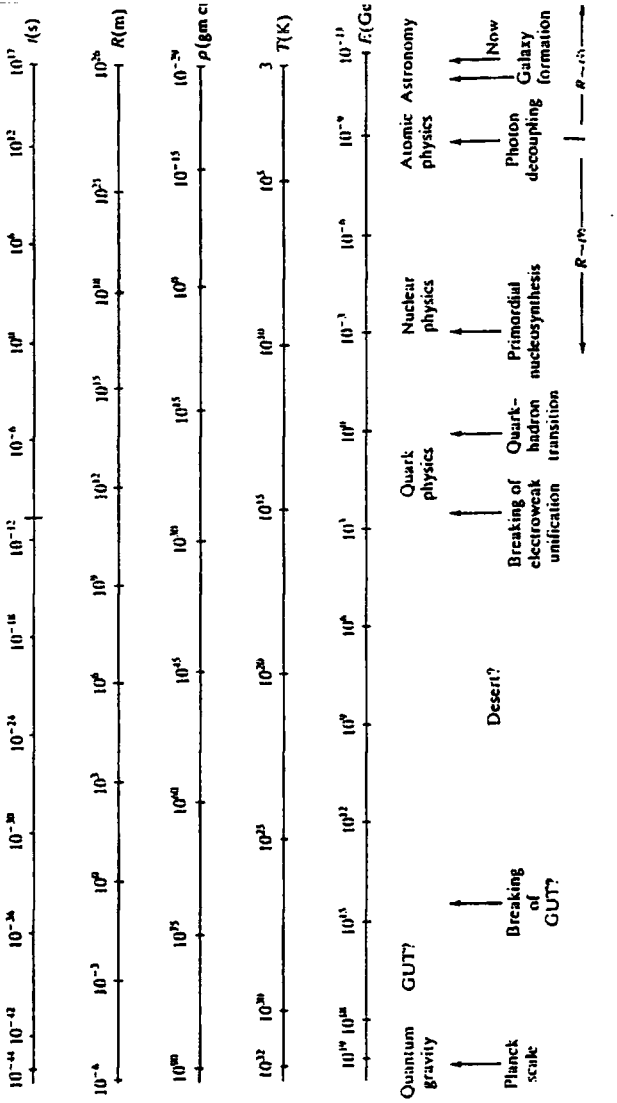

Figure 2.3: A brief history of the Universe (Collins, Marin and Squires (1989)).

verse and formation of structure could begin. Finally, at $t_d \approx 10^{13} sec$ photons decoupled form the surrounding matter releasing the $CMBR$. We conclude this chapter by displaying in figure (2.3) a snapshot of the history of the Universe from its very infancy up to now which shows all the important stages of its evolution.

Chapter 3

Inflationary Cosmology

Even though the standard model of cosmology provides a very satisfactory framework for the study of the evolution of the Universe it is plagued by several problems that cannot be solved unless one prescribes rather artificial initial conditions. In the next section we shall review some of these problems and show how attempts to solve them naturally lead to the idea of inflation.

3.1 Problems of the Standard Model

The naturalness problem:

The only dimensionful parameter appearing in Friedmann's equation is the gravitational constant G which in Planck units is given by

$$G = \frac{\hbar c}{{M_P}^2}.$$

If we set $\hbar = c = 1$ Friedmann's equation can be rewritten as

$$H^2 = \frac{8\pi\rho}{3{M_P}^2} - \frac{k}{R^2} + \frac{\Lambda}{3} \tag{3.1}$$

and we might argue that all the parameters in this equation should be of order 1 in these units. This, however, would give $H^{-1} \approx t_P \approx 10^{-44} sec$ rather than ${H_0}^{-1} \approx 10^{17} sec$ as observed. It also predicts that $\Lambda \approx {t_P}^2$ whereas we have seen

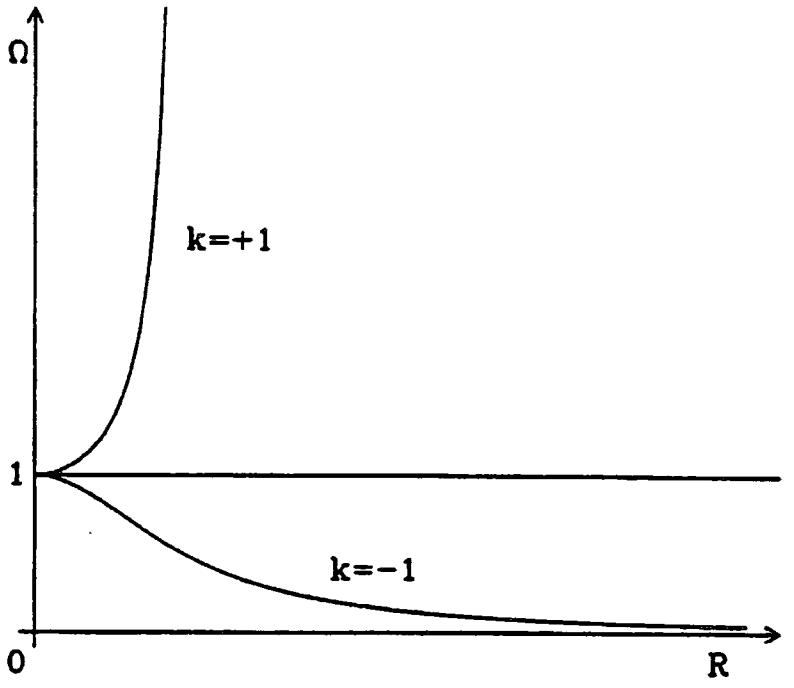

Figure 3.1: An illustration of the unstable nature of Ω. For $\Omega > 1$ Ω diverges to infinity whereas for $\Omega < 1$ it rapidly approaches 0.

that the cosmological constant should be vanishingly small ($\leq 10^{-122} t_P{}^2$) and there is no natural mechanism that can achieve this automatically.

The flatness problem:

The flatness problem is the difficulty of understanding in the context of the Big Bang theory why the Ω-parameter is of order 1. If we neglect the cosmological constant we can rewrite Friedmann's equation in terms of Ω as follows

$$\frac{\Omega - 1}{\Omega} = \frac{3kc^2}{8\pi G\rho R^2} \tag{3.2}$$

and, taking into account the time dependence of ρ and R,

$$\frac{\Omega - 1}{\Omega} \sim \begin{cases} t & \text{radiation dominated} \\ t^{2/3} & \text{matter dominated} \end{cases} \tag{3.3}$$

and so $\Omega = 1$ represents a state of unstable equilibrium (see figure (3.1)). It turns out that, for Ω to be of order 1 today, at the Planck time it must have been 1 ± 10^{-60}. To appreciate this problem in a different way we recall that for

both the radiation-dominated and the matter-dominated eras the energy density falls off more rapidly than the curvature term which should be overwhelmingly dominant today if it is non-zero.

The horizon problem:

On very large scales the Universe appears to be homogeneous and isotropic. For example, the $CMBR$ that was released about 10^6 years after the Big Bang is received uniformly from all directions in the sky and has the same effective temperature of about $2.76K$ to about one part in 10^5. The smoothness of the $CMBR$ is very puzzling if one recalls that it extends over regions that would seem to have been causally disconnected in the early Universe. The horizon size is defined to be the maximum distance a light signal could have travelled since the beginning of the Big Bang,

$$d_H(t) = R(t) \int_0^t \frac{cdt'}{R(t')}.$$

Thus,

$$\frac{d_H(t)}{R(t)} = \begin{cases} t^{1/2} & \text{radiation dominated} \\ t^{1/3} & \text{matter dominated.} \end{cases} \tag{3.4}$$

For the $CMBR$, for example, that was released at $t_d \approx 5 \times 10^{12} sec$ we obtain

$$\frac{d_H(t_0)}{d_H(t_d)} = \left(\frac{t_0}{t_d}\right)^{1/3} \approx 40$$

and the observable Universe at decoupling consisted of roughly 10^5 causally disjoint regions. How is it possible that radiation emitted from different parts of the Universe that were not causally connected have the same temperature?

Topological defects

In the context of GUTs, symmetry breaking mechanisms may give rise to topological defects such as magnetic monopoles, cosmic strings and domain walls. The mechanism of formation of such defects was studied by Kibble (1976) who

argued that their production in the early Universe is unavoidable. Although a detailed analysis of this topic is beyond the scope of this thesis, their cosmological implications are profound as we will briefly discuss below.

Magnetic monopoles are point-like defects which arise if the vacuum manifold contains non-contractible surfaces. The existence of monopole solutions was first demonstrated by t' Hooft (1974) and Polyakov (1974) in a gauge theory possessing $SO(3)$ symmetry which is broken by a Higgs triplet. Although their solution approaches the ground state σ for $r \to \infty$, as $r \to 0$ the Higgs field vanishes and so at that point the potential energy is a maximum. This solution, often referred to as the hedgehog solution, is topologically stable because there is no way to deform it into a configuration in which the vacuum expectation value is σ everywhere. By considering the magnetic field associated with this hedgehog solution it has been shown that it corresponds to a magnetic monopole. These point-like defects are called t'Hooft-Polyakov monopoles and, since it is expected that each causally disconnected region will have approximately one such defect associated with it, with a mass of order of the energy scale of the symmetry breaking, their contribution to the energy density of the Universe is predicted to be far greater than is observed. In particular, given the fact that the monopole density is unlikely to have decreased much through annihilation, monopoles produced through GUT symmetry breaking would have a total mass density about 10^9 times the critical density (see, for example Collins, Martin and Squires (1989)) so such a universe would have collapsed long ago.

Cosmic strings, on the other hand, are one-dimensional defects which arise in models where the vacuum manifold contains non-contractible loops. In the simplest case, where ϕ is a complex scalar with a 'mexican hat' potential, then the values of ϕ which minimise the potential energy of the theory can be such

that $\phi = \sigma \exp i\theta$, where θ is arbitrary. After the phase transition the Universe is made up of different regions where the 'direction' of ϕ is chosen at random, but its value must match smoothly accross boundaries. Because ϕ must be single-valued the total phase change around any closed path must be zero. However, it is possible for paths with $\Delta\theta = 2\pi n, \quad n = 1, 2...$ to exist as well. In this case shrinking the path would eventually lead to a point where the phase of ϕ is undefined, that is where the vacuum expectation value of ϕ must be zero and so the potential is at its maximum. The resulting defects resemble thin tubes of false vacuum along which ϕ vanishes. Since these tubes or strings can have no ends they must be either closed loops or of infinite length. They will have a huge mass per unit length, $\mu \sim \sigma^2$, where σ is the symmetry breaking scale of the theory (so for example, for GUTs $\mu \sim 10^{30} GeV^2$), and it has been proposed that these cosmic strings could be the seeds of galaxies (see section (4.4)).

Finally, domain walls are two-dimensional structures, generally associated with the breaking of a discrete symmetry whereby the field ϕ can take one of the two ground states of the system. Since the choice of the minimum depends on random fluctuations, it can be expected to be different in different regions of space, so it is possible that neighbouring regions of space will fall into different minima. These regions will be separated by a two-dimensional boundary or domain wall, a region of false vacuum where $\phi = 0$. It has been shown that the surface energy density of such structures is of order $\sigma \sim \sqrt{\lambda}\eta$, where λ is the coupling constant and η is the symmetry breaking scale of the theory, and thus, unless either λ or η is exceedingly small, the mass per unit area would be unacceptably large, destroying the homogeneity of the Universe on large scales.

The kinematics, evolution and gravitational effects of such defects is beyond the scope of this thesis. This brief review has been intended to show that symme-

try breaking in particle physics theories could produce various kinds of topological defect whose mass scale is of the order of the energy scale at which symmetry breaking occurs. Only cosmic strings would seem to be compatible with the observed inhomogeneity of the Universe (see section (4.4)). Monopoles or domain walls would destroy its large scale homogeneity and isotropy. The mechanism of inflation was developed as a means of diluting the overproduction of such unwanted cosmological defects. For a detailed account of topological defects and their implications for Cosmology see Vilenkin and Shellard (1994), from which this review has been drawn.

The structure formation problem:

The Universe on small scales is, of course, not homogeneous. It is thought that structure on small scales most likely resulted from the growth of small density perturbations but in the context of the standard model of Cosmology their origin, spectrum and nature is not explained.

3.2 Inflation

The idea of inflation as a means of solving some of the long–standing problems of the Big Bang of Cosmology was first introduced by Guth in 1981 who noticed that if there was a period when the energy density in the early Universe was dominated by the vacuum energy density so that $\rho \sim U \sim$constant then the Universe would expand exponentially since

$$H^2 \equiv \left(\frac{\dot{R}}{R}\right)^2 = \frac{8\pi G\rho}{3} = \text{constant}$$

and hence

$$R \sim e^{Ht}.$$

Such an expansion could solve the flatness problem since the curvature term would be suppressed exponentially. The horizon problem would be solved as well since the observable universe could have evolved from just one causally connected region that was small enough for the observed homogeneity and isotropy to be achieved quite easily. Similarly the region that inflated to become our observable Universe could contain ≤ 1 monopoles in accordance with observations. Cosmic strings, domain walls or other topological defects that were produced before inflation would similarly have been diluted exponentially.

How could such an exponential expansion have taken place? Guth's answer was that it could have resulted from a first order *GUT* phase transition that did not occur instantaneously but was preceeded by a period of supercooling. Before going into this, however, we shall briefly review an important result relating to symmetry restoration at high temperatures.

Since ϕ is a quantum field interacting with itself and with other fields, the classical potential $U(\phi)$ must be modified by radiative corrections. The corrected potential, called the effective potential, is evaluated by a perturbative expansion in powers of coupling constants and can be written as

$$U_{eff}(\phi) = U_{cl}(\phi) + U_n(\phi)$$

where $U_{cl}(\phi)$ is the classical potential and $U_n(\phi)$ accounts for the contribution of Feynman diagrams with closed loops. In some models these radiative corrections can completely alter the character of symmetry breaking (Vilenkin and Shellard (1994)). At high temperatures the calculation of higher order quantum corrections to the classical potential should take into account the effect of all the background particle fields. The vacuum expectation value of ϕ is thus temperature dependent.

For example, at high temperatures the usual Higgs potential

$$U(\phi) = -\frac{1}{2}\mu^2\phi^2 + \frac{1}{4}\lambda\phi^4 \tag{3.5}$$

must be replaced by the temperature dependent effective potential given by (see, for example, Collins, Martin, Squires (1989))

$$U(\phi, T) = -\frac{1}{2}\mu^2\left(\phi^2 + \frac{T^2}{12}\right) + \frac{1}{4}\lambda\phi^4 + \frac{1}{8}\lambda\phi^2T^2 - \frac{\pi^2}{90}T^4 \tag{3.6}$$

plus higher order terms in λ. The minima of the potential are then given by

$$\begin{aligned} \frac{\partial U(\phi,T)}{\partial\phi} &\approx (-\mu^2\phi + \lambda\phi^3 + \frac{\lambda}{4}T^2\phi) = 0 \\ &\Longrightarrow \quad \phi = 0 \text{ or } |\phi|^2 = \frac{4\mu^2 - \lambda T^2}{4\lambda}. \end{aligned}$$

There is thus a critical temperature

$$T_c = \frac{2\mu}{\lambda^{1/2}} = 2v$$

above which the Higgs potential is minimised at $\phi = 0$ and the symmetry is maintained. Below T_c the symmetric state becomes unstable and ϕ develops a non-zero expectation value at

$$|\phi|^2 = \frac{\mu^2}{\lambda}\left[1 - \frac{T^2}{T_c^2}\right],$$

corresponding to the true minimum of the theory, which reduces to the usual limit $|\phi|^2 = v^2 \equiv \frac{\mu^2}{\lambda}$ for $T = 0$. As described above the evolution of ϕ between the two phases is 'smooth' since $|\phi|$ grows continiously from zero as the temperature decreases below T_c, indicating a second-order phase transition.

Of more interest to us will be first-order phase transitions in which the evolution of ϕ is discontinious. A graph showing the temperature-dependent effective potential for a first-order phase transition is shown in figure (3.2). For $T \gg T_c$

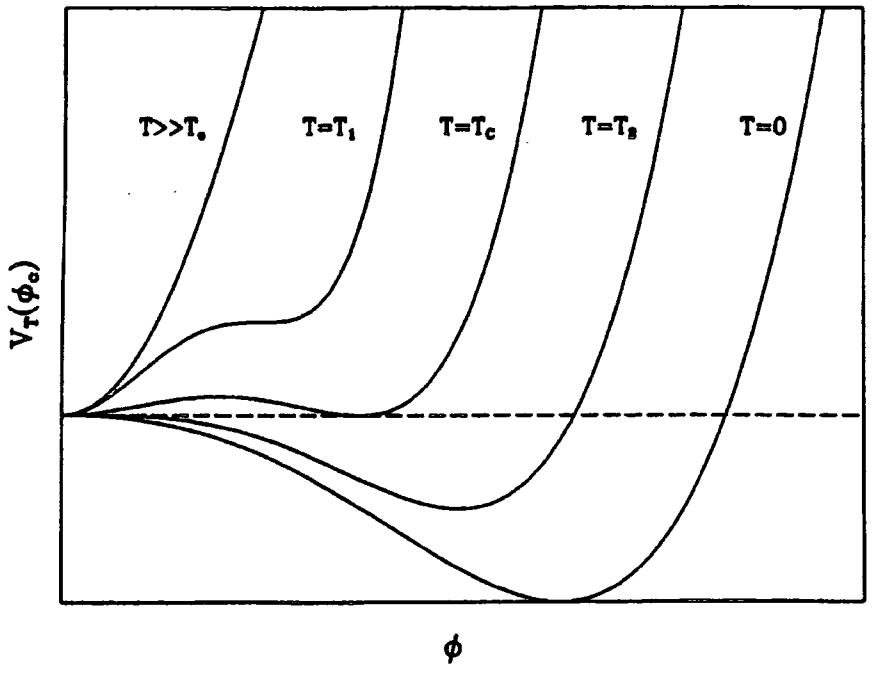

Figure 3.2: The temperature-dependent effective potential for a first-order phase transition (Kolb and Turner (1990)).

the potential is quadratic with just one minimum at $\phi = 0$. As the temperature lowers a second minimum develops at $\phi \neq 0$ and at $T = T_c$ there are exactly two degenerate minima. For temperatures below T_c the minimum at $\phi \neq 0$ corresponds to the true vacuum state while the $\phi = 0$ minimum corresponds to a false vacuum which is unstable. For $T > T_2$ there is a barrier that separates the two ground states and initially the ϕ-field is trapped behind this barrier in the region $\phi \sim 0$. The phase transition will not occur immediately resulting in an effective vacuum energy density

$$\rho_v = U(\phi = 0) - U(\phi = \phi_{min}) \approx \frac{\mu^4}{4\lambda}$$

(because the rapid expansion causes rapid cooling) which is equivalent to an effective cosmological term

$$\Lambda = 8\pi G \rho_v \approx \frac{8\pi G \mu^4}{4\lambda}.$$

During this time the potential energy of the so-called inflaton-field can, as we saw earlier, cause a period of exponential expansion, at the end of which the inflaton field will overcome the barrier as a result of quantum or thermal tunnelling. Supposing that the phase change occured at the GUT scale M_x,

$$\Lambda \approx \frac{{M_x}^4}{{M_P}^2} \approx 10^{18} GeV^2.$$

After the phase transition is complete $\rho_v \rightarrow 0$ and hence $\Lambda \rightarrow 0$, to agree with observation, and the energy released by the decay of the ϕ-field will reheat the Universe to $T \approx T_c {g_*}^{-1/4}$ and the subsequent evolution of the Universe will resume as in the Big Bang model.

It was soon realised, however, that the original model of inflation was not completely free of problems either. The main difficulty concerned the termination of the false vacuum phase, usually referred to as the 'graceful exit' problem. If the tunnelling rate is too small the phase transition will never be completed and if eventually bubbles of true vacuum coalesce a very inhomogeneous universe will result. If, on the other hand, the tunnelling rate is too large there will not be sufficient inflation to solve the problems of the Big Bang (Guth, Weinberg (1983)). However, even though Guth's original model had its problems the key features were too attractive for cosmologists to ignore. It was realised that the difficulties could be solved if the whole of the observable Universe resulted from just one bubble, as required by new inflation (Albrecht and Steinhardt (1982), Linde (1982)).

We should mention here a proposal by Hawking and Moss (1982) who argued that homogeneity and isotropy can be achieved through a homogeneous bubble solution in which tunnelling occured everywhere at the same time.

In particular, Hawking and Moss introduced a cosmological 'no hair' theo-

rem according to which perturbations of the de Sitter metric are exponentially suppressed so that after a time $t \gg H^{-1}$ the Universe becomes indistinguishable from a completely homogeneous and isotropic de Sitter space. Because of the existence of event horizons, all processes in a given domain of de Sitter space are independent of anything that goes on outside them. With a suitable choice of the parameters their potential leads to the nucleation of bubble solutions in flat spacetime whose radius is greater than that of the de Sitter space, H^{-1}. Their solution to the equations of motion, apart from the trivial $\phi = 0$, is $\phi = \phi_1$, where ϕ_1 is the position of the local maximum of the potential. The Universe continues in the de Sitter state until the transition to $\phi = \phi_1$ occurs everywhere. Finally, because the $\phi = \phi_1$ solution is unstable, the field will evolve according to the classical equations of motion to the true minimum from which it will decay through damped harmonic oscillations. The classical evolution of the ϕ field in de Sitter space is equivalent to that in a closed space with curvature of the order of the radius of the de Sitter space. Thus, by taking into account the curvature and finite horizon-size of the Universe, Hawking and Moss are able to achieve a graceful exit from the exponential expansion of the Universe without introducing too much inhomogeneity.

3.3 New inflation

The main difference between new inflation and Guth's original model is that inflation occurs not while the ϕ-field is trapped in the supercooled false vacuum state but as it is slowly 'rolling' towards its equilibrium value so that the whole observable Universe results from a single bubble. This can be achieved by choosing the field that implements inflation to be the Higgs multiplet that causes the breakdown of the $SU(5)$ GUT symmetry, corresponding to the Coleman-Weinberg

potential which, at zero temperature, is given by (Brandenberger (1985))

$$U(\phi) = A\phi^4\left[\log\frac{\phi^2}{\sigma^2} - \frac{1}{2}\right] + \frac{1}{2}A\sigma^4 \tag{3.7}$$

where $A = (5265/64){\alpha_{GUT}}^2$, α_{GUT} being the GUT gauge coupling and σ the GUT energy scale (we will see, however, that this potential in not flat enough and that for any normal values of the coupling λ a highly inhomogeneous Universe results (c.f. section (3.5))). The phase transition in this case procceeds via the 'slow-roll' mechanism. In this regime the Higgs fields are excited from their initial zero value through quantum or thermal fluctuations and slowly roll alongside the flat part of the potential before reaching its steep part whereupon they will evolve rapidly and subsequently decay through coherent field oscillations. The Universe in this model is reheated not because of bubble wall collisions but because of the creation of elementary particles due to the decay of the ϕ-field.

The crucial difference between the two models is that since the field is already emerging from its false vacuum state before the inflationary era began, instead of having many bubbles making up the observable Universe, we just have one such bubble and so the Universe on large scales can be homogeneous and isotropic. The potential is arranged so that the time taken for the ϕ-field to overcome any barriers (if they exist) is very much smaller than the time it takes to start oscillating and that is the reason why the scalar potential has to be very flat near its origin (see figure (3.3)). Provided that the scalar potential is flat enough, the time taken for the ϕ-field to reach its true ground state can be long compared to the expansion time and, once $T \ll T_c \approx \sigma$, where σ is the energy scale of the theory, the potential energy of the ϕ-field becomes $U(0) \approx \sigma^4$ and will dominate the energy density of the Universe since $\rho \sim (kT)^4 \ll (kT_c)^4 = \mathcal{O}(\sigma^4)$, and thus cause the Universe to expand exponentially. In the next section we will give a

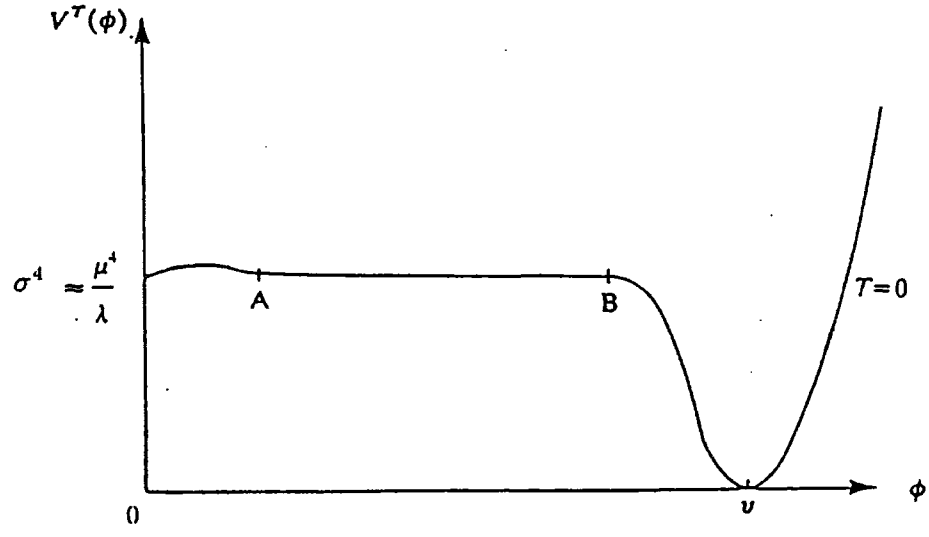

Figure 3.3: An example for the zero temperature potential required for new inflation.

somewhat more mathematical analysis of the subject.

3.4 Scalar Field Dynamics

Consider a classical scalar field ϕ that possesses some potential of self-interaction $U(\phi)$ with Lagrangian density

$$\mathcal{L} = -\frac{1}{2}\partial_\mu\phi\partial^\mu\phi - U(\phi)$$

and stress-energy tensor

$$T_{\mu\nu} = -\partial_\mu\phi\partial_\nu\phi - \mathcal{L}g_{\mu\nu}.$$

Asssuming that ϕ is spatially homogeneous, $T_{\mu\nu}$ can take the form of a perfect fluid with energy density and pressure given by

$$\rho = \frac{1}{2}\dot{\phi}^2 + U(\phi) \tag{3.8}$$

$$P = \frac{1}{2}\dot{\phi}^2 - U(\phi). \tag{3.9}$$

Provided that the potential energy dominates the kinetic it then follows that

$$\rho + 3P = 2\left[\dot{\phi}^2 - U(\phi)\right] < 0,$$

in which case $P \sim -U(\phi) \sim -\rho$ and the energy density of the Universe acts as an effective cosmological constant with $\Lambda = 8\pi G U(\phi)$. The equation describing the motion of ϕ in the self-interacting potential is obtained using conservation of energy-momentum and is given by

$$\ddot{\phi} + 3H\dot{\phi} + \Gamma\dot{\phi} + U'(\phi) = 0 \tag{3.10}$$

where the second term accounts for the expansion of the Universe and the $\Gamma\dot{\phi}$ term accounts for the particle creation that results from the decay Γ of ϕ-field to matter. The evolution of the ϕ-field can be divided into two qualitatively different regimes.

Slow-roll:

This period refers to the flat part of the potential ($A - B$ in fig.(3.3)) where ϕ rolls at constant velocity and the particle creation term is suppressed. We can neglect $\ddot{\phi}$ provided that

$$\ddot{\phi} \ll 3H\dot{\phi} \tag{3.11}$$

or,

$$|U''(\phi)| \ll 9H^2. \tag{3.12}$$

During this time the necessary condition for inflation to occur holds as well,

$$|U(\phi)| \gg \frac{1}{2}\dot{\phi}^2, \tag{3.13}$$

and since the potential energy dominates the dynamics of our system we can have $H^2 = 8\pi G U(\phi)/3$ as required and the total number of e-folds of expansion in time Δt is given by

$$N = e^{H\Delta t}.$$

coherent field oscillations:

During this regime (beyond B in fig.(3.3)) the potential steepens and ϕ evolves rapidly on the expansion time scale

$$|U''(\phi)| \gg 9H^2. \tag{3.14}$$

Once ϕ reaches the potential well it will start oscillating with frequency $\omega = (U''(\sigma))^{1/2}$. Using (3.8) we can rewrite the equation of motion for ϕ as follows

$$\dot{\rho}_\phi + 3H\dot{\phi}^2 + \Gamma\dot{\phi}^2 = 0. \tag{3.15}$$

As ϕ is rapidly oscillating around σ, $\dot{\phi}^2$ oscillates sisnusoidally and can be replaced by its average over a cycle,

$$\langle\dot{\phi}^2\rangle_{cycle} = \rho_\phi,$$

and hence

$$\dot{\rho}_\phi + 3H\rho_\phi + \Gamma\rho_\phi = 0. \tag{3.16}$$

This is the equation governing the evolution of the energy density of massive particles with decay rate Γ whose solution is given by

$$\rho_\phi = \sigma^4\left(\frac{R}{R_B}\right)^{-3} e^{-\Gamma(t-t_B)} \tag{3.17}$$

where we have assumed that coherent field oscillations commense at $t = t_B$, when $\phi = \phi_B$ and $R = R_B$, when the vacuum energy density is σ^4. From this time until $t \approx \Gamma^{-1}$ the energy density of the Universe is dominated by ρ_ϕ and since $\rho_\phi \sim R^{-3}$ we have $R \sim t^{2/3}$ and so the Universe is matter-dominated. When $t \approx \Gamma^{-1}$ the ϕ-field oscillates around the true minimum of its potential and decays into particles and the Universe is reheated untill it reaches

$$T_{rh} \approx g_*{}^{-1/4}\left(\Gamma M_P\right)^{1/2}.$$

Provided that $\Gamma^{-1} < H^{-1}$, so that the Universe reheats in less than one expansion time, all of the vacuum energy density is converted to radiation and $T_{rh} \approx {g_*}^{-1/4}\sigma$.

To solve the flatness, horizon and monopole problems we need to ensure that the initial smooth domain contains an entropy at least as great as that of our Universe. If we take the initial inflating patch to be of size $H^{-1} \approx M_P/(\sigma^2)$, during inflation it will exponentially grow by a factor of e^N, followed by a further increase during reheating of

$$\frac{R_{rh}}{R_B} \approx \left(\frac{\sigma^4}{{T_{rh}}^4}\right)^{1/3}.$$

Hence the total entropy at the end of reheating is

$$S \approx \left[H^{-1}e^N\left(\frac{\sigma^4}{{T_{rh}}^4}\right)^{1/3}\right]^3 S_{rh} \tag{3.18}$$

where $S_{rh} \approx k{T_{rh}}^3$ is the entropy density at the end of reheating. Thus,

$$S \approx \frac{ke^{3N}{M_P}^3}{\sigma^2 T_{rh}} \tag{3.19}$$

and to obtain $S > 10^{88}k$ we need

$$N_{total} \gtrsim 68 + \frac{2}{3}\ln\left(\frac{\sigma}{10^{14}GeV}\right) + \frac{1}{3}\ln\left(\frac{T_{rh}}{10^{10}GeV}\right). \tag{3.20}$$

The exponential increase of the scale factor and the huge increase in entropy ensures that the curvature decreases exponentially and that the whole observable Universe evolves from just one causally connected region that contains ≤ 1 monopoles in accordance with observations and is highly homogeneous and isotropic because of the high degree of uniformity within the initial patch that evolved to become our Universe. In figure (3.4) we show a comparison of standard and inflationary cosmologies.

As we have described it so far the new inflationary scenario does not explain the growth of structure on small scales and of course it still gives no explanation

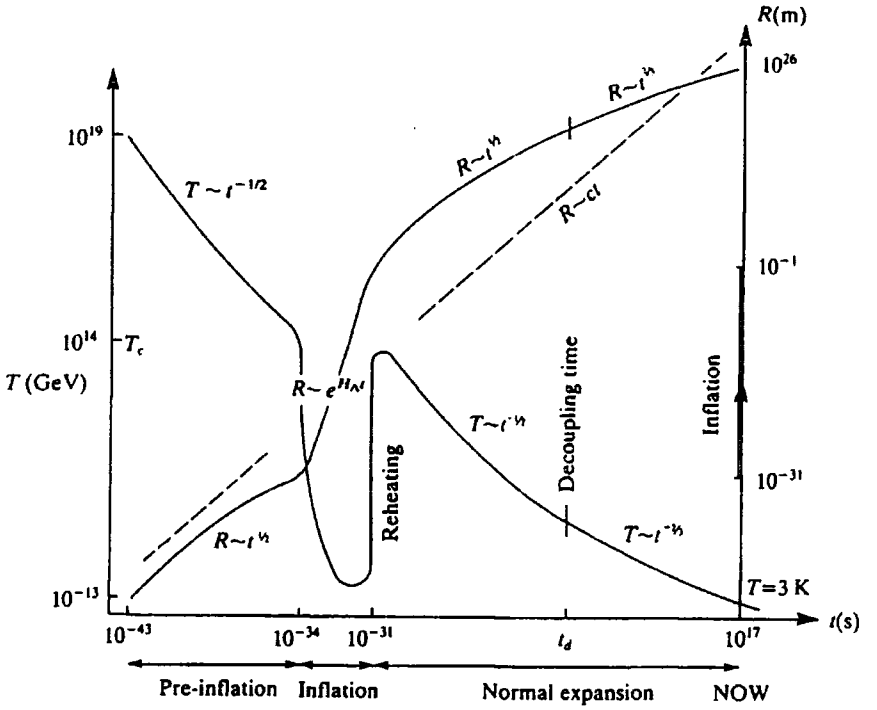

Figure 3.4: Variation of the temperature T and the scale factor R with time t in inflationary cosmology (Collins, Martin and Squires (1989)).

for the smallness of the cosmological constant in the present era. In the next section we will examine how it is possible to account for small scale inhomogeneities from which structure has grown.

3.5 The Origin of Density Inhomogeneities

So far we have assumed that ϕ is spatially perfectly uniform. However, because of quantum fluctuations in de Sitter space such a scalar field has a spectrum of quantum fluctuations associated with it given by (Collins, Martin and Squires (1989))

$$(\Delta\phi)^2 \equiv \frac{H^2}{4\pi^2}. \tag{3.21}$$

In standard cosmology perturbations on cosmologically interesting scales would have started outside the horizon ($\lambda_{phys} \geq H^{-1}$) and crossed inside when their size became comparable to the horizon length. Microphysical processes in the early Universe, however, can only operate on scales $\leq H^{-1}$ and it is very difficult to

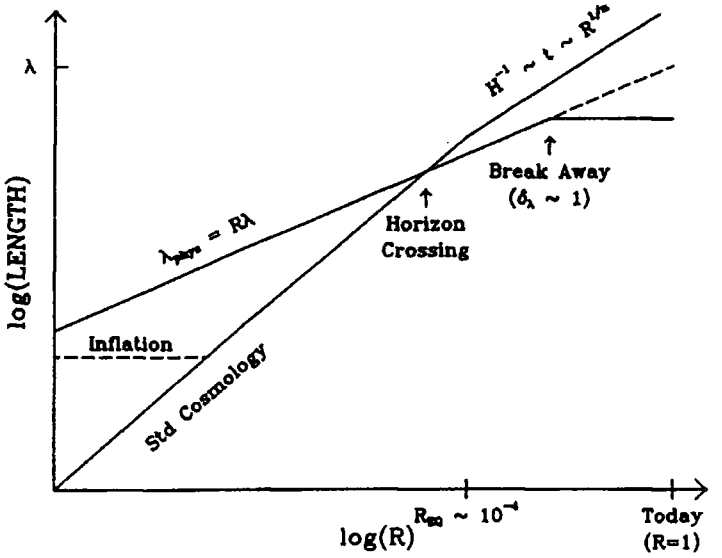

Figure 3.5: The physical size of a length scale λ_{phys} and the Hubble radius H^{-1}, as a function of the scale factor R. In standard cosmology all length scales begin super-horizon sized and subsequently cross back into the horizon at a later time. In inflationary cosmology, on the other hand, all scales begin sub-horizon sized, cross outside the horizon during inflation and finally re-enter at a later stage (Kolb and Turner (1990)).

imagine how structure could have evolved. In inflationary cosmology, on the other hand, a given length scale starts inside the horizon where quantum fluctuations in ϕ can produce density perturbations (see figure (3.5)).

As the scale crosses outside the horizon during inflation microphysical processes become impotent and $\delta\rho/\rho$ 'freezes out' at a value

$$\begin{aligned} \frac{\delta\rho}{\rho} \approx \frac{\delta U}{U} &\approx \frac{1}{U}\frac{\partial U}{\partial \phi}\delta\phi \\ &\approx \frac{\dot{\phi}H^2}{\sigma^4}. \end{aligned} \tag{3.22}$$

There is a quantity ζ which in the uniform Hubble constant gauge is gauge-invariant and which at horizon crossing is given by $\zeta = \delta\rho/(\rho + P)$ (Bardeen, Steinhardt and Turner (1983)). For superhorizon modes ζ remains constant and hence at horizon crossing we can write

$$\left(\frac{\delta\rho}{\rho + P}\right)_{t_1} = \left(\frac{\delta\rho}{\rho + P}\right)_{t_2} \tag{3.23}$$

where t_1 and t_2 are the times when a given perturbation crosses out and then back into the horizon. At t_2, $\rho + P = n\rho$, (where $n = 4/3,\ 1$ for the radiation and the matter dominated epochs respectively), and hence, up to a numerical factor,

$$\left(\frac{\delta\rho}{\rho+P}\right)_{t_2} = \left(\frac{\delta\rho}{\rho}\right)_{t_2}. \tag{3.24}$$

During inflation, however, when the perturbation crosses outside the horizon at t_1, $\rho + P = \dot{\phi}^2 \ll \rho \approx \sigma^4$ and so

$$\left(\frac{\delta\rho}{\rho+P}\right)_{t_1} \simeq \frac{\delta\rho}{\rho}\frac{\sigma^4}{\dot{\phi}^2} \tag{3.25}$$

and hence

$$\left(\frac{\delta\rho}{\rho+P}\right)_{t_1} = \frac{H^2}{\dot{\phi}}, \tag{3.26}$$

using (3.22). Thus at t_2

$$\left(\frac{\delta\rho}{\rho}\right)_{t_2} = \frac{H^2}{\dot{\phi}}. \tag{3.27}$$

Since H and ϕ are very nearly constant during inflation, the amplitude of $\delta\rho/\rho$ is nearly scale invariant (the Harrison-Zel'dovich spectrum).

To account successfully for galaxy formation an initial scale invariant spectrum of density perturbations of magnitude 10^{-5}–10^{-4} is needed since perturbations of this size that started growing at t_{eq} can now have reached $\delta\rho/\rho \gtrsim 1$. The prediction of a scale-invariant spectrum is an impressive feature of inflationary models. Somewhat less satisfactory is the achievement of the required magnitude of perturbations since very flat potentials are required as we will now show. For our purposes we will consider the Coleman-Weinberg potential (cf. (3.7)). The absence of a $m^2\phi^2$ mass term ensures that the potential is very flat near the origin and for $\phi \ll \sigma$ it can be approximated by

$$U(\phi) \simeq \frac{1}{2}A\sigma^4 - \frac{1}{4}\lambda\phi^4$$

$$\begin{aligned} U'(\phi) &\simeq -\lambda\phi^3 \\ \lambda &= 4A\left[\frac{1}{2} - \ln\frac{\phi^2}{\sigma^2}\right] \sim 10^{-1} \end{aligned} \tag{3.28}$$

During the slow-roll period

$$\frac{\delta\rho}{\rho} \approx -\frac{H^3}{(\partial U/\partial\phi)} \approx \frac{H^3}{\lambda\phi^3}. \tag{3.29}$$

At the end of the slow roll period when $\phi \approx \phi_B$, $|U''(\phi_B)| \simeq 9H^2$, and so (from the second equation in (3.28))

$$\phi_B{}^2 \approx \frac{3H^2}{\lambda}.$$

During this time the number of e-folds of expansion from ϕ_A to ϕ_B is

$$\begin{aligned} N_\phi = \int_{t_\phi}^{t_B} H dt &\simeq \int_{\phi_A}^{\phi_B} \frac{H}{\dot\phi} d\phi \simeq 3\int_{\phi_A}^{\phi_B} \frac{H^2}{(\partial U/\partial\phi)} d\phi \\ &\simeq \frac{3H^2}{2\lambda}\left(\frac{1}{\phi_A{}^2} - \frac{1}{\phi_B{}^2}\right) \\ &\simeq \frac{3H^2}{2\lambda\phi^2} \end{aligned}$$

and hence

$$\frac{\delta\rho}{\rho} \approx \frac{H^2}{\dot\phi} = \frac{-3H^3}{(\partial U/\partial\phi)} \approx \frac{3H^3}{\lambda\phi^3} \sim \lambda^{1/2}N^{3/2} \tag{3.30}$$

and, since we need $N \gtrsim 68$, to obtain $\delta\rho/\rho \approx 10^{-4}$ we must have $\lambda \lesssim 10^{-14}$, which demonstrates just how flat the potential has to be. Unfortunately, is is difficult to see how such a small coupling could arise naturally from a particle physics model.

The reason for this is that the size of the one-loop quantum corrections is fixed by the gauge coupling constant and that in order to have $A \approx 10^{-15}$ (say), the gauge coupling would have to be $\alpha \sim 3 \times 10^{-8}$, far too small to be compatible with any unification scheme. Such a small value of λ can be achieved naturally in SUSY theories but, since in this case ϕ couples to ordinary matter only through

interactions of gravitational strength, its decay rate would be too small and consequently adequate reheating would be problematic. The other problem lies in the fact that in order to solve the cosmological problems associated with Big Bang cosmology we need $N \gtrsim 68$, which can be achieved if initially $\phi_A \ll H$. We have seen, however, that quantum fluctuations in ϕ are of order H and so it is unlikely that the above condition will be met. Furthemore, if $\phi_A \ll H$ initially, the semiclassical analysis based on (3.10) would be invalidated as it only applies for $\phi_A \gg H$ (Collins, Martin and Squires (1989)).

To summarise then, almost all inflationary models that have been proposed so far can be classified in two main categories. In *slow − roll* models, such as new inflation examined earlier, the scalar field is misplaced from the true minimum of its potential and, provided that its kinetic energy in negligible, the evolution of the Universe is dominated by the potential energy of this field which is equivalent to an effective cosmological constant. There is a wide choice of possible inflaton fields that might drive inflation as is evident from the large number of slow-roll models that have been proposed. The major problem suffered in such models is the required fine tuning of the parameters of the potential because it has to be very flat to produce enough inflation. This, in turn, leads to the second problem of slow-roll models, namely that flat potentials give rise to anacceptably large density perturbations.

The second major category includes models such as Guth's original scenario where inflation occurs because of a first order phase transition that proceeds by quantum tunnelling of the ϕ-field to the true minimum of its potential which leads to the formation of bubbles of true vacuum. As mentioned before the problem here lies in the fact that such a phase transition produces a very inhomogeneous Universe which is often refered to as the 'graceful exit' problem.

Recently it has been proposed that the graceful exit problem might be avoided by modifying Einstein's theory of gravity so that the gravitational constant G varies with time, as in Brans-Dicke (BD) theory of gravity (Brans and Dicke (1961)). Extended inflation based on BD theory was first introduced by La and Steinhardt in 1989 and it not only avoids the fine tuning required in slow-roll models but, more importantly for our own work, allows the phase transition to be completed through bubble nucleation proccesses and hence could have resulted in large scale structures via bubble wall collisions. In the next section we will introduce the main ideas underlying this new model, reserving a discussion of its implications to structure formation and to the uniformity of the CMBR to chapter 4.

3.6 Extended Inflation

In extended inflation the Universe undergoes a first order phase transition and, as in Guth's original model, it supercools in a false vacuum state that is separated from the true vacuum by an energy barrier. The key difference, however, lies in introducing a modified theory of gravity such as BD theory of gravity where Newton's gravitational constant is replaced by a time-varying scalar field $\Phi(t)$. The effect of this, as we will see below, is to slow the exponential increase of the cosmic scale factor during the inflationary epoch into a power law expansion.

In the original extended inflation model (La and Steinhardt (1989a)) the BD scalar was a free field. It has been argued, however, that extended inflation via a pure BD theory is incompatible with astrophysical constrains and furthermore theories with completely free scalar fields are not well motivated physically (La, Steinhardt and Bertschinger (1989), hereafter as (LSB)). Instead a scalar potential $V(\Phi)$ for Φ is included in the BD action, chosen to have a minimum such that

$\Phi \rightarrow {M_{pl}}^2$ where $M_{pl} \approx 10^{19} GeV$ is the value of the Planck mass today. Making the substitution $\Phi \equiv ((1/8b)\phi^2)$ where ϕ has dimensions of mass and b is the BD parameter the action can be written as (LSB)

$$A(\phi, \sigma) \equiv \int d^4x\sqrt{-g}\left[\xi\phi^2 R - \frac{1}{2}\partial_\mu\phi\partial^\mu\phi - V\left(\frac{\phi^2}{8b}\right) + 16\pi L(\sigma)\right] \tag{3.31}$$

where $\xi = 1/8b$ is the non-minimal coupling coefficient and $L(\sigma)$ contains the contributions of all matter fields including the scalar σ that drives inflation. Equations of motion for ϕ and $R(t)$ can then be derived whose solution show how these parameters vary during inflation and the more conventional radiation and matter dominated epochs. In the particular case that the potential $V(\phi)$ is chosen to have a minimum at $\phi = \sqrt{8b\Phi} = \sqrt{8b}M_{PL}$, the theory is known as induced gravity theory.

During the inflationary epoch the false vacuum energy density dominates the energy density of the Universe and $\rho_\sigma = -p_\sigma = \rho_F \equiv {M_F}^4$ where M_F defines the energy scale for the false vacuum energy density and the inflationary phase transition. Solutions to the equations of motion in this case yield

$$\phi(t) = \sqrt{8b}m_{PL}\left(1 + \frac{H_B t}{\alpha}\right), \tag{3.32}$$

$$R(t) = \left(1 + \frac{H_B t}{\alpha}\right)^{b+1/2} = \left(\frac{\phi(t)}{\phi(0)}\right)^{b+1/2}, \tag{3.33}$$

where $H_B = \sqrt{8\pi/3}{M_F}^2/m_{PL}$ is the Hubble parameter at the beginning of inflation ($t = 0$), $m_{PL} < M_{PL}$ is the effective Planck mass at the beginning of inflation and where $\alpha \equiv \sqrt{(3 + 2b)(5 + 6b)/12}$.

For short times the BD solution approaches the Einstein-de Sitter solution in that ϕ is nearly constant and $R(t)$ increases exponentially. However, for times such that $H_B t/\alpha > 1$ the scale factor increases as a power-law rather than exponentially and this is essentially all that is required to achieve a successful graceful

exit (La and Steinhardt (1989a)). After the successful termination of the phase transition, extended inflation closely resembles old inflation in the sense that most of the false vacuum energy is concentrated on the bubble walls and reheating is achieved through bubble wall collisions.

Just as in the case for slow-roll inflationary models it has been possible to derive the conditions required for a successful extended inflation model (LSB, Weinberg (1989)) by considering the various stages of the inflationary epoch and placing limits on M_F and m_{PL}. The problems of the Big Bang model of Cosmology can be solved as in the more conventional models of inflation with the exception that, to suppress the overproduction of topological defects, the phase change that produces these defects must have occured before the inflationary phase transition.

Contrary to the predictions of most inflationary models the spectrum of adiabatic density perturbations in extended inflation is not in general scale invariant because both H and ϕ vary with time

$$\frac{\delta\rho}{\rho} \approx \frac{H^2(t)}{\dot{\phi}(t)}, \tag{3.34}$$

where t corresponds to the time when a given comoving wavelength crosses outside the horizon during the inflationary epoch. Constraints on $\delta\rho/\rho$ on scales comparable to the present horizon length ${H_P}^{-1}$, can be obtained by considering the observed isotropy of the CMBR, that is

$$\left.\frac{\delta\rho}{\rho}\right|_{{H_P}^{-1}} < 10^{-4}. \tag{3.35}$$

In particular it can be shown (LSB) that

$$\left.\frac{\delta\rho}{\rho}\right|_{{H_P}^{-1}} \approx \alpha\sqrt{\frac{\pi}{8b}}\left(\frac{M_F}{M_{PL}}\right)^2\left(\frac{M_F}{T_P}\right)^{2/(b-1/2)} < 10^{-4}, \tag{3.36}$$

where $T_P \sim 3K$ is the present temperature of the CMBR.

Gravitational wave perturbations, on the other hand, can produce a quadrapole anisotropy in the CMBR due to the Sachs-Wolfe effect and it can be shown that

$$A_{GW} \approx \sqrt{\frac{8\pi}{3}}\left(\frac{M_F}{M_{PL}}\right)^2\left(\frac{M_F}{T_P}\right)^{2/(b-1/2)} < 2\times 10^{-5}. \tag{3.37}$$

Given that $M_F > 100GeV$ to achieve baryosynthesis after reheating, the last two equations can be satisfied provided that $b > 1.5$ (LSB).

We next consider the bubble nucleation rate. In chapter 5 we will show that for conventional models of inflation the critical quantity to calculate is Γ, the nucleation rate of bubbles of true vacuum per unit volume. In extended inflationary models, however, Γ has to compete with the inflationary expansion which is now characterised by a *time-varying* Hubble parameter $H(t)$. This is taken into account by introducing a dimensionless parameter ϵ (La and Steinhardt 1989b),

$$\epsilon(t) \equiv \frac{\Gamma}{H^4(t)}. \tag{3.38}$$

During the phase transition H decreases inversely with time and ϵ increases as $\epsilon_B[H(0)/H(t)]^4$, where ϵ_B is the value of ϵ at the beginning of inflation. It can then be shown that

$$\epsilon_B > \frac{16\pi}{3}\frac{{M_F}^4}{{M_{PL}}^4}. \tag{3.39}$$

Finally, another constraint on extended inflationary models can be obtained from the observation that the overproduction of large bubbles would destroy the observed large-scale isotropy. By considering the fractional volume of bubbles with radius greater than the horizon size at decoupling, it has been shown (LSB) that

$$b < \left(\frac{4}{C}\right) \times \left[25 + \log\frac{M_F}{10^{15}GeV}\right], \tag{3.40}$$

where $C \approx 4$. Extended inflation based on a pure BD theory requires $b > 500$ (Reasenberg *et al.*, (1979)). However, such a large value of b would produce too

many large bubbles which would destroy large scale isotropy and so extended inflation based on a pure BD theory can be ruled out. In the case where $V(\phi) \neq 0$ values for b in the range $1.5 < b < 25$ are allowed. Extended inflation can then be achieved in many different particle physics theories which makes it an attractive candidate for the 'ultimate' inflationary theory. What is more, because in extended inflation the phase transition is completed by bubble nucleation proccesses, it might be possible to account for the bubbly structure suggested in some recent astronomical surveys (see the next chapter) as resulting from collisions between true vacuum bubbles.

To conclude, we note that inflation has been studied in many different contexts such as in supersymmetry, supergravity, Kaluza-Klein theories or superstrings and indeed can occur in any theory that contains a weakly-coupled scalar field displaced from the minimum of its potential. The vast literature on inflationary cosmology reflects the continuing uncertainty as to the specific form of the potential $U(\phi)$ that should, on the one hand, be predicted by a fundamental particle theory and, on the other hand, allow for the successful implementation of inflation and the solution of the structure formation problem (Barrow (1988)).

Chapter 4

Structure Formation

Perhaps the most important and as yet unresolved question in Cosmology concerns the origin and evolution of the large scale structures, such as galaxies, clusters and voids. In this chapter we review the observational evidence concerning the structure of the Universe and the dark matter problem. Then, we consider a popular class of structure formation models based on the concept of gravitational instability and finally briefly mention some alternative ideas such as explosive galaxy formation and cosmic strings. We conclude with a discussion of the inhomogeneities observed in the CMBR and the possibility that structure may have resulted from a phase transition.

4.1 Observed Large Scale Structure

On very large scales the Universe is homogeneous and isotropic. This is one of the major assumptions on which the Big Bang model of Cosmology is based and the best evidence for it comes from the isotropy of the $CMBR$. Observational evidence for the large scale homogeneity and isotropy of the Universe, other than that obtained from the $CMBR$, is quite hard to obtain as it involves analysing very large samples of galaxies if the results are to be reliable. However, as figures (4.1) and (4.2) show, we can begin to discern its smoothness on very large scales.

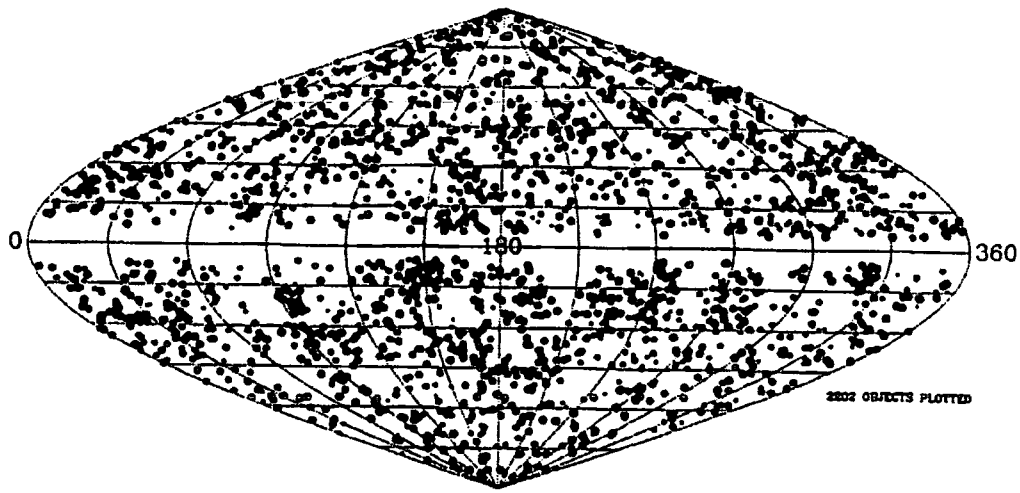

Figure 4.1: Distribution of distant IRAS galaxies (Strauss *et al* (1992))

On small scales, however, galaxies, clusters of galaxies and giant voids are quite common and one would like to know how they were formed and why they are so distributed in space. Recent studies of the redshifts of galaxies such as the CfA redshift survey extension (Geller and Huchra (1991)) has led people to speculate that galaxies lie predominantly on the surfaces of bubbles rather than along one-dimensional filaments. Some of the results of the survey are shown in figs.(4.3) and (4.4). Several of the voids are surrounded by thin structures in which the intergalaxy separation is small compared with the radius of the void. Typical voids have diameters of about $25Mpc$, the largest being $50Mpc$. The typical thickness of the sheets of matter that surround these voids is of order $5Mpc$ and they have a typical mass of about $10^{16}M_{\odot}$ (Geller and Huchra (1991). The most pronounced structure we can see in fig.(4.4) that runs across the entire right ascension range is the 'Great Wall'. A recent survey (Las Campanas Redshift survey, Doroshkevich *et al* (1995)) which examines the characteristics of structure along a straight line gives some support to the idea that on very large scales the structure in the Universe is sheet-like. There is also evidence that on much smaller scales the structure may be filamentary but, as the authors stress,

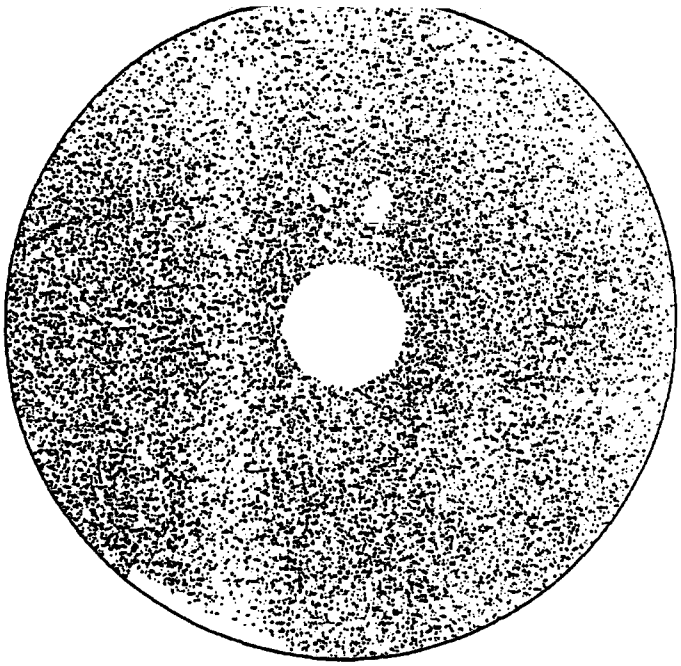

Figure 4.2: Angular distribution of the $\sim 31,000$ brightest $6cm$ radio sources (Gregory and Condon (1991)). The hole at the centre is caused by the range of the radio telescope, while the ragged edge at the lower left-hand side and the small holes just above the central one are caused from the interference by the sun and by other bright sources in the plane of the Milky Way respectively.

their results need to be tested with even deeper redshift surveys.

4.2 Dark Matter

During the past twenty years it has become increasingly clear that baryonic matter can only account for a fraction of the mass in the Universe. First, the observed light–element abundances are close to the theoretically predicted values in the context of the Big Bang provided the baryonic contribution to Ω is less than one. The second observation that led to the realisation that there is a dark matter problem came with the study of galaxy rotation curves which showed that most galaxies must be surrounded by an invisible halo of unknown composition. And finally, after the idea of inflation was introduced, it became clear that, since Ω is expected to be very close to 1 if the theory is correct, at least 90% of the total mass in the Universe has not been detected yet and is unlikely to be baryonic

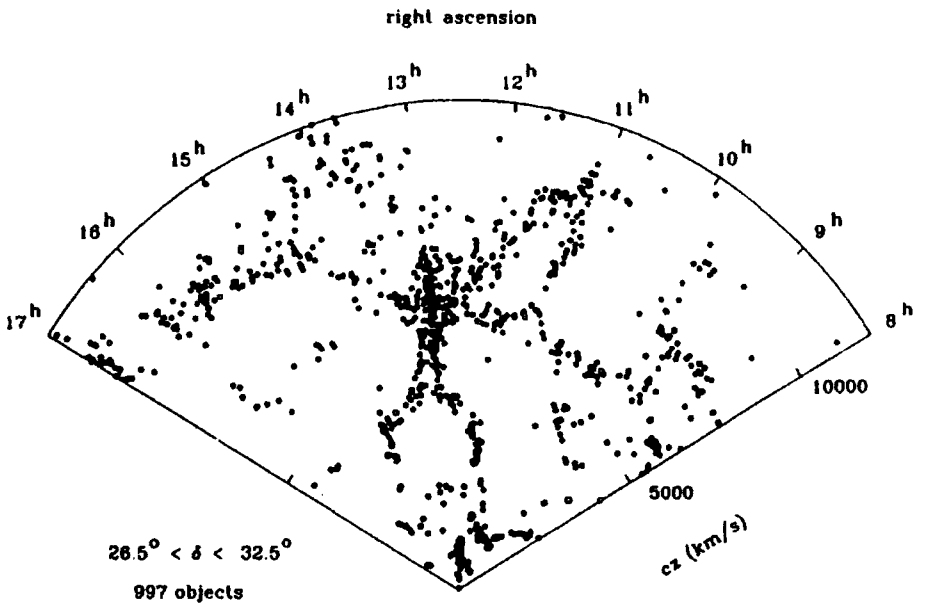

Figure 4.3: Observed velocity versus right ascension for the survey strip entered at $\delta = 29.5°$. The strip is 6° in declination (de Lapparent, Geller and Huchra (1986)).

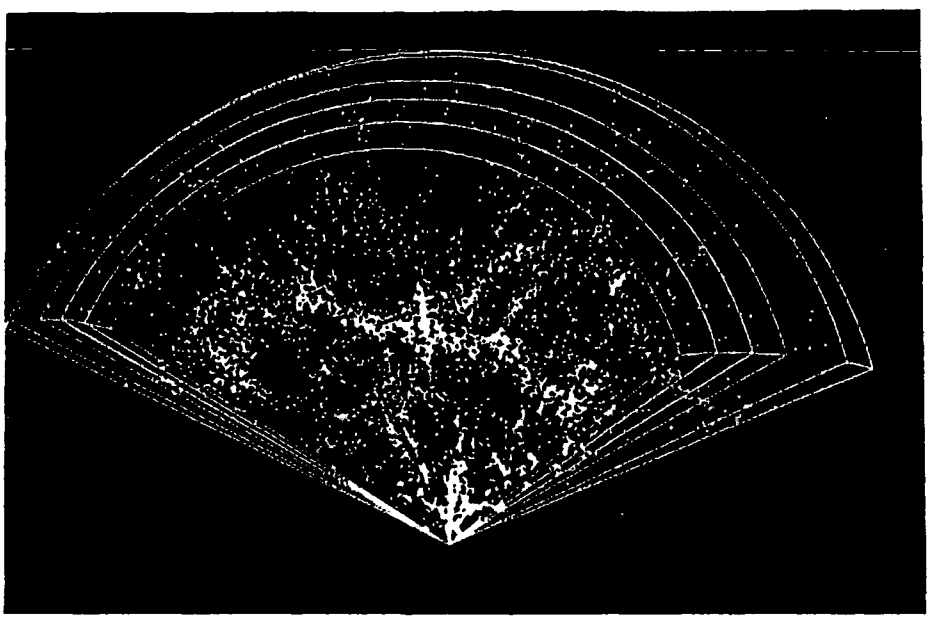

Figure 4.4: Projection of a three-dimensional display of four completed slices of the redshift survey (Geller and Huchra (1991)).

in origin. However, we should keep in mind that inflationary models have been proposed where $\Omega < 1$. In such models one has a two-field potential, one of which drives the slow-roll inflationary epoch while the other performs a phase transition in which the nucleation rate varies in such a way as to give an $\Omega_0 = 0.2$ Universe with maximum probability. In this scenario the Universe appears to be composed of infinitely many superhorizon underdense bubbles which resemble open universes (Amendola, Baccigalupi and Occhionero (1996)).

Non-baryonic matter can be divided into two categories, namely hot dark matter (HDM) and cold dark matter (CDM). HDM is the term used to describe light particles that decoupled from the hot plasma while they were still relativistic. Because they are moving very fast prior to the epoch of galaxy formation they can only be clustered on large scales. Thus, consider, for example, a light neutrino. Since neutrinos drop out of equilibrium while still relativistic, their abundance is roughly the same as that of photons. During e^+e^- annihilation extra photons are produced and from conservation of entropy we obtain

$$\left(\frac{T_\nu}{T_\gamma}\right)^3 = \frac{g_\gamma}{g_\nu} = \frac{4}{11}$$

and, therefore,

$$\frac{n_\nu}{n_\gamma} = \frac{3}{8}g_\gamma = \frac{3}{8}g_\nu\left(\frac{T_\nu}{T_\gamma}\right)^3 = \frac{3}{22}g_\nu.$$

Here ν and γ refer to neutrinos and photons respectively, n and g are the number density and the spin degrees of freedom, and T is the temperature. Thus,

$$\rho_\nu = m_\nu n_\nu = \frac{3}{22}n_\gamma \sum g_\nu m_\nu \sim 10^{-31}\sum g_\nu m_\nu gcm^{-3}$$

where the sum is taken over all neutrino species. Since now $\rho_c = 2\times10^{-29}h_0{}^2 gcm^{-3}$, the contribution of light neutrinos to the mean density of the Universe is given by

$$\Omega_{\nu_0} = \frac{g_\nu}{2}\left(\frac{\sum m_\nu}{100eV}\right)h_0{}^{-2} \tag{4.1}$$

where $g_\nu = 4$ ($g_\nu = 2$) for a Dirac (Majorana) fermion, which implies that closure density is obtained provided that

$$\sum m_\nu \lesssim \begin{cases} 100eVh_0{}^2 & g_\nu = 2 \\ 50eVh_0{}^2 & g_\nu = 4. \end{cases} \tag{4.2}$$

On the other hand there could be massive CDM particles that did not drop out of equilibrium until they were non-relativistic and were therefore moving slowly at the epoch of galaxy formation and clustered on very small scales. Examples of CDM candidates include $WIMPS$ that have masses in excess of $1GeV$. For example massive neutrinos, ones for which $kT \ll mc^2$ at decoupling, would be in equilibrium through the weak interaction while they were non–relativistic and since

$$\rho c^2 = \frac{mc^2 g}{\hbar^3}\left(\frac{mkT}{2\pi}\right)^{3/2} e^{-mc^2/kT}$$

their density relative to that of photons falls exponentially with the mass. The decoupling temperature of heavy neutrinos is of order $kT_d \sim m_\nu c^2/20$ and we can account for the missing mass provided $m_\nu \approx 2GeV$.

A similar analysis can be carried out for any other non–baryonic dark matter candidate and upper and lower bounds to their mass can be inferred. We will not go into any more detail except to note, on the one hand, the large number of possible candidates and the fact that most of them are hypothetical in the sense that they have not been directly detected and to stress, on the other hand, that any candidate chosen to solve the dark matter problem must be able to explain the structure formation problem as well.

4.3 Models of Structure Formation

Structure formation and the models that have been suggested to explain it is a huge topic that cannot be covered in any detail here. We will, therefore, only

briefly mention some of the main theories that have been put forward.

4.3.1 Gravitational Instability Models

According to this idea the range of structures we see today has resulted from the growth of small density fluctuations in the early Universe. The spectrum of primaeval density fluctuations can be described in one of two ways:

- Gaussian fluctuations in the density where the mass spectrum is taken to be a power law

$$\frac{\delta\rho}{\rho} \propto m^{-\alpha}. \tag{4.3}$$

- In Fourier space, where the fluctuations are treated as a sum of plane waves characterised by a wavenumber k. The power spectrum of the distribution in this case is given by

$$P_k = |\delta_k|^2 \propto k^n. \tag{4.4}$$

The two formalisms can be related by evaluating the mean square fluctuations predicted by the Fourier waves, the result being dependent on a window function describing the region that contains the fluctuation. In the case of a spherical boundary of radius r it can be shown that

$$\left\langle \left(\frac{\delta\rho}{\rho}\right)^2 \right\rangle \approx \frac{1}{2\pi^3} \int_{\frac{1}{r}}^{\infty} P(k) 4\pi k^2 dk \propto r^{-(3+n)} \propto m^{-\frac{3+n}{3}},$$

which, comparing with (4.3), gives $\alpha = (3+n)/6$. Restrictions can be placed on α and n by noting that the absence of very large structures suggests $\alpha > 0$. Also values of $\alpha > 2/3$ can be shown to be incompatible with the relatively smooth structure of the largest elliptical galaxies, and we therefore have

$$0 < \alpha < \frac{2}{3}, \quad or \quad -3 < n < 1. \tag{4.5}$$

Primaeval fluctuations can be either adiabatic, in which case

$$\frac{\delta\rho_r}{\rho_r} = \frac{4\delta\rho_m}{3\rho_m},$$

or isothermal, which implies fluctuations in the matter density only and

$$\delta\rho_r = 0,$$

where ρ_m and ρ_r are the matter and radiation densities respectively. In both cases there is a characteristic mass below which irregularities are damped out by pressure. For adiabatic perturbations the scale is set by the Silk mass, which is the minimum mass scale that can survive right through to decoupling, given that as $t \longrightarrow t_d$ the photon mean free path becomes larger enabling them to move out of overdense regions, dragging matter out as well, so damping out any inhomogeneities. It is estimated that, at decoupling, the Silk mass is of order $M_D(t_d) \approx 10^{12} M_\odot$. In the case of isothermal perturbations the damping scale is considerably smaller because of the dramatic drop in pressure once the baryons decouple from the photons. In this case, $M_D \approx 10^5 M_\odot$, similar to the size of a globular cluster.

The theory of the evolution of density inhomogeneities in an expanding Universe can be divided into two qualitatively different regimes, depending on whether or not a given scale is outside or inside the horizon at the time. For perturbations that are outside the horizon microphysical processes cease to have any effect and ideally a general relativity approach is required. However, as we saw in chapter 3, there is a simple gauge invariant quantity that characterises the size of a given perturbation once it has re–entered the horizon, $\zeta \equiv \delta\rho/(\rho + P)$. The evolution of density perturbations is related to that of the curvature k/R^2 relative to the energy density ρ_0 (Kolb and Turner (1990)). To demonstrate this we start by

considering adiabatic perturbations about a flat FRW model, for which

$$H^2 = \frac{8\pi G\rho_0}{3}.$$

A similar, though perturbed, region with a slightly higher density ρ_1 will have a positive curvature and

$$H^2 = \frac{8\pi G\rho_1}{3} - \frac{k}{R^2}.$$

Thus,

$$\delta = \frac{\rho_1 - \rho_0}{\rho_0} = \frac{k/R^2}{8\pi G\rho_0/3}$$

and so

$$\delta \propto \frac{R^{-2}}{\rho} \propto R^2 \sim t. \tag{4.6}$$

Thus, adiabatic perturbations grow as t while outside the horizon. Isothermal fluctuations, however, do not grow while they are ouside the horizon. The details of their subsequent evolution depend on whether they cross back into the horizon before or after matter-radiation density equality. The end result, however, is the same: after horizon crossing the difference between adiabatic and isothermal modes becomes irrelevant.

We now turn our attention to adiabatic perturbations that are inside the horizon where causal microphysical processes are important and a Newtonian treatment of their evolution will suffice. As we mentioned before, the evolution of perturbations once they have crossed back into the horizon depends on whether they do so in the radiation or matter dominated epoch. In a radiation dominated epoch the growth of perturbations is inhibited. One way of seeing this is to interpret the expansion of the Universe as a damping term that slows down the growth of perturbations. In particular, since the expansion rate of the Universe is faster than it would have been had there been only matter present, the growth of perturbations is almost nil. However, during the matter dominated epoch the

expansion of the Universe is only able to dampen the exponential collapse of a classical Jeans instability into a power law.

More formally, the first step towards the realisation of a structure formation theory based on the concept of gravitational instability involves the derivation of equations governing the decay or growth of density perturbations. This is done by perturbing the Euler equations of Newtonian motion after introducing a scale factor to take into account the expansion of the Universe. Solutions to these equations show how $\delta \equiv \delta\rho/\rho$ varies during the various stages of the evolution of the Universe (see, for example, Weinberg (1972), Kolb and Turner (1990), Peebles (1993)). The second step is to estimate the Jeans mass, that is the smallest mass that will collapse gravitationally. This depends on the nature of dark matter and on whether the Universe is matter or radiation dominated. The final step requires numerical simulation and it is here that model predictions are adjusted to match the observed distribution of matter (see, for example, Davis *et al* (1985), (1988), White *et al* (1983)).

There are two basic models of structure formation depending on the shape of the power spectrum and on the nature of dark matter.

- **(a) Pancake models.** These are based on adiabatic baryon or HDM models in which low-mass fluctuations are destroyed. The first structures to form are comparable to the size of clusters of galaxies. Smaller structures only emerge later as the bigger structures fragment into galaxies. However, numerical simulations of HDM models show that such structures take too long to form and that they would only acquire a small fraction of the baryonic matter.

- **(b) Hierarchical clustering.** This occurs in isothermal baryon or CDM models and the structure builds 'from the bottom up', initially on globular cluster scales. The problem here lies in the fact that CDM models fail to produce enough structure on very large scales and so are inconsistent with the observations which suggests that clusters of galaxies are strongly correlated. It seems that a biasing mechanism is needed to suppress the formation of galaxies in regions of lower than average density.

  The second 'problem' of CDM models, their preference for an $\Omega_0 = 0.2$ Universe, may perhaps be reconciled with inflation (Amendola, Baccigalupi and Occhionero (1996)), or there may be a residual positive cosmological constant which accounts for as much as 80% of the critical energy density of the Universe (Efstathiou, Sutherland and Madox (1990)).

4.4 Other Models

Though both types of model have some attractive features neither is entirely satisfactory, the main reason being the uncertainties in the nature of the dark matter. If the evidence presented earlier, that the structure in the Universe lies on the surfaces of bubbles, is correct it may be that other mechanisms of structure formation are needed, not based just on gravitational instabilities. One such mechanism is provided by the theory of explosive galaxy formation (Ostricker and Cowie (1981)). The key idea here is that at redshifts $z \lesssim 100$ massive stars in bound stellar systems have lifetimes which are short compared to the Hubble time and they will explode, releasing energy that will propagate as an adiabatic blast wave. The total mass swept up by the shock wave is estimated to be of order $M_s \simeq 10^{-2} - 10^{-3}M$ where M is the mass of the bound stellar system. The details of the structures resulting from this scenario depend on the era in which

it takes place, but in general it is predicted that unvirialised groups of galaxies should lie on two-dimensional surfaces and that large cavities will be produced. However, to account for voids larger than about $20h^{-1}Mpc$, a large amount of energy input is required which would cause unacceptably large fluctuations in the $CMBR$ (Peebles (1983)).

Another model of galaxy formation is based on the idea of cosmic strings (cf. section (3.1)). Strings produced in an early phase transition would form a tangled network spreading throughout the Universe. The evolution of such strings in an expanding Universe would depend on their density and the length distribution of the loops, a fairly involved topic that will not be reviewed here (for a detailed account on cosmic strings and their impact on Cosmology see Vilenkin and Shellard (1994)). It should be noted, however, that because of the large mass scales associated with such defects their cosmological implications would be significant. It has been argued, for example, (Ostriker *et al* (1986)) that each oscillating loop of string would grow a bubble of galaxies around it and that these bubbles might be comparable to the size of the voids which have been observed.

Severe tests of such models result from the anisotropies that cosmic strings would induce in the temperature of the CMBR and from examining the observational evidence for such defects due to gravitational lensing. If inflation occured in the early Universe, any cosmic strings which formed before inflation would be diluted away by the accelerated expansion. Thus, it is only possible to account for structure formation via cosmic strings which formed after, or near the end of, the inflationary epoch. It remains to be seen whether such models can be made realistic and whether they will be able to satisfy the constraints imposed by the CMBR when improved measurements from COBE become available (Vilenkin and Shellard (1994)).

As yet there is no 'standard model' of structure formation. The problem lies in developing a theory that, on the one hand, is compatible with the standard model of cosmology and inflation and, on the other hand, is able to reconcile the structures observed on small and medium scales with the large scale uniformity seen in figs. (4.1) and (4.2) and the high degree of isotropy of the $CMBR$.

4.5 Inhomogeneities in the Cosmic Microwave Background Radiation

Severe tests of the initial fluctuation spectrum and indeed of all structure formation models can be obtained from observations of the $CMBR$, since large scale density perturbations will lead to temperature fluctuations in the $CMBR$ of roughly the same magnitude (Sachs and Wolfe (1967)). Apart from a small dipole anisotropy which is attributed to our motion relative to the cosmic rest frame, temperature fluctuations in the $CMBR$ on large scales arise mainly from the Sachs-Wolfe effect. They result from the fact that fluctuations in the gravitational potential will induce redshifts in the $CMBR$ photon distribution which will appear as temperature fluctuations. Observations of large scale fluctuations by the $COBE$ satellite indicate that the temperature differences observed by two microwave antennae separated by almost any angle between 10 *arcsec* and 180° is

$$\frac{\Delta T}{T} = 1.1 \pm 0.1 \times 10^{-5}, \tag{4.7}$$

just within the range consistent with inflation (see, for example, Steinhardt (1995)). While the Sachs-Wolfe effect probes the fluctuation spectrum on large scales, comparable to ${H_0}^{-1}$, we should also note that there are other effects that will give rise to temperature fluctuations in the $CMBR$ on small scales. Unfortunately they are harder to compute as these smaller angular scales correspond

Milestone	Range of ℓ	What it tests
1. Large scale fluctuations	$2 \lesssim \ell \lesssim 30$	Spectral amplitude
2. Plateau at intermediate scales	$10 \lesssim \ell \lesssim 100$	Spectral shape/slope
3. First Doppler peak	$100 \lesssim \ell \lesssim 300$	
a. Value of ℓ at the maximum		Flatness
b. Height		Constraints on h, Ω_B, Ω_Λ and reionization?
4. Second & higher Doppler peaks	$300 \lesssim \ell \lesssim 800$	Constraints on $\Omega_B h^2$, CDM vs. MDM
5. Damping	$\ell \gtrsim 1000$	Silk effect, cosmo. parameters?

Table 4.1: Tests for inflation and dark matter models of large scale structure (Steinhardt (1995)), where the temperarure fluctuations have been expanded in spherical harmonics, $\frac{\delta T}{T} = \sum_{\ell m} \alpha_{\ell m} Y_{\ell m}(\theta, \phi)$, where θ and ϕ are spherical angles in the sky and where $\alpha_{\ell m}$ are the scalar and tensor multiple components respectively.

to comoving length scales that were sub-horizon sized at decoupling and so microphysical processes were important. Furthermore, re-ionisation effects reduce the small scale anisotropies, making them harder to study (for more details see Kolb and Turner (1990)). It is hoped that a series of experiments and observations during the next decade will allow us to test the inflationary hypothesis and place new constraints on most of the cosmological parameters (Steinhardt (1995)). A summary of the tests proposed is shown in table (4.1). If successful this programme should give overwhelming support to inflationary cosmology in general and severely constrain models of structure formation.

4.6 First-Order Phase Transitions and CMBR Constraints

As we have noted, recent large scale surveys (eg. de Laparent, Geller and Huchra (1988), Vogeley, Geller and Huchra (1991)) suggest that the large scale structure in the Universe may be bubble-like, concentrated around giant voids. The renewed interest in first-order inflation models such as in extended inflation (see last chapter) has led scientists to speculate that such large scale structures might be the direct result of the first order phase transition in the inflationary epoch

causing the nucleation of bubbles of true vacuum (La (1991)).

Even though it is still early days as far as the detailed observation of voids is concerned (in most surveys the void size is comparable with that of the sample as a whole) such a scheme for generating structure is an attractive alternative to CDM models which fail to produce enough structure on large scales.

Extended inflation (hereafter EI) models succeed in achieving a graceful exit from the false vacuum phase, allowing percolation of the bubbles of true vacuum and their subsequent thermalisation through bubble wall collisions, without requiring fine tuning of the parameters involved (La and Steinhardt (1989b)). However, severe constraints on all such models are imposed by the distortions that the bubble spectrum would produce in the CMBR (Weinberg (1989), Liddle and Wands (1991), Turner, Weinberg and Widrow (1992)). In particular it has been shown that the original EI model based on a pure BD theory with no potential for Φ is incompatible with these constraints (La, Steinhardt and Bertchinger (1989)). This, however, should not worry us too much because a non-zero Φ potential is better motivated physicaly and appears naturally in many particle physics models. Nevertheless, since too many large bubbles could still destroy the large-scale isotropy of the CMBR, the number of bubbles that are larger than the horizon size at decoupling must be constrained.

Before we examine how first-order inflation models may be able to account for the bubbly structure observed on large scales, we review why Guth's original model failed. We have mentioned before that this is due to the fact that bubbles of true vacuum do not percolate, the basic reason being that the expansion of the background space, $R \sim e^{Ht}$, overwhelms the bubble growth. To quantify this, consider a bubble nucleated at time t_0 with zero initial radius. From the moment of its nucleation it will expand with a speed approaching the speed of light and

at some later time $t > t_0$ its comoving radius will be given by

$$x(t,t_0) = \int_{t_0}^{t} dt' R^{-1}(t') = \frac{e^{-Ht_0} - e^{-Ht}}{HR_0} \longrightarrow \frac{e^{-Ht_0}}{HR_0}, \tag{4.8}$$

where R_0 is the scale factor at the beginning of the vacuum-dominated era at $t = 0$ and where the limit applies for $t \to \infty$. Equation (4.8) indicates that bubbles nucleated earlier than t_0 will reach larger comoving sizes than bubbles nucleated later. The physical size of a bubble at time t is $r(t,t_0) = R(t)x(t,t_0)$ and the physical volume occupied by it will be

$$V(t,t_0) = \frac{4\pi}{3} r^3(t,t_0) \longrightarrow \frac{4\pi}{3} \frac{e^{3H(t-t_0)}}{H^3} \tag{4.9}$$

where again the limit represents $t \to \infty$. The probability that any given point remains in the false vacuum phase during the bubble nucleation process (beginning at $t = 0$) is given by (Guth and Weinberg (1983))

$$p(t) = \exp\left[- \int_0^t dt_0 \Gamma V(t,t_0) \right] \longrightarrow \exp\left[- \frac{4\pi}{3} \left(\frac{\Gamma}{H^4} \right) Ht \right], \tag{4.10}$$

where Γ is the bubble nucleation rate per unit volume per unit time.

A measure of whether or not percolation will occur is the fraction of physical space that is still in the false vacuum, given by

$$f(t) = p(t) R^3(t) \longrightarrow \exp\left[\left(- \frac{4\pi}{3} \frac{\Gamma}{H^4} + 3 \right) Ht \right]. \tag{4.11}$$

Whether $f(t)$ increases or decreases with time depends on the competition between the decreasing probability of a point being in the false vacuum and the increasing volume of space occupied by the false vacuum (Kolb (1991)), which clearly depends on $\epsilon \equiv \Gamma/H^4$. If $\epsilon \ll 1$ the transition will never be completed whereas if $\epsilon \gg 1$ the period of inflation will be too short. Since in old inflation ϵ is constant there is no way these two conditions can be met. The obvious way to solve this graceful exit problem is to make ϵ a function of time by making

either Γ or H, or both, time dependent. In the last chapter we saw that in the original EI model H is a decreasing function of time and so percolation is eventually achieved. But unfortunately bubbles nucleated early in the inflationary epoch will grow to unacceptably large scales and hence would distort the CMBR (Weinberg (1989), La, Steinhardt and Bertschinger (1989), Liddle and Wands (1991)). In particular we see from (4.11) that ϵ must exceed $9/4\pi$ to ensure that the volume of physical space that still resides in the false vacuum decreases with time, but to prevent the overproduction of big bubbles, which would lead to large anisotropies in the CMBR, ϵ needs to be less than about 10^{-4} or so at the time when the bubbles were formed.

The solution, therefore, is to construct a model that satisfies both these conditions. In principle this can be achieved by modifying either the particle physics or the gravity sector., However, it still remains to be seen whether these requirements can emerge naturally from a fundamental theory of physics (for a review of some of these models see Kolb (1991) and refferences therein).

Amendola and Occhionero (1993) have run simulations to determine whether there is a preferred range of astrophysically interesting primordial bubbles that can explain the large scale structure in the Universe and concluded that the simplest EI models can be ruled out. In their simulations (following La (1991)) they approximate the number of bubbles that have radii larger than R in the present observable Universe, $N_B(R)$, by a power law

$$N_B(R) = \left(\frac{R}{R_M}\right)^{-p}, \quad p = 3 + 4(b - \frac{1}{2}), \quad R_m < R < R_M, \tag{4.12}$$

where R_M is the power law normalisation, b is the dimentionless coupling constant of the BD theory, and where

$$R_m = 23\zeta\Omega_0{}^{-1/2}h^{-2}Mpc$$

is an expression for the physical separation between bubbles at the present time (La (1991)). The limiting case $\zeta \rightarrow 0$ denotes collisionless CDM, while $\zeta \rightarrow 1$ denotes a photon-baryon plasma. They have found that for the primordial bubble model to fit the observed galaxy corelation function successfully the normalisation of the primordial bubble spectrum has to be such that

$$R_M/28h^{-1}Mpc = (p/10)^{-1.3}, \tag{4.13}$$

and concluded that, since we know the original EI model is ruled out, in order to retain a first-order phase transition that can result in a bubble-like structure, either the EI models have to be modified, or some mechanism to suppress very large bubbles has to be introduced.

As we mentioned before the original EI model achieved percolation by changing from Einstein gravity to BD gravity, thus making H a decreasing function of time. It has been noted, however, that percolation can also be achieved by making the tunnelling rate Γ increase with time, as in the case with two-field inflation (Adams and Freeze (1991)) in which one field tunnels from the false to the true ground state while the other slow-rolls along a suitable potential.

Recently (Occhionero and Amendola (1994)) such a mechanism for overcoming the graceful exit problem while not interfering with the CMBR constraints has been proposed in which the two-field inflation is implemented through "quadratic gravity" i.e. a theory in which the underlying gravity is not Einsteinian but also carries the quadratic corrections to the Ricci curvature in the Langrangian. Whereas in conventional EI models the size of bubbles is far below astrophysical interest, provided that the phase transition is completed *before* the end of inflation, as it does in this model, then the bubbly structure of the Universe can be reproduced for reasonable values of the spectral index p without interfering with

the CMBR constraints.

The CMBR constraints arise mainly from the Sachs-Wolfe effect because an empty bubble of radius L at decoupling distorts the microwave temperature by approximately $\Delta T/T \sim L^2/{L_d}^2$ where L_d is the horizon scale at decoupling. However this result must be corrected by a further factor of $L^2/{L_p}^2$, where $L_p > L$ is the scale corresponding to the size of a COBE pixel at decoupling, and by an extra factor ${z_{dec}}^{1/5} \approx 4$ to take into account the fact that as soon as the bubbles re-enter the horizon (assuming that they do so in the matter-dominated era) their radius will begin to grow faster than the universal expansion (Occhionero and Amendola (1994)). Through the Sachs-Wolfe effect the CMBR places constraints on both large and small bubbles. They thus determine a region of the parameters p and R_M which not only satisfies the CMBR constraints but also (4.13) which fits the galaxy corelation function. The results have been further improved in later work (Baccigalupi, Amendola and Occhionero (1996)) and it is found that, in order to achieve compatibility with the measured galaxy spectrum and with the CMBR constraints, the relevant parameter ranges for p and R_M are roughly

$$6 \leq p \leq 13, \quad 30h^{-1}Mpc \leq R_M \leq 130h^{-1}Mpc.$$

These results have been further explored (Amendola *et al* (1996)) with a detailed evaluation of the nucleation rate Γ of bubbles of true vacuum (following the method of Coleman (1977) and Callan and Coleman (1977) which we will discuss in the next chapter). Amendola and his coworkers have taken into account deviations from the thin wall limit and calculated explicitly the prefactor of the exponential (see (5.46) below), and have also taken into account gravitational effects ($G \neq 0$) which increase the nucleation rate Γ. The crucial quantity they evaluate is ϵ in (4.11). They conclude that, while passing the CMBR constraints,

their model can still give rise to sufficiently strong large scale structure. They are, thus, able to reconcile the inflationary two-field potential with observations.

This brief review of the latest advances in first order inflation models which can explain the formation of structure through bubble collisions shows that a variety of hypotheses can account for the large scale structure and yet satisfy the constrains imposed by the CMBR.

In our work we examine a different possibility, namely that the first order phase transition that leads to the formation of bubbles occurs *after* the phase transition responsible for inflation; possibly even associated with the phase transition responsible for electroweak symmetry breaking. To this end, following the work of Coleman, we shall derive, in the next chapter, the nucleation rate of bubbles of true vacuum and attempt to obtain the parameters of the Higgs field potential by demanding that the size, thickness and mass of the shells of matter produced by bubble wall collisions should match those that are observed. (Our derivation would have been more accurate had we used the improved nucleation rate as derived in Amendola *et al.* (1996), but almost all of our numerical calculations had been completed before we became aware of this paper. The implications of this new result for our work will be discussed briefly in the last chapter of this thesis.)

Finally, it should be noted that constraints from the CMBR apply to any theory that produces a bubble spectrum, irrespective of whether or not they result from the primordial phase transition, and consequently we shall need to consider whether our model can produce sufficient large scale structure through bubble wall collisions without overly distorting the CMBR.

Chapter 5

The Decay of the False Vacuum

In most inflationary models the early Universe starts in a false vacuum state– a state in which some scalar field is displaced from the true minimum of its potential. Then the decay of the false vacuum proceeds, perhaps via quantum tunnelling, and bubbles of the true vacuum are formed which expand into the surrounding regions of false vacuum. Though homogeneity would seem to require that the whole of the observable Universe is in just one such bubble, it is possible that subsequent phase changes at lower energy scales may have produced bubbles within the observable Universe which can account for the observed large-scale structure. In order to explore this possibility, in this chapter we shall calculate the rate of nucleation of such bubbles for various kinds of scalar potential and the shape of the wavefront corresponding to the bubble surface. Following the work of Coleman (1977, 1985) and Branderberger (1985), we shall first examine tunnelling effects in quantum mechanics and then convert our results into those of quantum field theory.

5.1 Tunnelling in Quantum Mechanics

The path integral formulation in Quantum Mechanics is based on the notion of a propagator or transition matrix element $M(x_f t_f; x_i t_i)$. The development of an

expression for M requires 'a summation over histories' corresponding to all the different ways of reaching (x_f, t_f) from (x_i, t_i) (see for example Ryder, 1985). If $\psi(x_i, t_i)$ is the wavefunction describing the state of a particle at time t_i then the corresponding wavefunction at a later time can be obtained from M by

$$\psi(x_f, t_f) = \int M(x_f t_f; x_i t_i)\psi(x_i, t_i)dx_i. \tag{5.1}$$

A critical property that will prove useful in our calculations is that if we divide the time interval (t_i, t_f) into two, with an intermediate time t, the propagator M must satisfy

$$M(x_f t_f; x_i t_i) = \int\int M(x_f t_f; xt).M(xt; x_i t_i)dx_i dx \tag{5.2}$$

In general the propagator M is given by

$$M(x_f t_f; x_i t_i) =< x_f|T(t_f, t_i)|x_i > \tag{5.3}$$

where $T(t_f, t_i)$ is the translation operator linking the states of a system at different times,

$$|\psi(t_f) >= T(t_f, t_i)|\psi(t_i) > . \tag{5.4}$$

Consider, for example, the theory of a particle moving in a one-dimensional potential $U(x)$ characterised by a local minimum at $x = 0$ (see fig. (5.1) and described by a Hamiltonian H given by

$$H(p, x) = \frac{p^2}{2m} + U(x). \tag{5.5}$$

The translation operator in this case is given by

$$T(t_f, t_i) = e^{-iH((t_f - t_i)/\hbar}$$

so that the propagator can be expressed as

$$M(x_f t_f; x_i t_i) < x_f|e^{-iH((t_f - t_i)/\hbar}|x_i > . \tag{5.6}$$

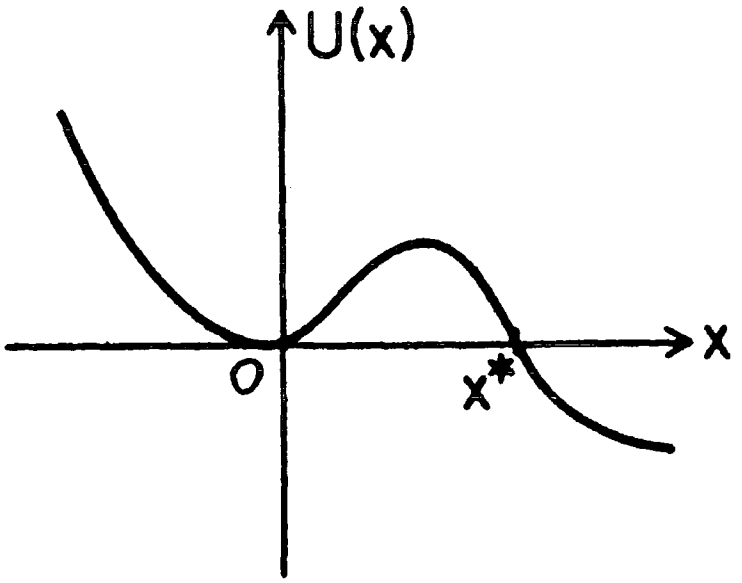

Figure 5.1: A typical one-dimensional potential showing the false ground state at $x = 0$ and the escape point x^*.

We are interested in the decay rate per unit time of the false vacuum, which is an unstable state. Since unstable states have complex energy, the probability that the system has remained in that state decreases exponentially with time and the decay rate is proportional to the imaginary part of the energy of the state. Thus, if a wave function $\Psi(t)$ has energy $E_0 = ReE_0 + iImE_0$ then its decay rate per unit time Γ is given by

$$\Gamma = -\frac{2}{\hbar} ImE_0. \tag{5.7}$$

The imaginary part of the energy of the state, is determined by the transition matrix element as we will now show.

In Euclidean space (in which we treat $i\delta t = T$ as real) we expand the matrix element (5.6) in terms of a set of energy eigenstates states $|n>$

$$< x_f|e^{-HT/\hbar}|x_i >= \sum_n e^{-E_nT/\hbar} < x_f|n >< n|x_i >$$

where $|x_i>$ and $|x_f>$ are position eigenstates and the states $|n>$ are a complete

set of energy eigenvalues of H with energies E_n, given by

$$H|n>=E_n|n> .$$

If $|\Omega>$ is the lowest energy state not orthogonal to $|x_i>$ or $|x_f>$ and has energy E_0, then

$$<x_f|e^{-HT/\hbar}|x_i> \stackrel{T\to\infty}{\longrightarrow} e^{-E_0T/\hbar} <x_f|\Omega><\Omega|x_i> . \tag{5.8}$$

Choosing the local minimum to be at $x=0$ and setting $|x_i>=|x_f>=0$ the energy of the false vacuum is then given by

$$E_0 = -\hbar \lim_{T\to\infty} \frac{1}{T} \ln <0|e^{-HT/\hbar}|0> . \tag{5.9}$$

Note that (5.8) is different from (5.6) in the sense that the former is evaluated in Euclidean space whereas the latter is the corresponding expression in Minkowski space. To obtain results in Minkowski space we will analytically continue those in Euclidean space by treating iT as real.

We want to express the matrix element in (5.6) as a path integral. To proceed we generalise the argument given in (5.2) and divide the time interval (t_i, t_f) into n segments $(t_i,t_1),(t_1,t_2),....(t_{n-1},t_f)$ each of length $\delta t = (t_f - t_i)/n$. We can then write

$$\begin{aligned} M = \int [dx] <x_f|e^{-iH(t_f-t_{n-1})/\hbar} \quad & |x_{n-1}> \quad <x_{n-1}|e^{-iH(t_{n-1}-t_{n-2})/\hbar}|x_{n-2}> \times \ldots \\ & \ldots \qquad \times <x_1|e^{-iH(t_1-t_i)/\hbar}|x_i> \end{aligned} \tag{5.10}$$

where we have used the closure relations

$$\int |dx_j><dx_j|dx_j = 1$$

and where

$$[dx] \equiv \prod_{i=1}^{n} dx_i$$

. For sufficiently small δt,

$$\begin{aligned} < x_{j+1}|e^{-iH(\delta t)/\hbar}|x_j > &= < x_{j+1}|1 - \frac{iH}{\hbar}\delta t + \mathcal{O}(\delta t^2)|x_i > \\ &\simeq \delta(x_{j+1} - x_j) - \frac{i}{\hbar}\delta t < x_{j+1}|H|x_j > . \end{aligned} \quad (5.11)$$

Using the Hamiltonian (5.5) in the second term on the RHS of (5.11) we have

$$\begin{aligned} < x_{j+1}|H|x_j > &= < x_{j+1}|\frac{p^2}{2m} + U(x)|x_j > \\ &\simeq < x_{j+1}|\frac{p^2}{2m}|x_j > + < x_{j+1}|U(x)|x_j > . \end{aligned}$$

Using the standard results

$$< x_{j+1}|x_j >= \delta(x_{j+1} - x_j) = \int \frac{dp}{2\pi\hbar} e^{ip(x_{j+1}-x_j)/\hbar}$$

$$< x_j|p >= \frac{1}{2\pi\hbar} e^{ipx_j/\hbar}$$

and the notation

$$\bar{x}_j \equiv \frac{x_{j+1} + x_j}{2}$$

we get:

$$< x_{j+1}|H|x_j >= \int \frac{dp}{2\pi\hbar} e^{ip(x_{j+1}-x_j)/\hbar} \left\{ \frac{p^2}{2m} + U(\bar{x}_j) \right\}.$$

Thus (5.11) becomes:

$$\begin{aligned} < x_{j+1}|e^{-iH(\delta t)/\hbar}|x_j > &\approx \int \frac{dp}{2\pi\hbar} e^{ip(x_{j+1}-x_j)/\hbar} \left\{ 1 - \frac{i\delta t}{\hbar} \left[\frac{p^2}{2m} + U(\bar{x}_j) \right] \right\} \\ &\approx \int \frac{dp}{2\pi\hbar} e^{ip(x_{j+1}-x_j)/\hbar} \exp\left\{ -\frac{i\delta t}{\hbar} H(p, \bar{x}_j) \right\}. \end{aligned} \quad (5.12)$$

Expression (5.12) gives the matrix element for a segment of one possible path. To account for the full propagator between t_i and t_f we substitute (5.12) into (5.10) and obtain

$$\begin{aligned} M \simeq \int \left(\frac{dp_1}{2\pi\hbar}\right) ..... \left(\frac{dp_n}{2\pi\hbar}\right) \int dx_1 ..... dx_{n-1} \\ \times \exp\left\{ \frac{i}{\hbar} \sum_{j=1}^{n} \left[p_j \left(x_j - x_{j-1} \right) - \delta t H(p, \bar{x}_j) \right] \right\} \end{aligned}$$

which in the $\delta t \to 0$ limit becomes

$$\begin{aligned} M &= \lim_{n\to\infty} \int (\frac{dp_1}{2\pi\hbar}) \cdots (\frac{dp_n}{2\pi\hbar}) \int dx_1 \cdots dx_{n-1} \\ &\times \exp\left\{ \frac{i}{\hbar} \sum_{j=1}^{n} \delta t \left[p_j \frac{(x_j - x_{j-1})}{\delta t} - H(p, \bar{x}_j) \right] \right\} \\ &\equiv \int \left[\frac{dpdx}{2\pi\hbar} \right] \exp\left\{ \frac{i}{\hbar} \int_{t_i}^{t_f} dt \, [p\dot{x} - H(p,x)] \right\}. \end{aligned} \tag{5.13}$$

When the Hamiltonian is of the form (5.5) the momentum space integral can be evaluated explicitly. Thus, for small δt we have

$$\int \frac{dp_i}{2\pi\hbar} \exp\left[\frac{-i}{2m\hbar} \delta t {p_j}^2 + i p_j (x_j - x_{j-1}) \right] = \left(\frac{m^2}{2\pi i\hbar\delta t} \right)^{1/2} \exp\left[\frac{im}{2\hbar\delta t} (x_j - x_{j-1})^2 \right]$$

where we have used the Gaussian integral

$$\begin{aligned} \int_{-\infty}^{+\infty} dp e^{-ap^2+bp} &= \int_{-\infty}^{+\infty} dp e^{-a(p+b/2a)^2 + b^2/4a} \\ &= \left(\frac{\pi}{a} \right)^{\frac{1}{2}} e^{b^2/4a}. \end{aligned}$$

Thus, (5.13) becomes

$$\begin{aligned} M &= \lim_{n\to\infty} \left(\frac{m}{2\pi i\hbar\delta t} \right)^{n/2} \int \prod_{j=1}^{n} dx_j \exp\left\{ \frac{i}{\hbar} \sum_{j=1}^{n} \delta t \left[\frac{m}{2} \left(\frac{x_j - x_{j-1}}{\delta t} \right)^2 - U(x) \right] \right\} \\ &= N \int [dx] \exp\left\{ \frac{i}{\hbar} \int_{t_i}^{t_f} dt \left[\frac{m}{2} \dot{x}^2 - U(x) \right] \right\} \end{aligned} \tag{5.14}$$

where the normalisation constant N is given by

$$N = \lim_{n\to\infty} \left(\frac{m}{2\pi i\hbar\delta t} \right)^{n/2} = \lim_{n\to\infty} \left(\frac{nm}{2\pi i\hbar(t_f - t_i)} \right)^{n/2}.$$

If we now take $t_i = -T/2$ and $t_f = +T/2$ and continue into Euclidean space by treating $i\delta t$ as real, we obtain

$$< x_f | e^{-HT/\hbar} | x_i > = N \int [dx] e^{-S_E(x)/\hbar} \tag{5.15}$$

with boundary conditions

$$x(-T/2) = x_i \tag{5.16}$$
$$x(+T/2) = x_f.$$

Here $S_E(x)$ is the Euclidean action along the path $x(t)$ given by

$$S_E(x) = \int_{-T/2}^{+T/2} dt \left\{ \frac{1}{2} m \left(\frac{dx}{dt} \right)^2 + U(x(t)) \right\}. \tag{5.17}$$

In the path integral approximation to quantum mechanics, in order to evaluate M we have to take into account an infinity of possible paths that the particle can take, a fact best shown in the first line of equation (5.14). However, according to the principle of least action the path that the particle actually takes is determined by the extrema of S_E which are given by the solutions to the Euler–Lagrange equations of motion. If we choose to simplify to a particle of unit mass this translates into solving

$$\ddot{\overline{x}} = U'(\overline{x}) \tag{5.18}$$

subject to the boundary conditions

$$x(-T/2) = x_i \tag{5.19}$$
$$x(+T/2) = x_f.$$

Consider a potential like that shown in fig.(5.1) and choose $x_i = x_f = 0$. The equation of motion (5.18) is equivalent to that for a particle moving in an inverted potential $-U(x)$ (see fig.(5.2)). The trivial solution in this case is clearly $\overline{x}(t) = 0$ for all t. However, for theories characterised by a potential with an unstable ground state there are non–trivial solutions of (5.18) corresponding to a particle which starts to roll down the slope of the potential at time $t = -\infty$ with zero initial kinetic energy, turning around at some time t_c at $x = x^*$ and

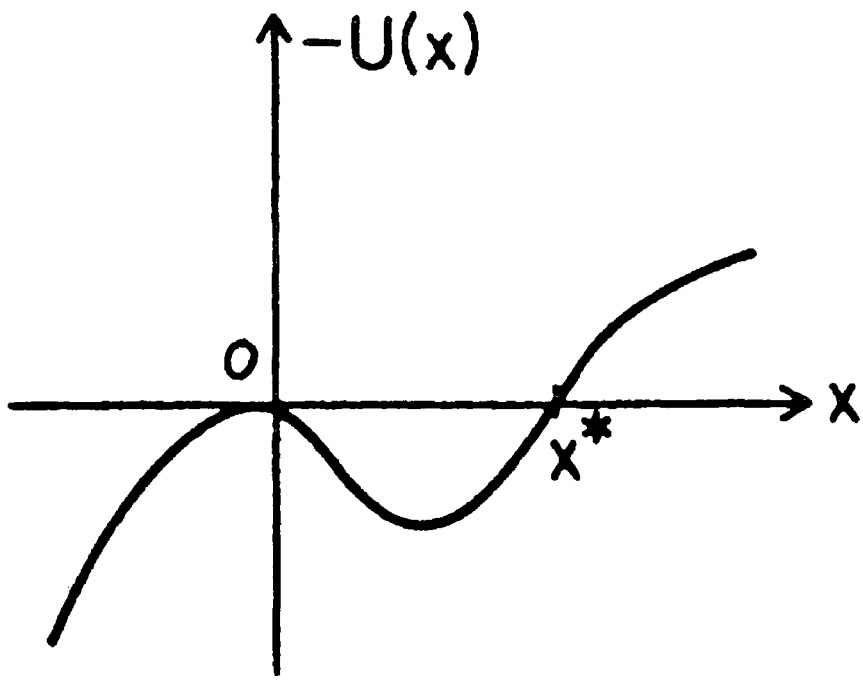

Figure 5.2: The inverted potential $-U(x)$.

returning to rest again at $x = 0$ at $t = +\infty$. The time t_c is called the center of the instanton. Coleman has termed this non–trivial solution 'the bounce solution'.

We shall first calculate the functional integral (5.15) in the case of a single instanton and later develop our result for an n–instanton configuration. The standard procedure is to perform a Gaussian approximation by expanding S_E about $\bar{x}$ and keeping only terms quadratic in the fluctuation $z \equiv x - \bar{x}$,

$$S_E(x) = \int_{-T/2}^{T/2} dt \left\{ \frac{1}{2} \left(\frac{d(z+\bar{x})}{dt} \right)^2 + U(\bar{x}) + U'(\bar{x})z + \frac{1}{2}U''(\bar{x})z^2 + \mathcal{O}(z^3) \right\}$$

with boundary conditions $z(\pm T/2) = 0$. Dropping terms of $\mathcal{O}(z^3)$ and integrating by parts the action becomes

$$\begin{aligned} S_E(x) &= \int_{-T/2}^{T/2} dt \left(\frac{1}{2}\dot{\bar{x}}^2 + U'(\bar{x}) \right) + \int_{-T/2}^{T/2} dt z \left(-\ddot{\bar{x}} + U'(\bar{x}) \right) \\ &+ \frac{1}{2} \int_{-T/2}^{T/2} dt z \left(-\frac{\partial^2}{\partial t^2} + U''(\bar{x}) \right) z \end{aligned}$$

$$= S_E(\bar{x}) + \frac{1}{2}\int_{-T/2}^{T/2} dtz\left(-\frac{\partial^2}{\partial t^2} + U''(\bar{x})\right)z. \tag{5.20}$$

With the approximation (5.20), (5.15) becomes a Gaussian integral and can be evaluated explicitly. We get

$$N\int [dx]e^{-S_E(x)/\hbar} = Ne^{-S_E(\bar{x})/\hbar}\int [dx]\exp\left\{-\frac{1}{2\hbar}\int dtz\left(-\partial_t{}^2 + U''(\bar{x})\right)z\right\}. \tag{5.21}$$

To proceed we introduce a diagonal matrix $\mathbf{A}$ such that

$$\mathbf{A} = \mathbf{diag}(\mathbf{a_1}\cdots\mathbf{a_n})$$

and a vector $\mathbf{x}$ defined by

$$\mathbf{x} = (\mathbf{x_1}\cdots\mathbf{x_n})$$

with inner product

$$(\mathbf{x}, \mathbf{Ax}) = \sum \mathbf{a_n}\mathbf{x_n}{}^{\mathbf{2}}. \tag{5.22}$$

Now since

$$\int_{-\infty}^{+\infty} dxe^{-ax^2/2\hbar} = \left(\frac{2\pi\hbar}{a}\right)^{1/2}$$

it follows that

$$\int dx_1\cdots dx_n \exp\left(-\frac{1}{2\hbar}\sum_{i=1}^{n} a_i{x_i}^2\right) = \frac{(2\pi\hbar)^{n/2}}{\prod_{i=1}^{n} a_i{}^{1/2}} \tag{5.23}$$

and (5.22) can be written as

$$\int d^n x \exp\left(-\frac{1}{2\hbar}(\mathbf{x}, \mathbf{Ax})\right) = (2\pi\hbar)^{n/2}\,(det\mathbf{A})^{-1/2}$$

or

$$\int [dx]\exp\left(-\frac{1}{2\hbar}(\mathbf{x}, \mathbf{Ax})\right) = (det\mathbf{A})^{-1/2} \tag{5.24}$$

where we have chosen the measure to be

$$[dx] \equiv d^n x(2\pi\hbar)^{-n/2}.$$

The above argument can be extended to the case of a single real variable $z(t)$ for which

$$(z,z) = \int dt[z(t)]^2.$$

In this case, with the aid of (5.24), the path integral (5.21) can be written as

$$N\int [dx]e^{-S_E(x)/\hbar} \simeq Ne^{-S_E(\bar{x})/\hbar}\left\{det(-\partial_t{}^2 + U''(\bar{x}))\right\}. \tag{5.25}$$

Thus the functional integral (5.15) can be fully determined provided that we can calculate the Euclidean action along $\bar{x}(t)$. This can be done easily by using conservation of energy and the expression for S given in (5.17). Along the path of the particle of unit mass we have

$$E = \frac{1}{2}\dot{x}^2 - U(x) = 0 \Rightarrow \frac{dx}{dt} = (2U(x))^{1/2}.$$

Thus,

$$\begin{aligned} S_E(\bar{x}) &= \lim_{T\to\infty}\int_{-T/2}^{T/2} dt\dot{\bar{x}}^2 \\ &= 2\int_0^{x^*} dx \frac{dt}{dx}\bigg|_{x=\bar{x}} \left(\frac{d\bar{x}}{dt}\right)^2 \\ &= 2\int_0^{x^*} (2U(x))^{1/2}dx \equiv B. \end{aligned} \tag{5.26}$$

Obviously the solution $\bar{x}$ is not unique since, by time–translation invariance, the center t_c of the instanton can be anywhere on the time axis. Furthermore combinations of instantons with widely separated centers provide equally good solutions and should be included as well. The functional integral (5.15) should thus be determined by taking into account all these contributions as well. In the dilute gas approximation we consider an approximate solution consisting of n instantons with widely separated centers $t_1 > t_2 \cdots > t_n$. Assuming that all the instantons are independent, we calculate the contribution of this configuration to

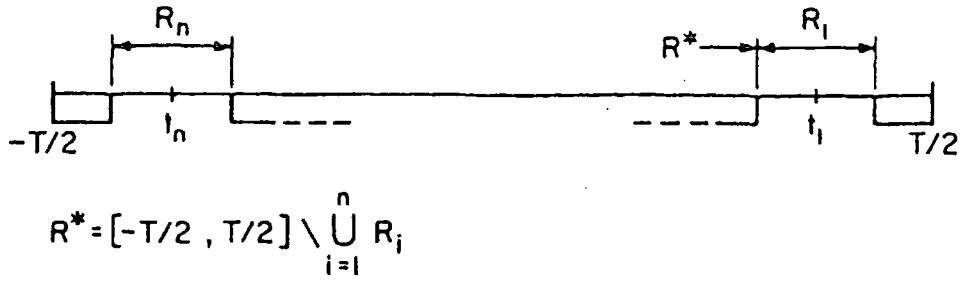

Figure 5.3: Division of the time interval for an n-instanton configuration.

(5.15) by summing over all possible instanton centers as well as over n. We denote our n–instanton configuration by $\bar{x}$, and the fluctuation about it by $z \equiv x - \bar{x}$. We then divide the interval $(-T/2, T/2)$ as in fig.(5.3) into non-overlapping regions R_i on which the single instantons are concentrated. The remaining part of the interval corresponding to the regions where $\bar{x} \approx 0$ is denoted by R^* (see fig.5.3). We also denote the fluctuation field on R_i by z_i and that on R^* by z^*. With this notation (5.15) becomes

$$\begin{aligned} N\int [dx] e^{-S_E(x)/\hbar} &= N\int [dz] e^{-S_E(\bar{x}+z)/\hbar} \\ &\simeq \left\{ \prod_{i=1}^{n} \int [dz_i] e^{-S_E(\bar{x}+z_i)/\hbar}\Big|_{R_i} \right\} N\int [dz^*] e^{-S_E(\bar{x}+z^*)/\hbar}\Big|_{R^*} \end{aligned} \tag{5.27}$$

We will evaluate the two terms on the RHS of (5.27) in turn. Since in the regions R^* we are considering fluctuations about $\bar{x} = 0$ we can approximate the integral by (5.25):

$$N\int [dz^*] e^{-S_E(\bar{x}+z^*)/\hbar}\Big|_{R^*} \simeq N\Big\{ det(-\partial_t{}^2 + \omega^2) \Big\}^{-1/2} \tag{5.28}$$

where we have denoted $U''(0)$ by ω^2, ω being the angular frequency of vibration of the particle at the bottom of the potential well at $x = 0$. The next step in the evaluation of the R^* contribution to the path integral is the evaluation of the determinant in (5.28). Since our final result will depend only on the ratio of determinants we write

$$N det^{-1/2}(D + \omega^2 I) \equiv N' det^{-1/2}(I + \omega^2 D^{-1}),$$

where $D \equiv -\partial_t{}^2$ acts on the space of functions with period T. Hence its eigenvalues are

$$\lambda_n = \left(\frac{\pi n}{T}\right)^{1/2}, \quad n \in Z_+.$$

Using the standard representation of $\sin \pi x$ as an infinite product,

$$\sin \pi x = \pi x \prod_{n=1}^{\infty} \left(1 - \frac{x^2}{n^2}\right)^2$$

and setting $x = i\omega T/\pi$ we can express the determinant as

$$\begin{aligned} det^{-1/2}(I + \omega^2 D^{-1}) &= \left(\frac{\sin i\omega T}{i\omega T}\right)^{-1/2} \\ &= (\omega T)^{1/2}(\sinh \omega T)^{-1/2} \\ &\simeq (2\omega T)^{1/2} e^{-\omega T/2}, \end{aligned}$$

for large T. Returning to (5.28), by adjusting the normalisation factor N we have

$$N \int [dz^*] e^{-S_E(\bar{x}+z^*)/\hbar}\Big|_{R^*} \simeq \left(\frac{\omega}{\pi\hbar}\right)^{1/2} e^{-\omega T/2}. \tag{5.29}$$

Also, if we define

$$\int [dz_i] e^{-S_E(\bar{x}+z_i)/\hbar}\Big|_{R_i} \equiv e^{-B/\hbar} K,$$

where B defined in (5.26) is the Euclidean action for a single instanton, then the first term on the RHS of (5.27) becomes

$$\left\{ \prod_{i=1}^{n} \int [dz_i] e^{-S_E(\bar{x}+z_i)/\hbar}\Big|_{R_i} \right\} \equiv e^{-nB/\hbar} K^n \tag{5.30}$$

where $B \equiv S_E(\bar{x})$ is the Euclidean action for a single instanton. Integration over all instanton centers gives a factor

$$\int_{-T/2}^{T/2} dt_1 \int_{-T/2}^{t_1} dt_2 \ldots \int_{-T/2}^{t_{n-1}} dt_n = \frac{T^n}{n!}. \tag{5.31}$$

Inserting (5.29), (5.30), (5.31) into (5.27) we obtain

$$\begin{aligned} N \int [dx] e^{-S_E(x)/\hbar} &\simeq \left(\frac{\omega}{\pi\hbar}\right)^{1/2} e^{-\omega T/2} \sum_{n=0}^{\infty} \frac{T^n}{n!} e^{-nB/\hbar} K^n \\ &\simeq \left(\frac{\omega}{\pi\hbar}\right)^{1/2} e^{-T(\omega/2 - Ke^{-B/\hbar})}. \end{aligned} \tag{5.32}$$

Thus, from (5.9)

$$E_0 = \frac{\hbar\omega}{2} - \hbar K e^{-B/\hbar},$$

and hence, from (5.7) the decay rate is given by

$$\Gamma = 2(ImK)e^{-B/\hbar}. \tag{5.33}$$

It is worth noting here that for the trivial solution $\bar{x}(t) = 0$ we would have $S = 0$, so there would be no K term and the result would correspond to a particle moving in a potential with a *stable* true ground state of energy $E_0 = \hbar\omega/2$ as expected.

We determine K introduced in (5.30) by demanding that we should get the correct answer for a one–instanton configuration, i.e.

$$\int [dx] e^{-S_E(x)/\hbar}\Big|_{one\ instanton} = K e^{-B/\hbar}\Big\{det(-\partial_t{}^2 + \omega^2)\Big\}^{-1/2}. \tag{5.34}$$

As we shall shortly show K is complex because the operator $-\partial_t{}^2 + U''(\bar{x})^2$ which arises in (5.20) has a negative eigenvalue for which the Gaussian approximation used in (5.21) is invalid because the curvature of S_E at $x = \bar{x}$ has the wrong sign. If $\bar{x}(t)$ is any solution to the classical Euclidean equation of motion obeying the boundary conditions then a general function obeying the boundary conditions can be written as

$$x(t) = \bar{x}(t) + \sum c_n x_n(t), \tag{5.35}$$

where the x_n are a complete set of orthonormal functions vanishing at the boundaries, i.e. such that

$$\int_{-T/2}^{T/2} dt x_n(t) x_m(t) = \delta_{mn} \tag{5.36}$$

and

$$x_n(\pm\frac{T}{2}) = 0,$$

the measure being

$$[dx] = \prod_n (2\pi\hbar)^{-1/2}\, dc_n.$$

We denote fluctuations about the single instanton by $z_i(t)$. These z_i are the eigenfunctions of the operator appearing in (5.25) with eigenvalues λ_i, i.e.

$$\left[-\partial_t{}^2 + U''(\bar{x})\right] z_i(t) = \lambda_i z_i(t), \quad i = 0, 1, 2, \ldots \tag{5.37}$$

In the case of the trivial solution $\bar{x}(t) = 0$ all eigenvalues of the second variational derivative of S_E are positive, making K real. Since S_E is independent of the instanton centre the fluctuation, $z_0(t)$, corresponding to a shift in the instanton centre by t, is an eigenfunction of (5.37) with zero eigenvalue. But z_0 has a node corresponding to the turning point of $\bar{x}$ and is not, therefore, the eigenfunction with lowest eigenvalue. So there must exist an eigenfunction $z_1(t)$ with a negative eigenvalue. Thus the bounce is not a minimum of the action but a saddle point and the Gaussian integral diverges. We must therefore treat z_0 and z_1 separately, but can use the Gaussian approximation for the remaining fluctuations.

For the z_0 mode we have:

$$x_0 = B^{-1/2}\frac{d\bar{x}}{dt}$$

where the normalisation comes from (5.36) and (5.26). Now since, from (5.35),

$$dx = \frac{d\bar{x}}{dt}dt = x_0 dc_0$$

we have

$$(2\pi\hbar)^{-1/2}dc_0 = \left(\frac{B}{2\pi\hbar}\right)^{1/2} dt.$$

So by integrating over all possible instanton centres we have already integrated in the z_0 direction, up to a normalisation factor. Thus, in evaluating the determinant, the zero eigenvalue should not be included as it corresponds to a stable ground state, but we should include instead a factor $(B/2\pi\hbar)^{1/2}$. To perform the rest of the integral we split $[dx]$ into the product of one–dimensional integrals

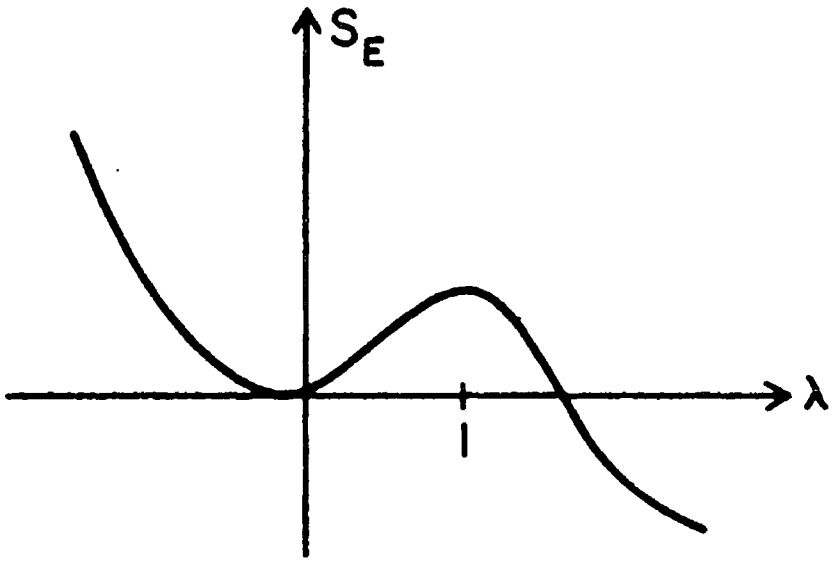

Figure 5.4: Euclidean action for the one-parameter family of paths.

over a specific one–parameter family of paths and an integral over the remaining paths. Denoting this parameter by λ, we choose the family x_λ to contain the trivial solution $x = 0$ for $\lambda = 0$ and the bounce solution $x = \bar{x}$ for $\lambda = 1$, and so that the negative mode has $\lambda > 1$. If $z_i(t)$ denotes the eigenfunctions of (5.37) with eigenvalues λ_i and with $\lambda_i > 1$ for $(i = 2, 3, \ldots)$ then the functional integral can be written as

$$\int [dx] = \int_{-\infty}^{+\infty} d\lambda \prod_{i=2}^{\infty} \int [dz_i] \, (2\pi\hbar)^{-1/2} \, .$$

Using the Gaussian approximation for the $[dz_i]$, the integral over $[dx]$ in (5.34) decouples into an infinite product of one–dimensional Gaussian integrals each contributing a factor ${\lambda_i}^{-1/2}$. Thus,

$$\int [dx] e^{-S_E(x)/\hbar} = \int_{-\infty}^{+\infty} d\lambda e^{-S_E(x_\lambda)/\hbar} \times \prod_{i=2}^{\infty} {\lambda_i}^{-1/2} (2\pi\hbar)^{-1/2}. \tag{5.38}$$

The action S_E as a function of λ is sketched in fig.(5.4). To keep the integral over λ finite we must distort the path for positive λ into the complex plane, as in fig.(5.5). Using the method of steepest descent

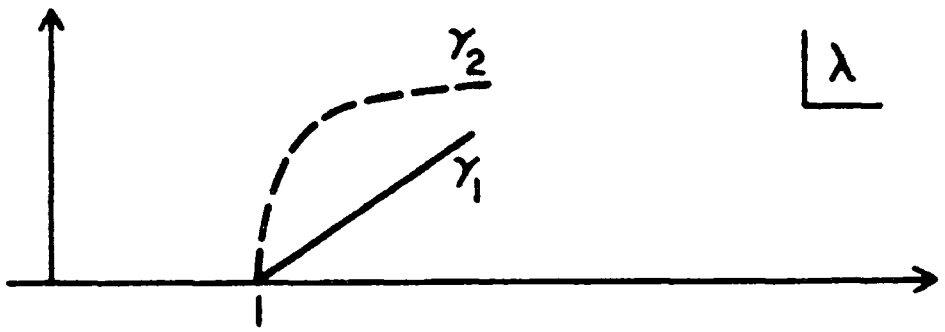

Figure 5.5: Distortion of the contour into the complex λ plane. γ_1 is the initial distorted contour whereas γ_2 is the contour for the steepest descent method.

$$\begin{aligned}\int_{-\infty}^{+\infty} d\lambda e^{-S_E(x_\lambda)/\hbar} &= \int_{-\infty}^{1} d\lambda e^{-S_E(x_\lambda)/\hbar} + \int_{\gamma_2} d\lambda e^{-\lambda_1 \frac{1}{2}(\lambda-1)^2/\hbar - B/\hbar} \\ &= R + \frac{1}{2} i e^{-B/\hbar} \prod_{i=1}^{\infty} |\lambda_i|^{-1/2} (2\pi\hbar)^{1/2}\end{aligned}$$

where R is real and γ_2 is the contour for the steepest descent method. Thus,

$$\begin{aligned}Im\left(\int [dx] e^{-S_E(x)/\hbar}\right) &= \frac{1}{2} e^{-B/\hbar} \prod_{i=1}^{\infty} |\lambda_i|^{-1/2} \\ &= \frac{1}{2} e^{-B/\hbar} \left\{ det'\left(-\partial_t{}^2 + U''(\bar{x})\right) \right\}^{-1/2}, \qquad (5.39)\end{aligned}$$

where det' indicates that in evaluating the determinant we omit any zero eigenvalues that correspond to translation modes and that we take the modulus of any negative eigenvalues.

Combining (5.34) and (5.39), and including the factor $(B/2\pi\hbar)^{1/2}$ from the integration over z_0, we obtain

$$ImK = \frac{1}{2} \left[\frac{det\left(-\partial_t{}^2 + \omega^2\right)}{det'\left(-\partial_t{}^2 + U''(\bar{x})\right)} \right]^{1/2} \left(\frac{B}{2\pi\hbar}\right)^{1/2}, \qquad (5.40)$$

and so, from (5.33) our final expression for the decay rate of a particle in a one-dimensional double well potential $U(x)$ is (Callan and Coleman (1977))

$$\Gamma = \frac{1}{2} \left[\frac{det\left(-\partial_t{}^2 + \omega^2\right)}{det'\left(-\partial_t{}^2 + U''(\bar{x})\right)} \right]^{1/2} e^{-B/\hbar} \left(\frac{B}{2\pi\hbar}\right)^{1/2}, \qquad (5.41)$$

where B is the Euclidean action defined in (5.26), $\omega^2 \equiv U''(0)$ and $\bar{x}$ is the solution of (5.18) with boundary conditions (5.19).

5.2 The Decay Rate in Quantum Field Theory

Converting the results obtained in the previous section for quantum mechanics into those applicable in quantum field theory is fairly straightforward. Consider, for example, a scalar field ϕ described by the Lagrangian density

$$\mathcal{L} = \frac{1}{2}\partial_\mu\phi\partial^\mu\phi - U(\phi), \tag{5.42}$$

where $U(\phi)$ is the potential energy density. Its decay rate is given by the analogue of (5.7) and (5.9), namely

$$\begin{aligned}\Gamma &= -2\lim_{T\to\infty}\frac{1}{T}\ln Im\left\{ < \phi_f|e^{-HT/\hbar}|\phi_i > \right\} \\ &= -2\lim_{T\to\infty}\left\{N\int[d\phi]\,e^{-S_E(\phi)/\hbar}\right\}\end{aligned} \tag{5.43}$$

with

$$\begin{aligned}\phi(-\frac{T}{2}) &= \phi_i \\ \phi(+\frac{T}{2}) &= \phi_f,\end{aligned}$$

ϕ_i and ϕ_f being the initial and final field configurations. The Euclidean action S_E is given by (c.f (5.17))

$$S_E(\phi) = \int d^4x\left[\frac{1}{2}\partial_\mu\phi\partial_\mu\phi + U(\phi)\right] \tag{5.44}$$

with boundary conditions

$$\begin{aligned}\lim_{\tau\to\pm\infty}\phi(\tau,\mathbf{x}) &= \phi_- \\ \lim_{|x|\to\infty}\phi(\tau,\mathbf{x}) &= \phi_-\end{aligned}$$

where τ is the Euclidean time, ϕ_- is the false minimum ground state and x is a point in Euclidean 3-space.

The first of these conditions ensures that the bounce solution goes from the false vacuum at $\tau = -\infty$ to false vacuum at $\tau = +\infty$ and corresponds to setting $|x_f >= |x_i >$ in our treatment of quantum mechanical tunnelling. The second condition ensures that the solution has finite action. The Euclidean action is again obtained by minimising the action and is given by (c.f (5.18))

$$\partial_\mu \phi \partial_\mu \phi = U'(\phi). \tag{5.45}$$

All possible solutions to (5.45) contribute to the tunnelling rate and, similar to our treatment of tunnelling in quantum mechanics, it is the solution with least action that makes the largest contribution to the tunnelling rate. The calculation of the tunnelling rate in quantum field theory follows along the same lines as that for quantum mechanics in the previous section except that the Euclidean action is now invariant in the four space–time directions and not just in time. Hence the factor $T^n/n!$ in (5.31) translates into $(TV)^n/n!$ and the decay rate is now given by (c.f. (5.33))

$$\Gamma = 2\,(ImK)\,e^{-B/\hbar}V.$$

Similarly we have now four factors of $(B/2\pi\hbar)^{1/2}$ instead of the one in (5.40). Generalising the argument given in (5.22)-(5.24) to the case of a scalar field $\phi(x)$, where x is a point in four-dimensional space-time, the decay rate of the ϕ-field from the false vacuum to the true vacuum state is given by (c.f. (5.41)

$$\frac{\Gamma}{V} = \frac{B^2}{4\pi^2\hbar^2} e^{-B/\hbar} \left[\frac{det\left(-\partial^2 + U''(\phi_+)\right)}{det'\left(-\partial^2 + U''(\bar{\phi})\right)} \right]^{1/2}, \tag{5.46}$$

where $B \equiv S_E$, $\bar{\phi}$ corresponds to non-trivial bounce solutions of the equation of motion, ϕ_+ is the true vacuum ground state and where the prime on *det*

indicates that the four zero eigenvalues corresponding to the freedom to translate the instanton centers in the four space-time directions are to be omitted.

In flat space the least action Euclidean solution has an $O(4)$ symmetry and its action S_E is lower than that for any non-$O(4)$-invariant solution (Coleman, Glaser, Martin, (1978)). When this is the case ϕ can be expressed in terms of a single variable ρ defined by

$$\rho \equiv (x_\mu x_\mu)^{1/2} = \left(|\mathbf{x}|^2 + \tau^2\right)^{1/2} \tag{5.47}$$

and the Euclidean action can be written as

$$S_E(\rho) = 2\pi^2 \int_0^\infty d\rho \rho^3 \left\{ \frac{1}{2} \left(\frac{d\phi}{d\rho} \right)^2 + U \right\} \tag{5.48}$$

with the equation of motion transformed into

$$\frac{d^2\phi}{d\rho^2} + \frac{3}{\rho} \frac{d\phi}{d\rho} - U'(\phi) = 0. \tag{5.49}$$

The boundary conditions for the $O(4)$ invariant solution are

$$\lim_{\rho \to \infty} \phi(\rho) = \phi_-. \tag{5.50}$$

If we now interpret ρ as a time variable and ϕ as the position of the particle, (5.49) is the equation of motion for a particle moving in the inverted potential $-U(\phi)$ subject to a time-dependent damping force. As we will now show, conservation of energy requires that there must be some value of $\phi = \phi^*$ for which the boundary conditions (5.50) are satisfied (see fig.(5.6)). Suppose that the particle starts from rest ($\rho = 0$) with zero initial kinetic energy from a position ϕ^* with $\phi_+ > \phi^* > \phi_-$. If ϕ^* is such that $\phi^* < \phi_1$ and $U(\phi_1) = U(\phi_-)$ the particle will never aquire enough energy to climb "up the hill" to ϕ_- and will undershoot; after some finite time ϕ will come to rest and reverse its direction. If, on the other hand, ϕ^* starts very close to ϕ_+ it will remain close to ϕ_+ for a long time during which the

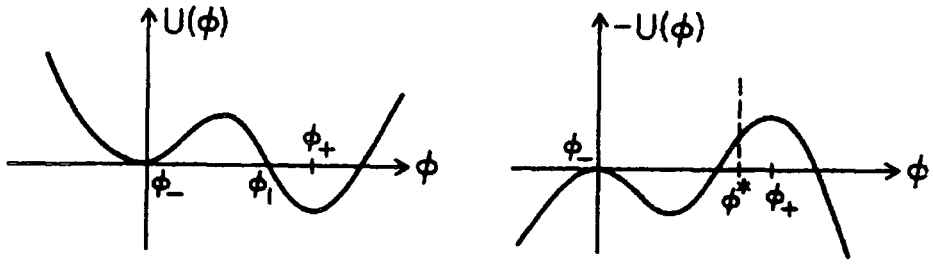

Figure 5.6: A typical potential $U(\phi)$ with an unstable false vacuum state ϕ_- and a true vacuum state ϕ_+. The graph on the right represents the inverted potential $-U(\phi)$, showing ϕ^* the initial value of ϕ.

damping will be negligible. When the particle finally rolls away from ϕ_+ it will speed up and reach ϕ_- with non-zero kinetic energy and so will overshoot. By continuity there must, therefore, be some value ϕ^* between ϕ_+ and ϕ_- for which the boundary conditions are satisfied.

In general a closed-form analytic solution to (5.49) cannot be found. However, in the 'thin wall' approximation where the difference in energy between the false and true vacua is small compared to the height of the barrier, it is possible to find an approximate solution for the Euclidean action. We start with a symmetric potential U_s (see figure (5.7)) with minima $\pm\alpha$, $+\alpha$ being the true minimum and $-\alpha$ being the false minimum, with

$$\begin{aligned} U_s(\phi) &= U_s(-\phi) \\ U_s'(\pm\alpha) &= 0 \\ \mu^2 &\equiv U_s''(\alpha) \end{aligned} \tag{5.51}$$

and we introduce a small energy difference between the two vacua given by

$$U_\alpha = U_s + \frac{\epsilon}{2\alpha}(\phi - \alpha)\,. \tag{5.52}$$

For $\epsilon \ll 1$ the nature of the instanton for U_a is qualitatively the same as that for U_s, since ϕ stays close to ϕ_+ for a long time after which it rolls down the valley

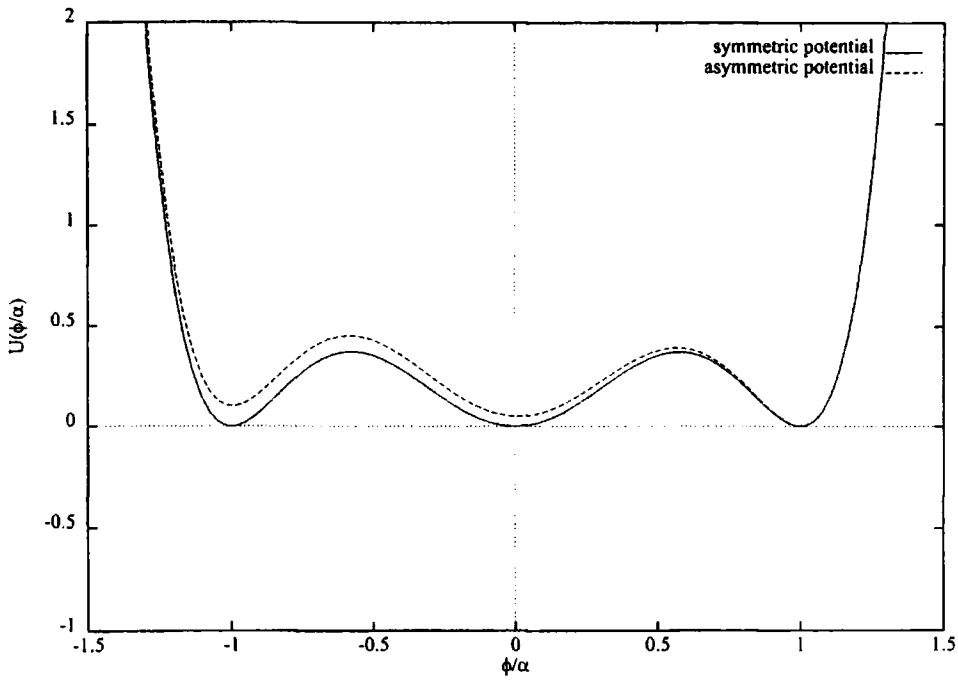

Figure 5.7: The symmetric potential U_s. Also shown an impression of the corresponding asymmetric potential where there is a small energy difference between the minima.

of the inverted potential, ending up at ϕ_- as $t \to \infty$. The friction term in (5.49) can, therefore, be neglected and we have

$$\frac{d^2\phi}{d\rho^2} = U_\alpha{}'(\phi) \simeq U_s{}'(\phi).$$

whose solution $\phi_1(\rho)$ is given by

$$\rho = \int_0^{\phi_1} \frac{d\phi}{[2U_s(\phi)]^{1/2}}$$
$$\frac{d\phi}{d\rho} = -\left(2U_s(\phi)\right)^{1/2}.$$

The corresponding action is given by

$$\begin{aligned} S_1 &= \int d\rho \left[\frac{1}{2}\left(\frac{d\phi}{d\rho}\right)^2 + U_s\right] \\ &= \int_{-\alpha}^{\alpha} d\phi \, [2U_s(\phi)]^{1/2}. \end{aligned} \tag{5.53}$$

Thus, the approximate solution is given by

$$\phi = \begin{cases} +\alpha & \rho \ll R \\ \phi_1(\rho - R) & \rho \simeq R \\ -\alpha & \rho \gg R. \end{cases} \tag{5.54}$$

Hence a spherical bubble of radius R is nucleated within which the field has transformed into the true vacuum state. Outside the bubble ($\rho \gg R$) the field is still in the false vacuum state and the two regions are separated by the bubble wall at $\rho \simeq R$ (see figure (5.8)). In this case the Euclidean action can be easily determined from (5.48), i.e.:

$$\begin{aligned} S_E &= 2\pi^2 \int_0^\infty d\rho \rho^3 \left[\frac{1}{2} \left(\frac{d\phi}{d\rho} \right)^2 + U \right] \\ &= -\frac{1}{2}\pi^2 R^4 \epsilon + 2\pi^2 R^3 S_1 \end{aligned} \tag{5.55}$$

where the first term comes from the interior of the bubble ($\rho \ll R$) and the second term from the bubble wall ($\rho \simeq R$), where the ϵ-dependent terms in U are negligible and thus $U_\alpha \approx U_s$. To determine the bubble radius we just minimise the action to obtain

$$R = \frac{3S_1}{\epsilon}.$$

Substituting back into (5.55) we get,

$$B \equiv S_E = \frac{27\pi^2 {S_1}^4}{2\epsilon^3}. \tag{5.56}$$

The above result is valid only for $\mu R \gg 1$, or equivalently

$$\frac{3S_1\mu}{\epsilon} \gg 1.$$

As $1/\mu$ defines the scale of the thickness of the bubble wall, the above expression is equivalent to saying that the size of the bubbles is large compared to their thickness, which is the thin-wall approximation that we used in the first place.

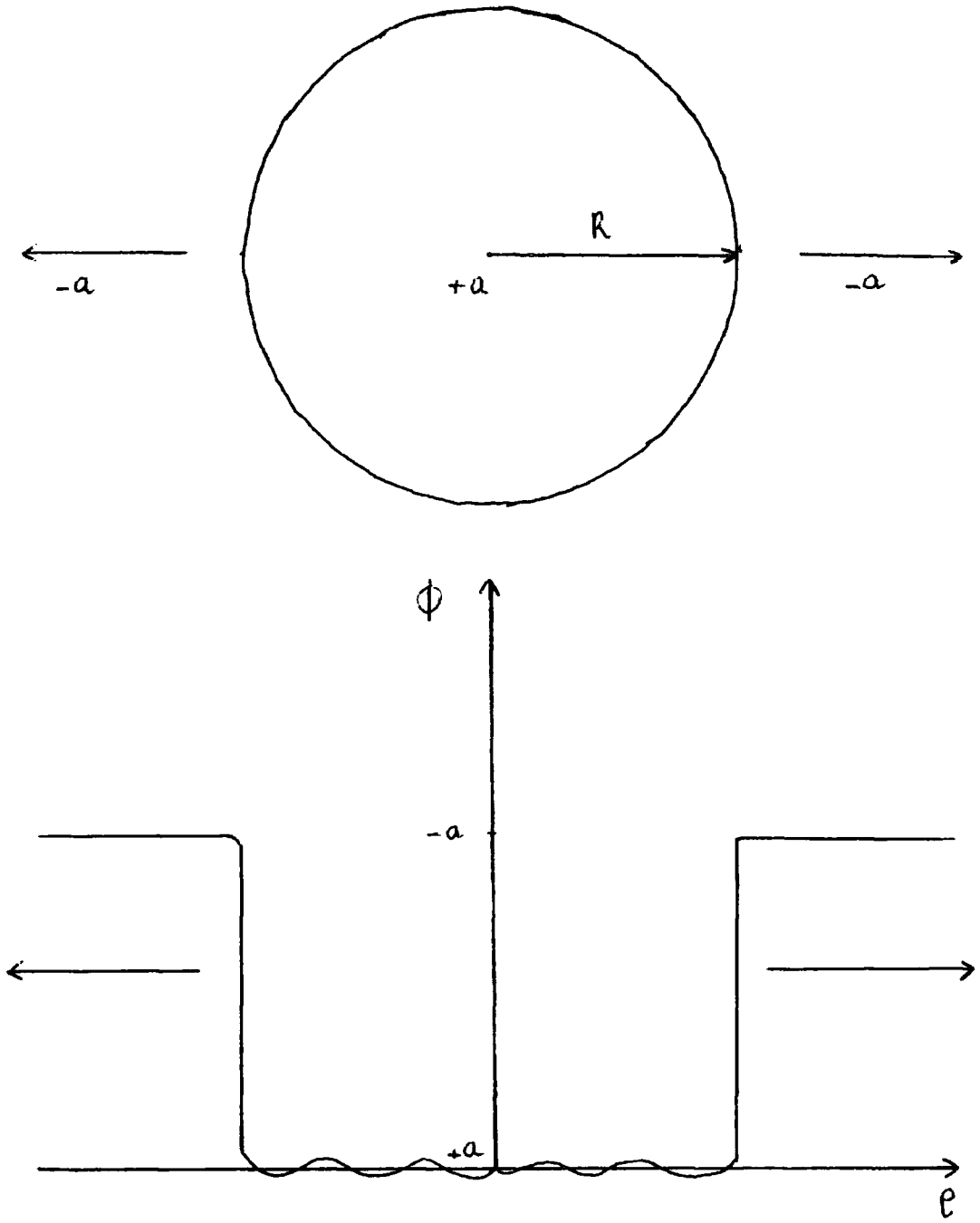

Figure 5.8: Qualitative picture of a bubble of true vacuum. Inside the bubble a region of true vacuum ($\phi = +\alpha$) is formed separated from the false vacuum ($\phi = -\alpha$) outside by the bubble wall at $\rho \approx R$. As the bubble expands (indicated by the arrows) false vacuum is being transformed into true vacuum.

5.3 Bubble Nucleation

So far we have obtained an expression for the tunnelling rate from the false to the true vacuum. In this section we are interested in the subsequent evolution of the ϕ field after tunnelling which can be studied in semiclassical terms.

In the quantum mechanical description of the decay of the false vacuum the particle makes a quantum jump at some time $t = 0$ from the false vacuum minimum of its potential at $x = 0$ to the escape point $x = x_e$ characterised by $U(x_e) = U(0)$, emerging with zero kinetic energy. Then for $t > 0$ the particle propagates classically. Similarly in quantum field theory, the field makes a quantum jump (say at time $t = 0$) to a state of zero kinetic energy and potential energy equal to that of the false vacuum. This state is the centre of the instanton $\bar{\phi}$ given by

$$\begin{aligned} \phi(x_0 = 0, \mathbf{x}) &= \bar{\phi}(\mathbf{x}, \tau = 0) \\ \frac{\partial}{\partial t}\phi(x_0 = 0, \mathbf{x}) &= \frac{\partial}{\partial \tau}\bar{\phi}(\mathbf{x}, \tau = 0) = 0. \end{aligned} \tag{5.57}$$

For $t > 0$ the field will evolve according to the classical equation of motion, which in Minkowski space is given by

$$\partial_\mu \partial^\mu \phi = -U'(\phi).$$

In Euclidean space this translates into

$$\partial_\mu \partial_\mu \phi = U'(\phi), \tag{5.58}$$

which is identical to (5.45). In terms of the variable ρ

$$\rho^2 \equiv \tau^2 + x^2 = x^2 - t^2$$

this becomes

$$\frac{d^2\phi}{d\rho^2} + \frac{3}{\rho}\frac{d\phi}{d\rho} = U'(\phi) \tag{5.59}$$

which is exactly the same as (5.49). Since the initial conditions are also the same, the classical field in Euclidean space is simply the instanton solution

$$\phi(\mathbf{x},\tau) = \bar{\phi}\left[\left(x^2+\tau^2\right)\right], \quad x^2+\tau^2 > 0.$$

If we analytically continue this solution back to Minkowski space

$$\phi(\mathbf{x},t) = \bar{\phi}\left[\left(x^2-t^2\right)\right], \quad |x| > t > 0.$$

It is worth noting here that the instanton appears not only as the dominant contribution to the path integral calculation of the tunnelling action, but it reappears as the classical field in Euclidean space after tunnelling. In other words, it gives the shape of the bubble at the moment of its materialisation in Euclidean space as well. To obtain the equation of motion for $|x| < t$ we set $\rho \to i\rho$ and (5.59) becomes

$$\frac{d^2\phi}{d\rho^2} + \frac{3}{\rho}\frac{d\phi}{d\rho} = -U'(\phi). \tag{5.60}$$

A qualitative picture of the solution in the $|x| > t$ regime is that the ϕ-field starts at $|x| = t$ with initial value ϕ^* and as $|x|$ increases it gradually approaches the false vacuum. On the other hand, for $|x| < t$ (5.60) represents the equation of motion for a particle moving in a potential $U(x)$ subject to a time-dependent damping force. Again the ϕ-field starts from rest at $\phi = \phi^*$, but this time it rolls down the hill towards the true minimum of the potential, ϕ_+. Once there, it will oscillate about ϕ_+ with the amplitude of the oscillations decreasing as energy is lost due to the damping term. To summarise then, we have (see fig. (5.9))

$$\phi(t,\mathbf{x}) = \begin{cases} \phi_- & |\mathbf{x}| \to \infty \quad \text{false vacuum} \\ \phi^* & |\mathbf{x}| = t \quad \text{bubble wall} \\ \phi_+ & |\mathbf{x}| = 0 \quad \text{true vacuum (only for } t \to \infty). \end{cases} \tag{5.61}$$

Suppose that at $t = 0$ a point on the bubble wall is given by $|\mathbf{x}| = {r_0}^2$. Then at time t it would be at

$$|\mathbf{x}| = \left(t^2 + {r_0}^2\right)^{1/2}$$

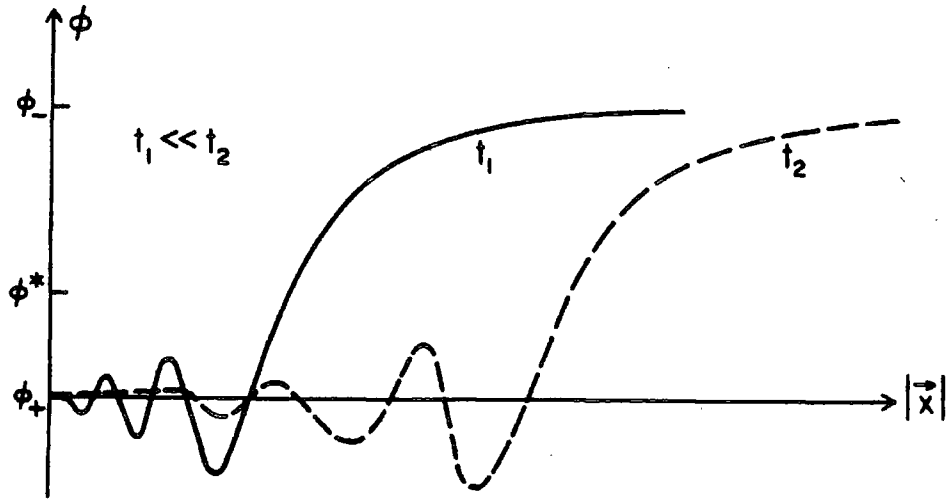

Figure 5.9: Qualitative picture of the solution (5.61). Also shown, an impression bubble growth between t_1 and t_2. The bubble profile separates the true vacuum phase on the left of each line from the false vacuum on the right. As the bubble expands the region of true vacuum increases.

and so the wall velocity is

$$v = \frac{d|\mathbf{x}|}{dt} = \frac{t}{(t^2 + r_0{}^2)^{1/2}} \simeq 1$$

since we expect r_0 to be a microphysical quantity. So, once formed, bubbles of true vacuum expand into the surrounding sea of false vacuum with a speed that approaches the speed of light ($c = 1$). In the next chapter we shall examine the large-scale structures that would result from the collision of such bubbles.

Chapter 6

Production of Structure from Bubble Collisions

If we suppose that a phase transition occurs which proceeds by the quantum tunnelling of some scalar field ϕ from a false vacuum state to its true vacuum state, the observed distribution of matter in the Universe may be the result of the collision of the true vacuum bubbles as they expand into the surrounding sea of false vacuum.

For tunnelling to occur the potential energy of the ϕ-field $U(\phi)$ must be of the double well form considered in the previous chapter with a potential barrier separating the two minima. To be consistent with our previous discussion we choose the false vacuum state to be at $\phi = 0$, and the true vacuum state to be at $\phi = \sigma$. The potential barrier separating the two ground states is the region where $U(\phi) > U(0)$. We also choose the scale of the potential such that $U(\sigma) = 0$ (see, for example, figures (6.1), (6.3)). Clearly there are many possible choices for the form of the potential, each of which will be described by various parameters. However, because so far there is no accepted theory that would explain and determine these parameters satisfactorily, we will work backwards and try to fix them by insisting that the structures formed by bubble wall collisions match those we observe.

Observation suggests that the structures in the Universe are bubble–like, consisting of voids surrounded by shells in which all the mass is concentrated. This suggests that we should attempt to fit three observations; the size of the voids, the thickness of the shells that surround them and the mass of the shells. We thus study potentials that can be described by three parameters and determine whether these potentials can result in structures that are compatible with observation. Our aim is therefore to choose suitable potentials, derive expressions for the size, mass and thickness of a typical shell and vary the parameters of the potentials to obtain results in agreement with the observed values. In what follows we will see that re–parametrisation of dimensionful quantities into dimensionless ones greatly reduces the amount of numerical calculation needed without any loss of generality so this approach will be used frequently.

We will first parametrise two similar forms of potential which can give rise to phase transitions, namely a polynomial potential and a modified Coleman-Weinberg potential, and then we will obtain a parametrisation of the decay rate for the ϕ field into matter.

6.1 Scalar Field Potentials

a) The Polynomial Potential

A suitable choice of a polynomial potential, shown in fig.(6.1), is

$$U_P(\phi) = \frac{A}{\sigma^2}\left(\phi^2 + \beta\sigma^2\right)\left(\phi^2 - \sigma^2\right)^2 \tag{6.1}$$

where ϕ and σ have dimensions of mass, A is the dimensionless coupling and β is a constant that determines the shape of the potential. Since for $\beta \geq 1/2$ the potential barrier between the two minima at $\phi = 0$ and $\phi = \sigma$ disappears, while for $\beta < 0$ the extrema at $\phi = 0$ and $\phi = \sigma$ become maxima, we restrict β to

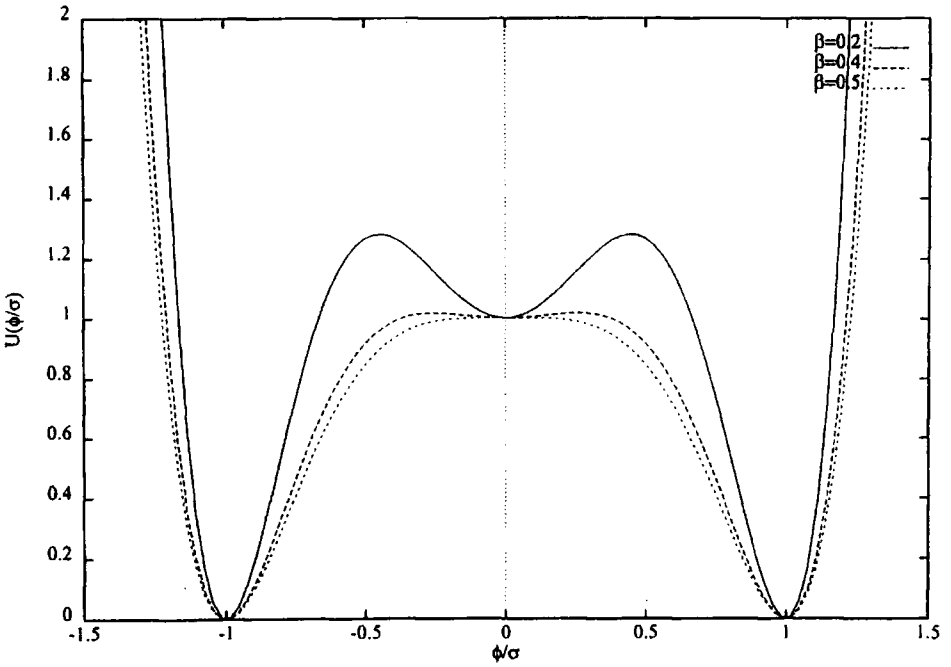

Figure 6.1: The polynomial potential for $\beta = 0.2, 0.4$ and 0.5.

lie between 0 and 1/2. We parametrise the potential in terms of a dimensionless quantity $\tilde{\phi}$, defined by

$$\tilde{\phi} \equiv \frac{\phi}{\sigma} \tag{6.2}$$

With this choice of parametrisation the polynomial potential can be re–written as

$$U_P(\tilde{\phi}) \equiv \tilde{A}\sigma^4 \tilde{U}_P(\tilde{\phi}) \tag{6.3}$$

where the scaled potential is

$$\tilde{U}_P(\tilde{\phi}) = \frac{1}{\beta}(\tilde{\phi}^2 + \beta)(\tilde{\phi}^2 - 1)^2 \tag{6.4}$$

and where $\tilde{A} \equiv A\beta$. With this notation the energy difference between the two ground states is given by

$$\epsilon = U_P(0) - U_P(\sigma) = \tilde{A}\sigma^4. \tag{6.5}$$

In fig.(6.1) the shape of the potential is shown for $\beta = 0.2, 0.4$ and 0.5.

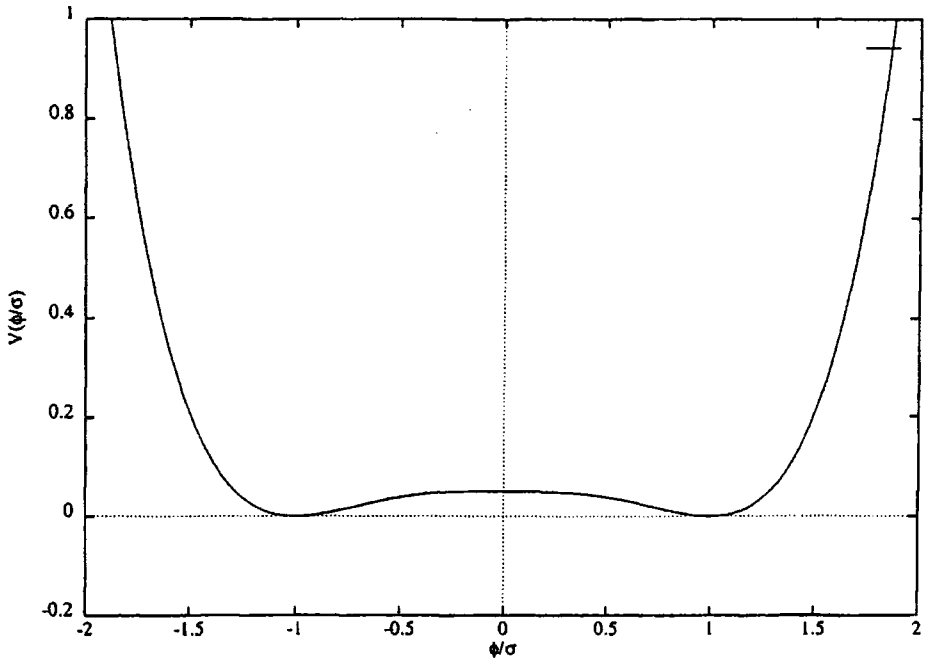

Figure 6.2: The Coleman-Weinberg potential.

b) The Modified Coleman-Weinberg Potential

The Coleman-Weinberg potential is obtained from the standard Higgs potential

$$U(\phi) = -\mu^2\phi^2 + \lambda\phi^4,$$

by setting the Higgs mass parameter μ to zero but including the one-loop vector boson radiative corrections. Thus, the original Coleman-Weinberg potential (see fig.(6.2)) is given by

$$U_{CW} = A\phi^4\left\{ \ln\left(\phi^2/\sigma^2\right) - \frac{1}{2}\right\} + \frac{1}{2}A\sigma^4. \tag{6.6}$$

The true minimum of the potential is again at $\phi = \sigma$ and A is dimensionless. In the SU(5) GUT $A = (5625/64){\alpha_{GUT}}^2$ where α_{GUT} is the GUT coupling constant. For $\alpha_{GUT} \approx 1/30$, we have $A \approx 10^{-1}$. We want to modify the Coleman-Weinberg potential to incorporate a barrier near $\phi = 0$. This is achieved by adding a term proportional to $\phi^2 \ln \phi^2$. Extra terms are then added to ensure that the true

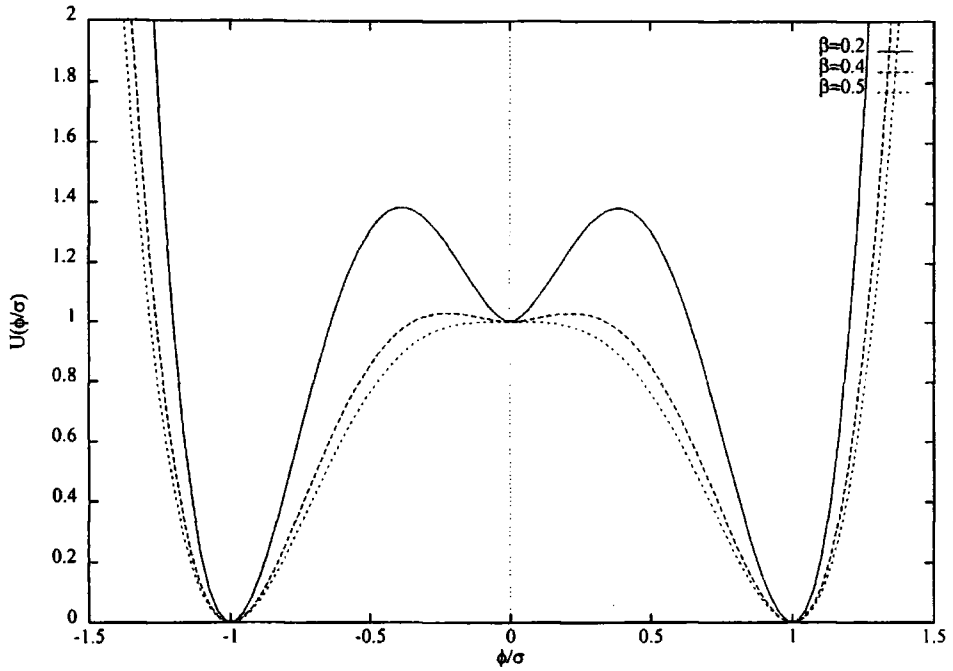

Figure 6.3: The modified Coleman-Weinberg potential for $\beta = 0.2, 0.4$, and 0.5.

minimum remains at $\phi = \sigma$ while $U_{CW}(\sigma) = 0$. The result, which we refer to as the modified Coleman-Weinberg potential, is given by

$$U_{CW} = A\left(\phi^4 - C\sigma^2\phi^2\right)\left\{\ln \phi^2/\sigma^2 - \frac{1}{2}\right\} + \frac{1}{2}A\sigma^4 + \frac{1}{2}AC\sigma^2\phi^2 - AC\phi^4, \quad (6.7)$$

where C is dimensionless. At $\phi = 0$,

$$U_{CW}(0) = A\sigma^4(\frac{1}{2} - C),$$

which can be written in the same compact notation as we used for the polynomial potential provided that we write $\tilde{A} = (1/2 - C)A \equiv \beta A$, so that

$$U_{CW}(0) = \tilde{A}\sigma^4.$$

If we now substitute for C in (6.7) and scale $\tilde{\phi}$ as in (6.2) we get

$$\begin{aligned} U_{CW}(\tilde{\phi}) &= \tilde{A}\sigma^4\tilde{U}_{CW} \\ \tilde{U}_{CW}(\tilde{\phi}) &= \frac{1}{\beta}\left[\beta + \tilde{\phi}^2(\frac{1}{2} - \beta) + \tilde{\phi}^2 \ln \tilde{\phi}^2\left\{\tilde{\phi}^2 - (\frac{1}{2} - \beta)\right\} - \frac{1}{2}\tilde{\phi}^4\right]. \end{aligned} \quad (6.8)$$

Here β has a similar significance to that which it has in the polynomial potential and for the same reasons it must lie within 0 and 1/2. In fact the shape of $\tilde{U}_{CW}$ for a given β is similar to that of $\tilde{U}_P$ with the same value (see fig.(6.3)).

We will next discuss the parametrisation of the decay rate of the ϕ-field to matter.

6.2 Coupling of ϕ to Matter

The amount of matter produced in bubble wall collisions is determined by Γ, the decay of the ϕ-field to matter. We will parametrise Γ in terms of the Standard Model Higgs decay rate.

If for simplicity we assume that the Higgs particle is heavy ($m_H > 2m_W$) so that the decays $H \longrightarrow W^+W^-$ and $H \longrightarrow Z^0Z^0$ are dominant then in the Standard Model (see, for example, Collins, Martin and Squires (1989))

$$\Gamma = \frac{3G_F}{16\pi\sqrt{2}} {m_H}^3, \tag{6.9}$$

where the Higgs mass m_H is determined in terms of the quartic Higgs self-coupling λ and the vacuum expectation value v,

$$m_H = \sqrt{2\lambda}v, \tag{6.10}$$

and where G_F is the Fermi weak coupling constant given by

$$G_F = \frac{1}{\sqrt{2}v^2}.$$

For the potentials under consideration the Higgs mass is determined by the condition

$${m_H}^2 = \frac{1}{2}\frac{d^2U(\phi)}{d\phi^2}\bigg|_{\phi=\sigma}. \tag{6.11}$$

In the case of the polynomial potential this reduces to

$$m_H = 2A^{1/2}(1+\beta)^{1/2}\sigma \tag{6.12}$$

whereas for the modified Coleman-Weinberg potential

$$m_H = A^{1/2}(3+2\beta)^{1/2}\sigma, \tag{6.13}$$

giving

$$\Gamma_P = \frac{3}{4\pi}A^{3/2}(1+\beta)^{3/2}\sigma \tag{6.14}$$

$$\Gamma_{CW} = \frac{3}{32\pi}A^{3/2}(3+2\beta)^{3/2}\sigma \tag{6.15}$$

respectively.

In the more general case where the coupling of the ϕ-field to matter is not that of the Standard Model but is instead some arbitrary coupling G, the decay rate is obtained by combining (6.9) and either (6.12) or (6.13) resulting in

$$\Gamma_P = \frac{3G}{2\pi\sqrt{2}}A^{3/2}(1+\beta)^{3/2}\sigma^3 \tag{6.16}$$

and

$$\Gamma_{CW} = \frac{3G}{16\pi\sqrt{2}}A^{3/2}(3+2\beta)^{3/2}\sigma^3. \tag{6.17}$$

As with the parametrisation of the potentials of the previous section, we want to work in terms of a dimensionless quantity $\tilde{G}$ and since $G \approx 1/\sigma^2$ we set

$$\tilde{G} = \sqrt{2}\sigma^2 G.$$

With this choice of parametrisation (6.16) and (6.17) yield

$$\Gamma_P = \frac{3}{4\pi}\tilde{G}A^{3/2}(1+\beta)^{3/2}\sigma, \tag{6.18}$$

$$\Gamma_{CW} = \frac{3}{32\pi}\tilde{G}A^{3/2}(3+2\beta)^{3/2}\sigma. \tag{6.19}$$

In the Standard Model $\tilde{G} = 1$.

If, on the other hand, the Higgs particle is light so that it decays primarily into fermions then (Collins, Martin and Squires (1989))

$$\Gamma(H \to f\bar{f}) = N_c \frac{G_F m_f m_H}{4\pi\sqrt{2}} \left(1 - \frac{4{m_f}^2}{{m_H}^2}\right)^{3/2},$$

where the colour factor N_c equals 3 for quarks and 1 for leptons, m_H is defined in (6.11) and m_f is the mass of the fermion species f. However, it seems likely that the Higgs particle is heavy ($m_H > 2m_W$) so that it decays primarily into bosons and hence its decay width is given by (6.9), and we will not consider further the possibility that it decays into fermions.

The only dimensionful quantity in our parametrisation of $U(\phi)$ and Γ is σ, the position of the global minimum, which sets the energy scale of the theory. If ϕ is to be identified by the scalar field responsible for SSB in the Weinberg-Salam model we will have $\sigma < 1TeV$ but otherwise we would expect $\sigma \gg 1TeV$. Apart from σ there are two other parameters that describe our trial potentials, namely A and β, both of which are dimensionless. A plays the role of a coupling constant and, as we saw in section (6.1) we might expect $A \approx 10^{-1}$ by analogy with the Coleman-Weinberg $SU(5)$ GUT. However, there are no essential restrictions on A from the form of the potential, though we are only able to use a perturbative approach if $A \ll 1$. The precise shape of the potential and in particular the height of the barrier is determined by β and we have seen that $0 < \beta < 1/2$. Once σ and β have been specified, the size of the energy difference between the false and true vacua is given by A. Finally, to determine the decay of the ϕ-field to matter we have introduced an extra parameter $\tilde{G}$ that takes into account the possibility that the coupling of ϕ to matter is not that of the Standard Model (which has $\tilde{G} = 1$).

6.3 Bounce Solution

In the last chapter we derived the decay rate of the ϕ-field from the false to the true vacuum state (c.f. (5.46))

$$\frac{\Gamma}{V} = \frac{B^2}{4\pi^2\hbar^2} e^{-B/\hbar} \left[\frac{det\left(-\partial^2 + U''(\phi_+)\right)}{det'\left(-\partial^2 + U''(\bar{\phi})\right)} \right]^{1/2}, \tag{6.20}$$

where $B \equiv S_E$ the tunnelling action , $\bar{\phi}$ corresponds to non-trivial solutions of the equation of motion and where the prime indicates that the 4 zero eigenvalues corresponding to the freedom to translate the instanton centers in the four space-time directions are to be omitted. To calculate the decay rate of the ϕ-field we must therefore be able to determine the following:

1. The bounce solution, $\overline{\phi}$
2. the tunnelling action between the two vacua
3. the ratio of the functional determinants

We will next examine ways of evaluating each of the above in turn.

As we have seen in the last chapter the bounce solution is the solution to the Euclidean equation of motion that is obtained by minimising the Euclidean action. In the notation introduced earlier (cf. (5.47)) ($\rho \equiv (|x|^2 + \tau^2)^{1/2} = (|x|^2 - t^2)^{1/2} > 0$) the bounce equation is given by

$$\frac{d^2\phi}{d\rho^2} + \frac{3}{\rho}\frac{d\phi}{d\rho} - U'(\phi) = 0 \tag{6.21}$$

with boundary conditions

$$\phi'(0) = 0 \tag{6.22}$$

$$\phi(\infty) = 0. \tag{6.23}$$

In the absence of the time-dependent damping term it reduces to

$$\frac{d^2\phi}{d\rho^2} = U'(\phi) \tag{6.24}$$

corresponding to the equation of motion of a particle moving in an inverted potential $-U'(\phi)$. To satisfy the boundary conditions the particle must start from rest at a point $\phi(0)$ such that it will end up at $\phi = 0$ as $\rho \to \infty$. In the absence of the damping term the energy of the system is conserved and so the particle must start at $\phi = \phi_e$ where $U(\phi_e) = U(0)$. Conservation of energy implies

$$\frac{1}{2}\left(\frac{d\phi}{d\rho}\right)^2 = U(\phi) - U(\phi_e).$$

Separating the variables and integrating we obtain

$$\rho(\phi) = \int_{\phi_e}^{\phi} \frac{d\phi}{\left[2\left(U(\phi) - U(\phi_e)\right)\right]^{1/2}}$$

which can be inverted to obtain $\phi(\rho)$.

In the presence of the damping term, however, it is no longer possible to find an analytic solution to the equation of motion, but, as we have seen in the last chapter, there must always exist a solution that satisfies the boundary conditions. The reason is that for different starting points $\phi(0)$, the particle will either have too little energy to climb the hill and reach $\phi = 0$ or, too much energy in which case it will reach $\phi(0)$ with non-zero kinetic energy and hence overshoot. Thus, by continuity, there is always a solution to the bounce equation satisfying the boundary conditions and such that

$$\phi_e < \phi(0) < \sigma.$$

Such a solution can only be found numerically. By trial (and mostly by error!) we choose possible values of $\phi(0)$ and for each we integrate our bounce equation

subject to the initial condition that the particle starts from rest. Depending on how close to σ we have chosen our starting value the particle will either overshoot or undershoot but somewhere in between we will find the correct value of $\phi(0)$ that ensures that $\phi(\infty) = 0$, and the corresponding solution $\phi(\rho)$.

There are two problems associated with the numerical solution of the bounce equation. Firstly, as we will have to start our integration at $\rho = 0$, we see that the damping term in (6.21) becomes undefined. This is dealt with by using L'Hôpital's rule which reduces the damping term to

$$\lim_{\rho \to 0} \frac{3}{\rho} \frac{d\phi}{d\rho} = 3 \frac{d^2\phi}{d\rho^2}.$$

Hence we start at $\rho = 0$ by integrating

$$\frac{d^2\phi}{d\rho^2} = \frac{1}{4} U'(\phi),$$

instead of the full bounce equation, for small values of ρ and then switch back to (6.21) once ρ is sufficiently large.

Secondly, for some values of the parameters of the potential the required value of $\tilde{\phi}(0)$ lies very close to 1 making an accurate computation of $\tilde{\phi}(\rho)$ difficult. This is dealt with by a change of variables to $z \equiv 1 - \tilde{\phi}$, and integrating z from its initial small value to some larger value (say 10^{-2}), then continuing the integration in terms of ϕ. As we have seen in chapter 5, the solution of the bounce equation gives the shape of the bubble wavefront for $|x| > t$. To obtain the equation of motion for $|x| < t$ we set $\rho \to i\rho$ and the bounce equation then becomes

$$\frac{d^2\phi}{d\rho^2} + \frac{3}{\rho} \frac{d\phi}{d\rho} = -U'(\phi) \tag{6.25}$$

with boundary conditions

$$\left. \frac{d\phi}{d\rho} \right|_{\rho=0} = 0$$

and

$$\phi(\infty) = \sigma.$$

The ϕ-field starts from the same $\phi = \phi(0)$ as in the case for $|x| > t$ but this time it rolls down the hill towards the true minimum of the potential, ϕ_+, where it oscillates until all of its energy is dissipated. The full wavefront is made up of the solutions to both (6.21) and (6.25) and is shown schematically in fig.(6.4), (6.5). The shape of the wavefront is relatively insensitive to the precise form of the potential but its width depends on the height of the barrier, as shown in fig. (6.4). More often than not the starting value of the ϕ-field lies quite close to 1, a fact that makes it hard to depict the oscillatory behaviour of the solution around the true minimum on the same scale as the rest of the wavefront which is why it appears as a straight line in the figures. If it is plotted on a suitable scale the decaying oscillations become evident, (see fig. (6.5)). We have plotted here the results for the polynomial potential only since the corresponding results in the case of the modified Coleman-Weinberg potential are very similar.

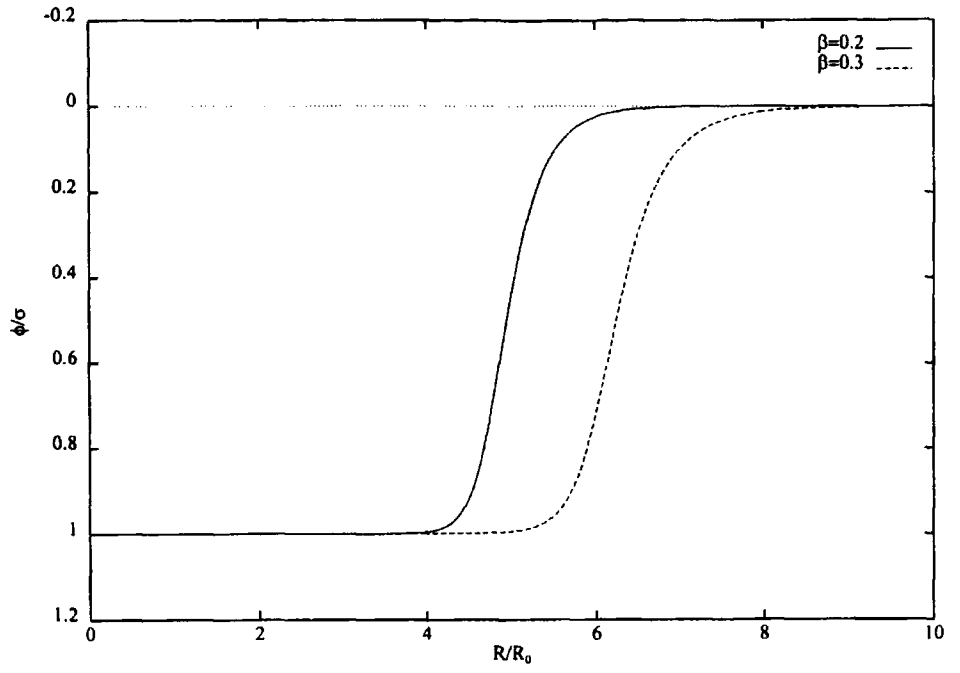

Figure 6.4: The shape of the bubble wavefront for the polynomial potential, with $\beta = 0.2$ and $\beta = 0.3$.

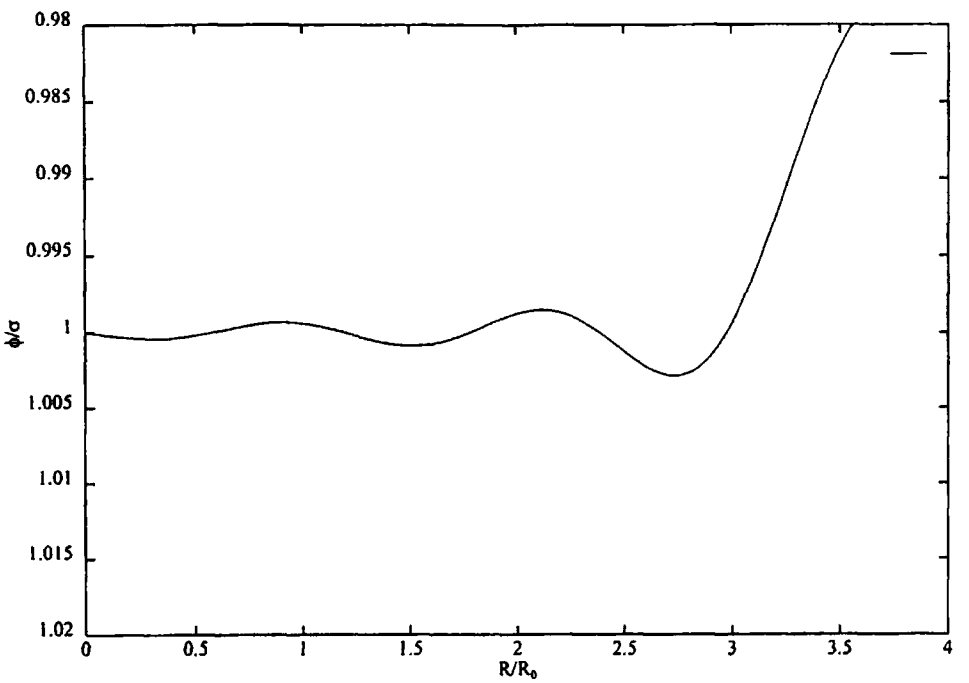

Figure 6.5: A graph showing the oscillatory behaviour of the solution to (6.21) for the polynomial potential with $\beta = 0.4$.

6.4 Tunnelling Action

The expression for the tunnelling action associated with the tunnelling of the ϕ-field through the potential barrier is given by (cf. (5.44))

$$S_E = \int d^4x \left[\frac{1}{2}\partial_\mu \overline{\phi}\partial_\mu \overline{\phi} + U(\overline{\phi})\right] \tag{6.26}$$

where $\overline{\phi} \equiv \overline{\phi}(x)$ minimises the action and is the solution to the equation of motion (6.21) with boundary conditions (6.22), (6.23). For the action to be finite we rescale $U(\phi)$ such that $U(0) = 0$ and $U(\sigma) = -\tilde{A}\sigma^4$. Since U is then negative one might worry about the possibility of S being negative as well. However, this is not the case as we will now show (Coleman (1985)). If we embed ϕ into a one-parameter family of functions

$$\phi_\lambda(x) = \bar{\phi}\,(x/\lambda)$$

then from (6.26),

$$S(\phi_\lambda) = \frac{1}{2}\lambda^2 \int d^4x \left(\partial_\mu\, \bar{\phi}\right)^2 + \lambda^4 \int d^4x U(\bar{\phi}) \tag{6.27}$$

Since $\bar{\phi}$ is a solution of the equation of motion it must minimise the action which means that $S(\phi_\lambda)$ must have a minimum at $\lambda = 1$. Thus,

$$\int d^4x \left(\partial_\mu\, \bar{\phi}\right)^2 = -4 \int d^4x U(\bar{\phi}),$$

so

$$S_E = \frac{1}{4} \int d^4x \left(\partial_\mu\, \bar{\phi}\right)^2 > 0.$$

Also,

$$\frac{d^2 S_E}{d\lambda^2} = -\frac{1}{2} \int d^4x \left(\partial_\mu\, \bar{\phi}\right)^2 < 0$$

and so at $\phi = \bar{\phi}$, the second variational derivative of S_E has at least one negative eigenvalue. Herein lies the second problem associated with the tunnelling action,

which is the possibility of there being more than one negative eigenvalue, a fact that would make our analysis in chapter 5 invalid. Fortunately this is not the case (Coleman (1985)). It has been shown (Coleman, Glaser, Martin (1978)) that the bounce solution is the absolute minimum of S_E for a fixed V, $V \equiv \int d^4x U$. However, there can not be two independent eigenvectors with negative eigenvalues for if there were, we could form a linear combination of these eigenvectors which was tangent to the surface of constant V, and the bounce would not even be a local minimum of S_E with fixed V, let alone an absolute minimum. Thus there can only be one eigenvector with a negative eigenvalue and the analysis of chapter 5 is valid.

To conclude this section we shall examine ways of determining the tunnelling action. The proper way of doing this is with the aid of the bounce solution. As we have seen, the bounce solution not only determines the shape of the bubble wavefront but also provides the tools for calculating S_E. The Euclidean action is given by

$$S_E = \frac{1}{4}\int d^4x (\partial_\mu \phi)^2. \tag{6.28}$$

If we introduce dimensionless scalar variables $\tilde{x}$ and $\tilde{\phi}$ such that $\tilde{x} = \sqrt{\tilde{A}}\sigma x$ and $\tilde{\phi} = \bar{\phi}/\sigma$, then S_E becomes

$$S_E = \frac{1}{4}\int \frac{d^4\tilde{x}}{\left(\sqrt{\tilde{A}}\sigma\right)^4}\sigma^2\left(\frac{\partial\tilde{\phi}}{\partial\tilde{x}_\mu}\right)^2\left(\sqrt{\tilde{A}}\sigma\right)^2 \tag{6.29}$$

$$= \frac{1}{4\tilde{A}}\int d^4\tilde{x}\left(\frac{\partial\tilde{\phi}}{\partial\tilde{x}_\mu}\right)^2. \tag{6.30}$$

Now, because the soliton of lowest action is $O(4)$ symmetric, we have

$$\int d^4\tilde{x}\left(\frac{\partial\tilde{\phi}}{\partial\tilde{x}_\mu}\right)^2 = 2\pi^2\int_0^\infty \tilde{x}^3\left(\frac{\partial\tilde{\phi}}{\partial\tilde{x}}\right)^2 d\tilde{x}.$$

Hence the tunnelling action is

$$S_E = \frac{\pi^2}{2\tilde{A}}\tilde{I} \tag{6.31}$$

where

$$\tilde{I} = \int_0^\infty \tilde{x}^3 \left(\frac{\partial \tilde{\phi}}{\partial \tilde{x}} \right)^2 d\tilde{x} \tag{6.32}$$

is determined numerically from the bounce solution which depends on the barrier height and hence on β. The potentials under investigation are described by three parameters which at the moment are unknown. However, the scaling method described above is a powerful tool for reducing the amount of numerical calculation as it enables the action to be computed in terms of just one variable β, since A has been scaled outside the integral $\tilde{I}$ (cf. (6.31)) and since the introduction of the dimensionless variables $\tilde{x}$ and $\tilde{\phi}$ has rendered the tunnelling action independent of σ. What makes this even easier is that there is a method of obtaining an approximate value for the tunnelling action using the thin-wall approximation which is valid provided that the size of the bubbles of true vacuum is large compared to their thickness (cf. section (5.2)).

We showed in the last chapter that in the thin-wall approximation where the energy difference ϵ between the false and true vacua is very much smaller than the height of the barrier, the tunnelling action is given by

$$B \equiv S_E = \frac{27\pi^2 {S_1}^4}{2\epsilon^3} \tag{6.33}$$

with $\epsilon = \tilde{A}\sigma^4$ and

$$S_1 = \int d\phi [2U_s(\phi)]^{1/2}.$$

In terms of scaled variables this becomes

$$S_1 = \sqrt{2\tilde{A}}\sigma^3 \int d\tilde{\phi} \left[\tilde{U}_s \left(\tilde{\phi} \right) \right]^{1/2} \equiv \sqrt{2\tilde{A}}\sigma^3 \tilde{I}_1 \tag{6.34}$$

where

$$|\tilde{I}_1| = 2 \int_0^1 d\tilde{\phi} \left[\tilde{U}_s \left(\tilde{\phi} \right) \right]^{1/2}$$

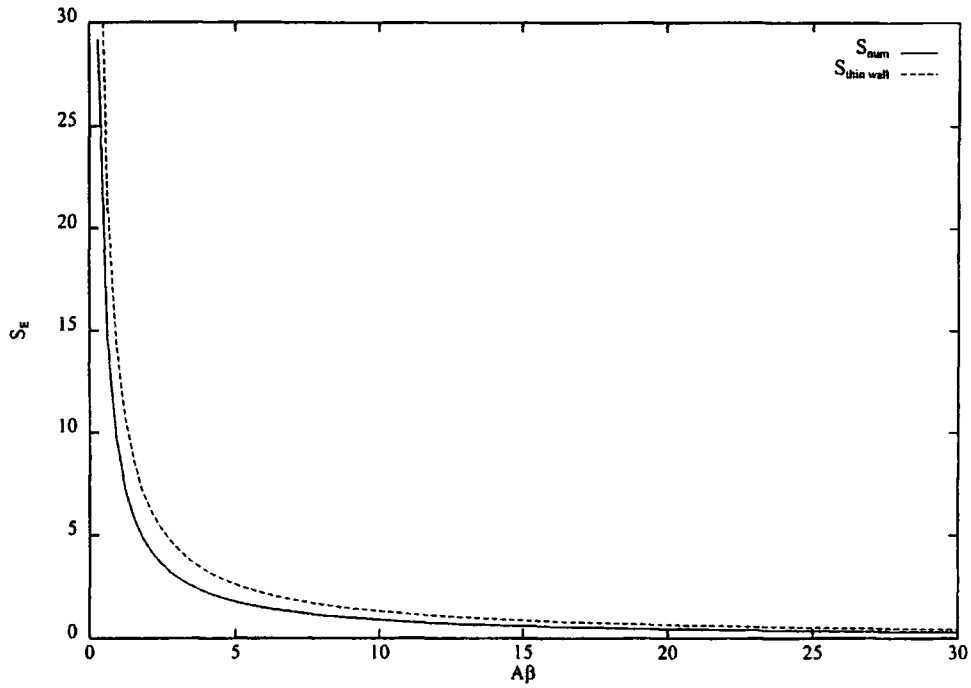

Figure 6.6: The tunnelling action for the polynomial potential computed numerically (solid curve) and in the thin wall approximation, for $\beta = 0.4$.

and so from (6.33)

$$B = \frac{54\pi^2 \tilde{I}_1^{\,4}}{\tilde{A}}. \tag{6.35}$$

In the limit of small β, the polynomial potential gives $\tilde{I}_1 = 0.25/\beta^{1/2}$, whereas for the modified Coleman-Weinberg potential, $\tilde{I}_1 \simeq 0.28/\beta^{1/2}$. The increasing accuracy of the thin wall approximations is illustrated in figs (6.6), (6.7), for the polynomial potential (for the modified Coleman-Weinberg potential the results are similar). Away from the thin wall regime B remains independent of σ and is still proportional to $1/A$ though its dependence on β becomes more complicated.

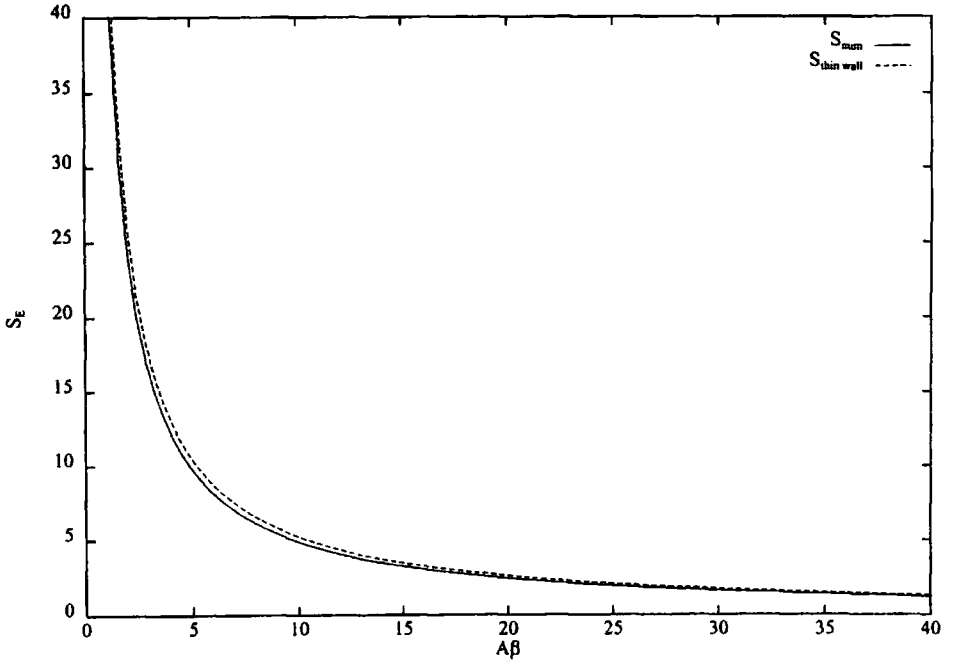

Figure 6.7: The tunnelling action for the polynomial potential computed numerically (solid curve) and in the thin wall approximation with $\beta = 0.2$.

6.5 Functional Integral

So far we have examined ways of determining the bounce solution that is needed in order to evaluate the tunnelling action and obtain the shape of the bubble wavefront, and we have also examined an approximate way of determining B without having to calculate the bounce solution. For the decay rate of the ϕ-field to be completely defined we now need to evaluate the ratio of the functional determinants that appear in the expression for Γ/V in (6.20), namely

$$D = \left[\frac{det\left(-\partial^2 + \omega^2\right)}{det'\left(-\partial^2 + U''\left(\bar{\phi}\right)\right)} \right]^{1/2} \tag{6.36}$$

where $\omega^2 = U''(0)$ and $\bar{\phi}$ is the solution of (6.21) with boundary conditions (6.22),(6.23). For both the polynomial and the Coleman-Weinberg potentials

$$\omega^2 = \frac{2(1-2\beta)}{\beta}\tilde{A}\sigma^2 \equiv \tilde{\omega}^2\tilde{A}\sigma^2. \tag{6.37}$$

As the evaluation of functional determinants is in general very difficult we will only obtain an approximate answer for D. We denote the eigenvalues of the differential operator $(-\partial^2+\omega^2)$ by μ_i and those of $(-\partial^2+U''(\bar{\phi}))$ by λ_i respectively. Now, since the determinant of any matrix is equal to the product of its eigenvalues (see Kleinert (1990)),

$$D^2 = \frac{det\,(-\partial^2+\omega^2)}{det'\left(-\partial^2+U''\left(\bar{\phi}\right)\right)} = \prod_{i=0}^{\infty}\left(\frac{\mu_i}{\lambda_i}\right). \tag{6.38}$$

In evaluating the primed determinant we take the modulus of the negative eigenvalue λ_0 and omit the four zero eigenvalues corresponding to the freedom to translate the instanton centres in the four directions in space-time (Coleman (1977), Callan and Coleman (1977)). The eigenvalues of the numerator are those of the simple harmonic oscilator (Vainstein *et al* (1982), Kleinert (1990))

$$\mu_n{}^2 = \frac{\pi^2 n^2}{T^2} + \omega^2, \quad n = 1, 2, ...$$

which in the dilute gas approximation (large T, cf. chapter 5) and for small n can be approximated by ω^2. Thus, since we have already accounted for 5 of the eigenvalues in the denominator, we approximate the five lowest eigenvalues of the numerator by ω^2, so that the ratio of the product of the other eigenvalues remains dimensionless. With these approximations (6.38) becomes

$$D^2 = \frac{\omega^{10}}{|\lambda_0|}\prod_{i=5}^{\infty}\left(\frac{\mu_i}{\lambda_i}\right) \equiv \frac{\omega^{10}}{|\lambda_0|}F^2. \tag{6.39}$$

λ_0 can be found numerically by converting $(-\partial^2+U''(\bar{\phi}))$ into a difference operator and obtaining the lowest eigenvalue of the resulting matrix, or, perhaps

more easily, by a phenomenological argument showing that the lowest negative eigenvalue depends on the critical bubble radius. This argument will be given in the next section. For now we will assume that λ_0 is known. It is again convenient to use scaling arguments such as those given at the beginning of this chapter. If we therefore set

$$U''(\phi) \equiv \tilde{A}\sigma^2 \check{U}''(\check{\phi})$$

so that

$$\lambda_0 = \tilde{A}\sigma^2 \hat{\lambda}_0, \tag{6.40}$$

by combining (6.39) with (6.40) we obtain

$$D = \frac{\tilde{\omega}^5 \tilde{A}\sigma^4}{\left| \tilde{\lambda}_0 \right|^{1/2}} F, \tag{6.41}$$

where $\omega^2 = \tilde{A}\sigma^2\tilde{\omega}^2$ and F is dimensionless. Thus the decay rate of the false vacuum per unit volume is given by

$$\frac{\Gamma}{V} = \frac{B^2}{4\pi^2\hbar^2} D e^{-B/\hbar} \tag{6.42}$$

where all the symbols have their previous meanings and D is given in (6.41). At this stage F is still undetermined but this is not really a problem as a rough estimate of its value will suffice since the magnitude of the expression for the decay rate is dominated by the exponential. For the forms of potential we examine, we can approximate the regions near each minimum by a harmonic oscillator potential. And since, in this case, the eigenvalues in the numerator and the denominator are expected to be similar in size, we set F to unity.

6.6 Negative Eigenvalue

In this section we will derive an approximate expression for the negative eigenvalue in terms of the bubble radius (Kleinert (1990)). The decay of the false

vacuum proceeds by the formation of bubbles of true vacuum that expand into the surrounding sea of the false vacuum. Since the inside of the bubble lies in the true ground state, which in the case of an asymmetric potential is lower than the metastable state by an amount ϵ, the volume energy of a bubble of arbitrary radius r, in D dimensions, is given by

$$E_V = -S_D \frac{r^D}{D} \epsilon, \tag{6.43}$$

where $S_D d^D/D$ is the bubble volume. The surface energy, on the other hand, is given by

$$E_S = \frac{r^{D-1}}{R^{D-1}} A \tag{6.44}$$

where A is a constant proportional to the surface tension and E_S is parametrised with respect to the critical radius R, determined by the equilibrium between the gain in volume energy and the loss in surface energy. Adding (6.43) and (6.44) and differentiating with respect to r at $r = R$ we have

$$R^D S_D \epsilon = (D-1)A, \tag{6.45}$$

and the critical energy is therefore given by

$$E_c = R^D S_D \epsilon \frac{1}{D(D-1)} = \frac{A}{D}. \tag{6.46}$$

Also,

$$\left.\frac{d^2 E}{dr^2}\right|_{r=R} = -A\frac{D-1}{R^2} = -DE_c \frac{D-1}{R^2} \quad . \tag{6.47}$$

Identifying E_c with the classical Euclidean action S_E, the above equation gives

$$\delta^2 S_E \approx -\frac{1}{2}(\delta r)^2 D S_E \frac{D-1}{R^2} \quad . \tag{6.48}$$

Consider now infinitesimal fluctuations of the ϕ-field such that

$$\delta\phi = \delta r \partial_r \phi. \tag{6.49}$$

Because of the rotational symmetry of the problem we can expand $\delta\phi$ into eigenfunctions of angular momentum ϕ_{nlm} such that

$$\delta\phi = \sum_{nlm} \phi_{nlm} Y_{lm}, \tag{6.50}$$

Y_{lm} being spherical harmonics. The lowest negative eigenvalue corresponds to the fluctuation ϕ_{000}, which when normalised (compare with the case in one dimension in the last chapter where we had from (5.26), (5.36) $x_0 = B^{-1/2}d\overline{x}/dt$), is given by

$$\phi_{000} = \frac{\partial_r \phi}{\sqrt{\int d^D x (\partial_r \phi)^2}} \ . \tag{6.51}$$

The expression under the square root is just D times the action of the critical bubble, S_E. Thus the ϕ_{000} contribution to $\delta\phi$ is

$$\delta\phi = \phi_{000} \frac{\partial_r \phi}{\sqrt{D S_E}} \tag{6.52}$$

which gives

$$\delta r = \frac{\phi_{000}}{\sqrt{D S_E}} \ . \tag{6.53}$$

Substituting back into (6.48) the second variational derivative of the Euclidean action is given by

$$\delta^2 S_E = -{\phi_{000}}^2 \frac{D-1}{2R^2}, \tag{6.54}$$

where ϕ_{000} is the normalised fluctuation of the solution to the bounce equation and R is the critical bubble radius. Thus, the negative eigenvalue is given by

$$\lambda_{00} = -\frac{D-1}{2R^2}. \tag{6.55}$$

In our case where we work in four dimensions this reduces to

$$\lambda_0 = -\frac{3}{2R^2}, \tag{6.56}$$

where

$$R = \frac{3S_1}{\epsilon},$$

and S_1 is the Euclidean action of the symmetric double well potential (cf. (6.33)–(6.35))). Substituting for S_1 and ϵ (cf. (6.6)) and using (6.56) it follows that

$$|\lambda_0| = |\tilde{\lambda}_0|\tilde{A}\sigma^2$$

where, for the polynomial potential and for small β, $\tilde{\lambda}_0 \approx 4\beta/3$ whereas for the modified Coleman-Weinberg potential $\tilde{\lambda}_0 \approx \beta$.

For large values of β, however, the thin wall approximation breaks down and we are not allowed to use $R = 3S_1/\epsilon$. In this case the critical bubble radius can be determined as follows. In section 6.3 we saw how to obtain the bounce solution and in figs.(6.5) and (6.6) we plotted the solution against $\tilde{R} = R/R_0$, where $R_0 = (\sqrt{\tilde{A}}\sigma)^{-1}$ is the unit of length. In this case

$$\begin{aligned} |\lambda_0| &= \frac{3}{2R^2} \\ &= \frac{3}{2\tilde{R}^2}\tilde{A}\sigma^2 \\ &\equiv |\tilde{\lambda}_0|\tilde{A}\sigma^2 \end{aligned}$$

where $|\tilde{\lambda}_0| = 3/(2\tilde{R}^2)$ and $\tilde{R}$ is the parametrised (dimensionless) critical bubble radius that can be estimated from the graph itself.

6.7 Bubble Collisions

So far we have determined the solution of the bounce equation that gives us the shape of the bubble wavefront at the moment of its materialisation. We have also shown in the last chapter that, once formed, bubbles of true vacuum expand into the surrounding false vacuum with a speed that approaches the speed of light, transforming it into true vacuum. As we are expecting the distribution of matter

to have resulted from the coalescing of true vacuum bubbles we next examine how to integrate the equation of motion for two such wavefronts moving towards each other.

The equation of motion for ϕ, obtained as usual by the minimisation of the action, is

$$\frac{\partial^2\phi(x,t)}{\partial t^2} - \frac{\partial^2\phi(x,t)}{\partial x^2} + \Gamma\frac{\partial\phi(x,t)}{\partial t} + U'(\phi) = 0 \tag{6.57}$$

where Γ is the decay width of ϕ into matter. In the thin wall approximation, where the radius of curvature of the bubbles is large compared to their width, the wavefronts depend only on x and t. Also, the third term, representing the decay of the ϕ-field due to its coupling to matter, being proportional to the velocity of ϕ, is only important when it is rapidly oscillating about the true minimum of the potential. Equation (6.57) is a hyperbolic partial differential equation that needs to be solved numerically.

The standard approach involves the setting up of an x,t lattice grid (see figure (6.8)) with lattice spacings δx and δt respectively and the transformation of (6.57) from a differential to a difference equation. At $t = 0$ the two wavefronts start by being well separated (see figure (6.9)) and we choose the point $x = 0$ to be midway between the two wavefronts. The initial conditions obeyed by our system, $\phi(x,0)$ and $\partial\phi(x,t)/\partial t$ at $t = 0$, are determined by the solution to the bounce equation which we computed in section (6.3). In the 'central differences' method we make the following approximations

$$\begin{aligned}
\ddot{\phi} &\simeq \frac{\phi(I,J+1) - 2\phi(I,J) + \phi(I,J-1)}{\delta t^2} \\
\phi'' &\simeq \frac{\phi(I+1,J) - 2\phi(I,J) + \phi(I-1,J)}{\delta x^2} \\
U'(\phi) &\simeq U'(\phi(I,J)) = a\tilde{U}'(\tilde{\phi}(I,J)) \\
\dot{\phi} &\simeq \frac{\phi(I,J+1) - \phi(I,J-1)}{2\delta t},
\end{aligned} \tag{6.58}$$

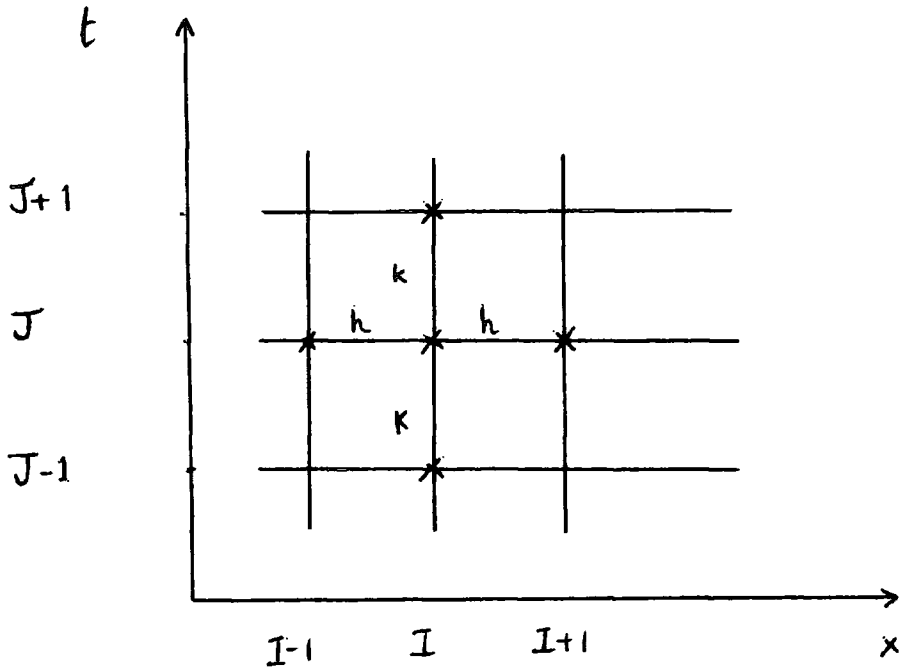

Figure 6.8: The type of lattice grid that we use in our calculation, where h and k are x and t lattice spacings respectively.

where $\phi(I,J)$ denotes the value of the ϕ-field at a point $(I\delta x, J\delta t)$ on the (x,t) lattice and $a = \tilde{A}\sigma^3$.

If our time step δt is sufficiently small the shape of the wavefronts will not change much in that time and hence the wavefronts at the next time step can be obtained by simply translating them. If we now substitute (6.58) into (6.57), scale ϕ as usual and solve for the most advanced time step we obtain:

$$\begin{aligned}\tilde{\phi}(I,J+1) &= \frac{1}{1+\frac{1}{2}\Gamma\delta t}\Big\{(\tilde{\phi}(I-1,J)-2\tilde{\phi}(I,J)+\tilde{\phi}(I+1,J))\left(\frac{\delta t}{\delta x}^2\right)+2\tilde{\phi}(I,J)\\ &- \tilde{\phi}(I,J-1)-\frac{a}{\sigma}\tilde{U}'(\tilde{\phi}(I,J))\delta t^2+\frac{1}{2}\Gamma\tilde{\phi}(I,J-1)\delta t\Big\}. \qquad (6.59)\end{aligned}$$

To simplify the above equation we again introduce dimensionless scalar variables and set

$$\frac{1}{2}\Gamma\delta t = \tilde{\Gamma}\lambda$$

$$\frac{a\delta t^2}{\sigma} = \tilde{a} = \tilde{A}\sigma^2\delta t^2, \tag{6.60}$$

where λ is defined in (6.61) and takes into account the fact that the numerical speed of propagation of the wavefronts is not equal to the physical speed of propagation but depends on the choice of the lattice spacings δx and δt respectively. The numerical and physical speeds of propagation for the problem under investigation are only equal if we choose $\delta x = \delta t$ so that $\lambda = 1$. However, the evolution algorithm is unstable for $\lambda \geq 1$ so we choose λ as follows:

$$\lambda \equiv \frac{\delta t}{\delta x} = \frac{1}{2}. \tag{6.61}$$

With these choices (6.59) becomes

$$\begin{aligned} \tilde{\phi}(I, J+1) &= \frac{1}{1+\tilde{\Gamma}\lambda}\Big\{(\tilde{\phi}(I-1,J) + \tilde{\phi}(I+1,J))\lambda^2 + 2\tilde{\phi}(I,J)(1-\lambda^2) \\ &- \tilde{a}\tilde{U}'(\tilde{\phi}(I,J)) + (\tilde{\Gamma}\lambda - 1)\tilde{\phi}(I,J-1)\Big\}. \end{aligned} \tag{6.62}$$

Since we made the approximation that the shape of the bubble wavefront will not change much in one time step, we want $\delta\tilde{\phi}(I, J+1) \ll \tilde{\phi}(I, J+1)$, and hence $\tilde{a} \ll 1$. Scaling arguments similar to those used before not only show that this is the case, but also show that $\tilde{a}$ is independent of the parameters of the potentials.

The width of the wavefront can be expressed either as the number of lattice spacings or in terms of the unit of length $(\sqrt{\tilde{A}}\sigma)^{-1}$. If the width of the wavefront is $\tilde{l}$ scaled units, or w_i lattice spacings, then

$$\begin{aligned} \frac{\tilde{l}}{\sqrt{\tilde{A}}\sigma} &= w_i\delta x = w_i\frac{\delta t}{\lambda} \\ &\Rightarrow \quad \delta t = \frac{\lambda\tilde{l}}{\sqrt{\tilde{A}}\sigma w_i}. \end{aligned} \tag{6.63}$$

Thus from (6.60),

$$\tilde{a} = \tilde{A}\sigma^2\delta t^2 = \left(\frac{l}{w_i}\right)^2\lambda^2.$$

Typically $\tilde{l} \sim 1$ and $w_i \sim 100$ and so $\tilde{a}$ is naturally of order $10^{-4}\lambda^2$, regardless of the values of $\tilde{A}$ and σ which at this stage are still undetermined. The integration of (6.62) proceeds by evaluating $\tilde{\phi}(I, J+1)$ for each point in the x direction and then advance to the next time step by relabelling $\tilde{\phi}(I, J)$ as $\tilde{\phi}(I, J-1)$ and $\tilde{\phi}(I, J+1)$ as $\tilde{\phi}(I, J)$.

Because we work with scaled variables our simulation gives the width of the matter distribution in terms of dimensionless quantities which have to be converted into physical units for comparison with observations.

If the width of the distribution determined by the simulation is w_0 lattice spacings, then from (6.63) the physical width of the distribution is

$$\delta r_i = w_0 \delta x = \frac{l}{\sqrt{\tilde{A}}\sigma} \frac{w_0}{w_i} \tag{6.64}$$

which gives the thickness of the shell at the time of its formation.

To find the total mass of the shell at the time of its formation we start by calculating the amount of matter produced by the decay of the ϕ-field in an infinitesimal box of size δx at time δt,

$$\delta M = \Gamma \dot{\phi}^2 \delta t \delta x^3,$$

and then obtain the total mass deposited in the box by the passage of the wavefront by summing over all time:

$$\begin{aligned} \sum_t \delta M &= \sum_t \Gamma \dot{\phi}^2 \delta t \delta x^3 \\ &= \sum_t \frac{(\tilde{\phi}_{t+1} - \tilde{\phi}_t)^2}{\delta t^2} \Gamma \delta t \delta x^3 \sigma^2 \\ &= \sum_t \frac{\Gamma}{\delta t} \Delta\tilde{\phi}^2 \sigma^2 \delta x^3 \\ &= \frac{1}{\lambda^3} \Gamma \sigma^2 \delta t^2 \sum_t \Delta\tilde{\phi}^2. \end{aligned} \tag{6.65}$$

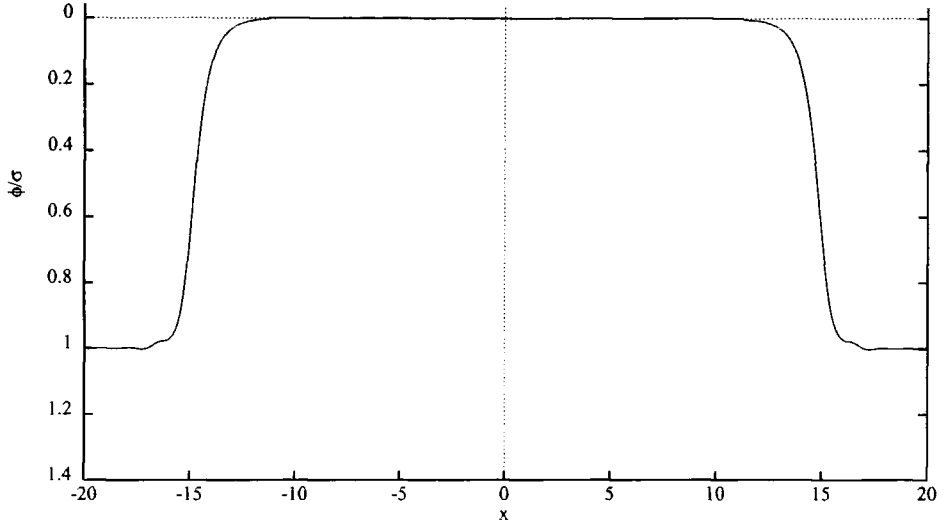

Figure 6.9: A graph showing the initial configuration of two bubble wavefronts facing each other at $t = 0$. As time increases the wavefronts move towards each other, transforming the false vacuum in between them into true vacuum. When they eventually collide at $x = 0$ all space has been converted to true vacuum and the decay of the ϕ-field results in a matter distribution similar to that shown in figure (6.10) below.

We have again scaled ϕ as usual and have used (6.61) in the last step. To find the total mass of a shell of radius r we sum over all x and obtain

$$\begin{aligned} M_0 &= \frac{4\pi r^2}{\delta x^2} \sum_x \left(\sum_t \delta M \right) \\ &= \frac{4\pi r^2}{\lambda^3} \left(\frac{\delta t}{\delta x} \right)^2 \Gamma \sigma^2 \sum_{x,t} \Delta \tilde{\phi}^2. \end{aligned} \tag{6.66}$$

If we denote the sum over x and t by $\sum_\phi$ the total mass of a shell of radius r at the time of its formation is given by

$$M_0 = 8\pi \Gamma r^2 \sigma^2 \sum\nolimits_\phi, \tag{6.67}$$

where $\sum_\phi$ is calculated in our simulation and where we have again used (6.61). An example showing the output of the collision simulation between two bubble wavefronts moving towards each other is shown in figure (6.10) for the polynomial potential.

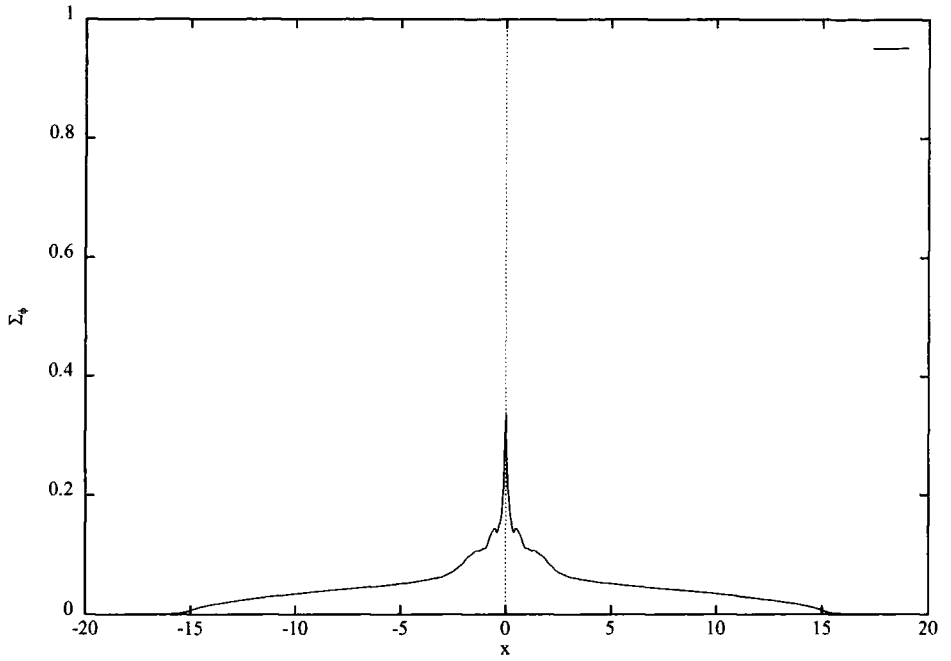

Figure 6.10: The shell of matter that is created at the point of collision between two bubble wavefronts, as determined by the quantity $\sum_\phi$. We have allowed enough time to ellapse after the collision of the bubble profiles at $x = 0$ so that all space has been converted into true vacuum.

6.8 Shell Sizes

In the last section we saw how the solution to the equation of motion for two wavefronts moving towards each other gives us information about the initial (the seed) mass of the resulting shell of matter. We shall now determine the size of the bubbles when they meet and consequently the scale of the resulting structures. The fraction of space occupied by bubbles increases due to the creation of new bubbles and the expansion of existing ones. Since shells of matter will be produced where bubbles collide these factors work in opposite directions as far as the scale of the shell structures is concerned, the first to decrease it and the second to increase it. For simplicity we shall first consider the formation of shells of matter in non-expanding space.

Ideally we should calculate the average size of the bubbles which are produced

by carrying out a numerical simulation in some volume of space by considering the creation of new bubbles at random time steps (remembering that new regions of true vacuum cannot form within existing bubbles) and let these bubbles expand at the speed of light between time steps. The simulation would end when the volume under consideration was completely filled with bubbles and the phase transition complete. Unfortunately, this is quite hard but, since there is as yet no detailed observation of the bubble spectrum, an order of magnitude estimate will be sufficient for our purposes. Purely from dimensional considerations we expect that a typical shell radius will be

$$r = r_i \left(\frac{c}{\Gamma/V} \right)^{1/4}, \tag{6.68}$$

where Γ/V is the bubble nucleation rate and where the constant of proportionality r_i is a dimensionless measure taking into account the fact that not all shells of matter are created with exactly the same radius. Since the main contribution to the above expression comes from the exponential of the action from expression (6.42) for Γ/V we can set this constant equal to unity.

In the rest of this chapter we shall derive general expressions for the thickness, mass and radius of the shells of matter based on these results.

6.9 Shell Thickness

Deriving an expression for the thickness of a shell as a function of time is a complicated matter as it requires a knowledge of the form of the gravitational potential Φ of the seed mass which is in turn dependent on the shape of the shell at the time of its formation. The final thickness of the shell will depend on the competition between gravity, which forces it to collapse, and pressure resulting from the internal motions of the constituent matter. One would expect, therefore,

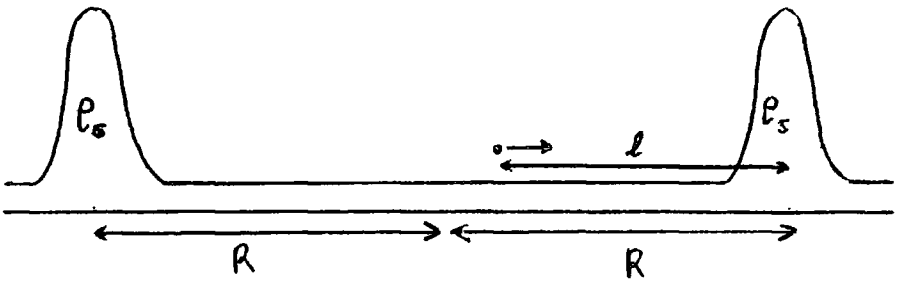

Figure 6.11: A planar model of accretion showing two shells of matter separated by a distance $2l$.

the thickness of a shell to increase initially because of the accretion of additional matter onto the shell, but then decrease as gravity compresses the whole shell. As long as there is still matter in the cavities between the shells, particles of matter will continue to accrete on the shell walls until the mass inside the cavity has reduced to zero.

We will make a number of simplifying assumptions, approximating the shell with a planar sheet of uniform surface density ρ_s and investigate its effect in attracting matter a distance l away from the sheet (see fig. (6.11)). The effects of any internal motion of the matter already inside the shell will be ignored. In flat space the equation of motion for a particle of matter is

$$\ddot{l} = -2\pi G\rho_s$$

where G is Newton's gravitational constant. Our approach, therefore, is based on Newtonian gravity which for subhorizon scales should be a good enough approximation. To take into account the expansion of the Universe we introduce the scale factor R by writing $l = xR$ where l is a physical distance, x is a coordinate distance and where, in general, $R \sim t^n$. With these substitutions the equation of motion for the particle becomes

$$\ddot{x} + \frac{2n\dot{x}}{t} + \frac{n(n-1)x}{t^2} = -\frac{2\pi G\rho_s}{t^n} \tag{6.69}$$

and the general solution to (6.69) is made up of the complimentary function plus the particular integral. To find the complimentary function we use $x \sim t^a$ as a trial solution, giving

$$a = \begin{cases} 1-n \\ n. \end{cases}$$

Thus, the complimentary function is

$$x = At^{-n} + Bt^{1-n}.$$

By inspection the particular integral is

$$x = Ct^{2-n},$$

where $C = -\pi G\rho_s$ is found by substituting back into (6.69). Thus, in terms of physical distances,

$$\begin{aligned} l = xR &= xt^n \\ &= A + Bt + Ct^2 \\ &= l_f - \pi G\rho_s(t - t_f)^2 \end{aligned} \tag{6.70}$$

where to obtain the last equality we have assumed that the test particle starts at rest a distance l_f away from the sheet at $t = t_f$, the time of formation of the shells of matter (this is yet another simplifying assumption since there is no reason why particles of matter inside the shell should not have an initial velocity). If we identify the thickness of the shell ΔR with the distance of the furthest particle from the sheet i.e one which has started a distance R away, at the midpoint between the sheets, then

$$\Delta R = R - \alpha\pi G\rho_s(t - t_f)^2,$$

so today the present thickness of the shells is given by

$$\Delta R_0 = R_0 - \alpha\pi G\rho_s(t_0 - t_f)^2 \tag{6.71}$$

where α is a model parameter of order unity.

6.10 Shell Mass

Since most of the matter inside the shell will eventually accrete onto the shell, we take the shell mass to be the seed mass (cf. (6.67)) plus the mass of matter inside the shell at the time of its formation, thus

$$M_{shell} = 8\pi\Gamma {r_f}^2\sigma^2\sum\nolimits_{\phi} + \frac{4\pi {r_0}^3\rho_0}{3}, \tag{6.72}$$

where r_f is the radius of the shell at the time of its formation, r_0 is its present radius and ρ_0 is the present average density of matter in the Universe.

6.11 Shell Radius

As we mentioned before, our aim is to account for a bubbly structure in the Universe by employing a first-order phase transition which occured after inflation. As in the case of the inflationary potentials introduced earlier in this thesis, our potentials are temperature-dependent and can result in a phase transition which, depending on the temperature T, can proceed either by thermal or by quantum tunnelling. Thermal tunnelling occurs at very high temperatures $T \gg T_c$ and in this case one has to use the finite temperature tunnelling rate. Quantum mechanical tunnelling of the kind examined in chapter 5, on the other hand, will be appropriate if $T \ll T_c$, however, since quantum tunnelling can be applied at finite temperatures provided that they are low enough (Linde (1990)). Supposing, therefore, that the phase transition occured when

$$kT \simeq U(0)^{1/4},$$

in other words above $T = 0$ but still low enough for the analysis in chapter 5 to be valid, then the time t_{pt} when the phase transition occurs is given by (cf.

(2.19))

$$t_{pt} = \left(\frac{45c^5\hbar^3}{16\pi^3 G g_*}\right)^{1/2} \frac{1}{(A\beta\sigma^4)^{1/2}}. \tag{6.73}$$

Hence, we can use a thermal argument to calculate the epoch of the phase transition but still use the quantum mechanical nucleation rate discussed in chapter 5, provided that the phase transition occurs at a temperature T such that $0 < T \ll T_c$. The typical separation of bubble centers at this time is (cf. (6.68))

$$r_{pt} = \left(\frac{c}{\Gamma/V}\right)^{1/4}. \tag{6.74}$$

To calculate the size of the shells when they are formed we must find the time taken for the bubbles to meet one another, allowing for the expansion of the Universe. The initial typical coordinate separation of bubble centers is

$$x_{pt} = \frac{r_{pt}}{R(t_{pt})} = r_{pt}\left(\frac{t_{eq}}{t_{pt}}\right)^{1/2}\left(\frac{t_0}{t_{eq}}\right)^{2/3} \tag{6.75}$$

assuming the phase transition occurs in the radiation-dominated era and where we have normalised the scale factor so that $R(t_0) = 1$. After time t_f, the time taken for neighbouring bubbles to meet one another, the wavefronts will have travelled a coordinate distance

$$x = c\int_{t_{pt}}^{t_f} \frac{dt}{R(t)} = \frac{c{t_{pt}}^{1/2}}{R(t_{pt})}\int_{t_{pt}}^{t_f} \frac{dt}{t^{1/2}}$$

and so neighbouring bubbles will meet at a time t_f given by

$$x_{pt} = \frac{2c(t_{pt})^{1/2}}{R(t_{pt})}\left({t_f}^{1/2} - {t_{pt}}^{1/2}\right), \tag{6.76}$$

where we have assumed that $t_f \leq t_{eq}$. Using (6.75) and solving (6.76) for t_f gives

$$t_f = t_{pt}\left(1 + \frac{r_{pt}}{2ct_{pt}}\right)^2 \tag{6.77}$$

at which time the size of the shells is

$$\begin{aligned} r_f &= r_{pt}\left[\frac{R(t_f)}{R(t_{pt})}\right] \\ &= r_{pt}\left(\frac{t_f}{t_{pt}}\right)^{1/2} \\ &= r_{pt}\left(1+\frac{r_{pt}}{2ct_{pt}}\right). \end{aligned} \tag{6.78}$$

Thus the present size, R_0, of the shells is given by

$$R_0 = r_f\left(\frac{t_{eq}}{t_f}\right)^{1/2}\left(\frac{t_0}{t_{eq}}\right)^{2/3} \tag{6.79}$$

where t_0 is the present age of the Universe, and t_{eq} is the time at which the Universe became matter-dominated.

In the next chapter we will present results on the shell radius, mass and thickness resulting from phase transitions produced by polynomial or modified Coleman-Weinberg potentials and compare them with the observed structure of the Universe.

Chapter 7

Results

In a problem such as that under investigation, one of the main difficulties in presenting the results is the large number of variables involved, in this case those describing the scalar field potential and its decay, and showing their relation to the properties of the shells of matter that are produced by the bubble collisions. We will, therefore, start by explaining how the results are obtained, followed by a section in which we will derive the explicit dependence of the shell parameters on those of the potential. In the rest of this chapter we present our results, but our conclusions are reserved for the next chapter.

7.1 Determining the Potential Parameters from Observation of the Shell Structure

For both the polynomial and the modified Coleman-Weinberg potentials (cf. (6.3), (6.8)) we introduced three parameters which describe particular features of the potential under consideration. In particular the position of the global minimum of $U(\phi)$ is given by σ and it is this parameter that sets the energy scale for the SSB. The shape of the potential including the height of the barrier separating the false from the true ground state is parametrised by β. Finally once σ is specified the energy difference between the false and the true minima is determined by

the coupling strength A. Since the shell properties are described by three quantities namely their size, mass and thickness, we might hope to determine all three potential parameters and hence deduce the form of the potential responsible for the phase transition and the epoch when the phase transition occured. However, because we cannot assume that the scalar field necesarily couples to matter in the same way as the Standard Model Higgs field we have introduced a fourth parameter, $\tilde{G}$ (cf. (6.18), (6.19)) which also appears in the expression for the shell mass (cf. (6.67)). Hence, we cannot determine both A and $\tilde{G}$. In presenting our results, therefore, we will consider two qualitatively different regimes; one in which we set $\tilde{G} = 1$, as in the standard model, and vary A, β and σ, and another where we can vary β, σ and $\tilde{G}$ but fix A at 10^{-1} as in the Coleman-Weinberg $SU(5)$ GUT.

To obtain our results we derive equations for the shell parameters in terms of the potential parameters and $\tilde{G}$. We could then, at least in principle, solve the equations and hence obtain A, β, σ and $\tilde{G}$ by requiring the shell parameters are equal to their observed values. Alternatively we could plot the dependence of the shell parameters for a range of possible values of the potential parameters. However, as we mentioned before, there are two factors that create uncertainties in the values of the parameters that we should use in our fits. The first, the fact that the observed shell parameters depend on the Hubble parameter which is only known up to a factor of two. So with $H_0 = h_0 \times 100 kms^{-1}Mpc^{-1}$ we have

$$\begin{aligned} R &\sim {h_0}^{-1} \\ \Delta R &\sim {h_0}^{-1} \\ M &\sim {h_0}^{-3}. \end{aligned}$$

Secondly the equations derived so far produce expressions for the *average* mass,

thickness and size of the shells. Since only a limited number of shells have been observed it is too early to say precisely what these average values should be. So our approach is based on order of magnitude estimates only rather than precise values and so we have adopted the second approach. This also gives a feeling for how the results vary over a range of possible values for the parameters that the first approach would not provide.

We shall next derive equations for the shell parameters in terms of the potential parameters.

7.2 Fitting the Shell Parameters

7.2.1 Calculating t_f and r_f

All the quantities that we calculate depend upon either the time of shell formation t_f, or the size of the shells at formation r_f, or both, and we will calculate these separately. We begin by finding the bubble nucleation rate which from (6.20) is given by

$$\frac{\Gamma}{V} = \frac{B^2}{4\pi^2\hbar^2} e^{-B/\hbar} \left[\frac{det(-\partial^2 + V''(\phi_+))}{det'(-\partial^2 + V''(\overline{\phi}))} \right]^{1/2} \tag{7.1}$$

where the tunnelling action $B = S_E$ is defined in (6.31) or (6.35) depending on whether we use the numerical result or the thin wall approximation, $\overline{\phi}$ is the bounce solution of section (6.3) and ϕ_+ is the position of the false minimum. Using (6.41) for the ratio of the determinants, (7.1) can be written

$$\frac{\Gamma}{V} = \frac{B^2}{4\pi^2} e^{-B} \frac{\tilde{A}^2 \tilde{\omega}^5 \sigma^4}{\left|\tilde{\lambda}_0\right|^{1/2}} \tag{7.2}$$

where $\tilde{\omega}$ is defined in (6.37) and $\tilde{\lambda}_0$ was determined in section (6.6), and where we have swiched into $\hbar = c = 1$ units. We will find later on that quite large values of β are required (i.e. larger than about 0.37) and so from this point we

will abandon the thin wall approximation. As far as the negative eigenvalue is concerned we have $\tilde{\lambda}_0 = 3/(2\tilde{R}^2)$ where $\tilde{R}$ can be estimated from the graph of the bounce solution (cf. section (6.6)). With these approximations, and with $c = 1$, the mean separation of nucleation sites at the end of the phase transition becomes (cf. (6.68))

$$r_{pt} = \left(\frac{1}{\Gamma/V}\right)^{1/4} = \frac{0.7697 e^{B/4}\beta^{5/8}}{\tilde{I}^{1/2}\tilde{R}^{1/4}(1-2\beta)^{5/8}\sigma} GeV^{-1}. \tag{7.3}$$

Also, from (6.73), the time at which the phase transition occurs is

$$t_{pt} = \left(\frac{45c^5\hbar^3}{16\pi^3 G g_*}\right)^{1/2} \frac{1}{(A\beta\sigma^4)^{1/2}} \tag{7.4}$$

where $\tilde{I}$ determines the bounce solution (cf. (6.31), (6.32)) and is evaluated numerically. If we take $g_* \sim 100$ at the end of the phase transition, set $c = \hbar = 1$ and $G = m_{pl}{}^{-2}$ it follows that

$$t_{pt} = \frac{3.678 \times 10^{17}}{(A\beta\sigma^4)^{1/2}} GeV^{-1}. \tag{7.5}$$

If we now define Q by

$$Q = 1 + \frac{r_{pt}}{2ct_{pt}}$$

then from (6.77) and (6.78) we have respectively

$$\begin{aligned} t_f &= Q^2 t_{pt} \\ r_f &= Q r_{pt}, \end{aligned}$$

or explicitly in terms of the potential parameters

$$t_f = \frac{3.678 \times 10^{17}}{(A\beta\sigma^4)^{1/2}}\left(1 + \frac{5.232 \times 10^{-19} e^{B/4} A^{1/2}\beta^{9/8}\sigma}{\tilde{I}^{1/2}\tilde{R}^{1/4}(1-2\beta)^{5/8}}\right)^2 GeV^{-1} \tag{7.6}$$

$$r_f = \frac{0.7697 e^{B/4}\beta^{5/8}}{\tilde{I}^{1/2}\tilde{R}^{1/4}(1-2\beta)^{5/8}\sigma}\left(1 + \frac{5.232 \times 10^{-19} e^{B/4} A^{1/2}\beta^{9/8}\sigma}{\tilde{I}^{1/2}\tilde{R}^{1/4}(1-2\beta)^{5/8}}\right) GeV^{-1}. \tag{7.7}$$

We will use (7.6) and (7.7) to obtain expressions for the mass, width and thickness of the shells.

7.2.2 Fitting the Shell Size

The present size of a shell is given by

$$R_0 = r_f \left(\frac{t_{eq}}{t_f}\right)^{1/2} \left(\frac{t_0}{t_{eq}}\right)^{2/3},$$

where $t_{eq} \approx 10^{12}s$ is the time when the Universe became matter-dominated, $t_0 \approx 2 \times 10^{17}s$ is the current age of the Universe and t_f and r_f are given by (7.6) and (7.7) respectively. Substituting (7.6) and (7.7) and dividing by 1.5637×10^{38} to convert from GeV^{-1} units into Mpc, we obtain for both the polynomial and the modified Coleman-Weinberg potential

$$R_0 = \frac{4.484 \times 10^{-26} e^{B/4} A^{1/4} \beta^{7/8}}{\tilde{I}^{1/2} \tilde{R}^{1/4} (1 - 2\beta)^{5/8}} Mpc, \tag{7.8}$$

where B and $\tilde{I}$ are defined in section (6.4) and where $\tilde{R}$ is a dimensionless measure of the critical bubble radius (cf. section (6.6)). The fact that the present size of a shell is the same for both potentials reflects their similarity which is evident from figures (6.1) and (6.3). Since β appears in the exponenntial of the action we expect the dependence of R_0 on β to be significant. On the other hand, the shell radius is not dependent on σ, i.e. it does not depend on the time when the phase transition occured. As can be seen from (7.6) and (7.7), the size of the shells at formation and the time of shell formation are both largely independent of σ, except that when either A or β become too large but σ stays relatively small the term in brackets becomes of order 1 and then $t_f \propto \sigma^{-2}$ and $r_f \propto \sigma^{-1}$ respectively. Even in this case, however, R_0 remains independent of σ and so it seems that the present size of the shells is determined not by the time when the phase transition occured but by the dynamics of the Universe, their initial size being stretched as the Universe expands. On the other hand, the energy scale σ, crucially determines the mass of the shells since they are created by the decay of the ϕ-field.

7.2.3 Fitting the Shell Mass

The present mass of a shell is given by

$$\begin{aligned} M_s &= 8\pi\Gamma {r_f}^2\sigma^2 \sum_{\phi} + \frac{4\pi\rho_0 {r_0}^3}{3} \\ &\equiv M + M_1 \end{aligned}$$

where all the symbols have their previous meanings and where Γ is the decay width of the ϕ-field to matter which for the potentials under consideration is given by

$$\begin{aligned} \Gamma_P &= \frac{3}{4\pi}\tilde{G}A^{3/2}(1+\beta)^{3/2}\sigma \\ \Gamma_{CW} &= \frac{3}{32\pi}\tilde{G}A^{3/2}(3+2\beta)^{3/2}\sigma \end{aligned}$$

respectively (see section (6.2)). The observed shell mass is of order $10^{16}M_\odot$, about 90% of which is accounted for by M_1. Thus, we constrain M to be of order $10^{15}M_\odot$. With the above expressions for Γ, substituting for r_f and dividing by 1.116×10^{57} to convert from GeV units to solar masses, it follows that

$$\begin{aligned} M_P &= \frac{3.185 \times 10^{-57} e^{B/2}\tilde{G}A^{3/2}(1+\beta)^{3/2}\sum_\phi \sigma}{\tilde{I}\tilde{R}^{1/2}(1-2\beta)^{5/4}} \times \\ &\quad \left[1 + \frac{5.232 \times 10^{-19} e^{B/4}A^{1/2}\beta^{9/8}\sigma}{\tilde{I}^{1/2}\tilde{R}^{1/4}(1-2\beta)^{5/8}}\right]^2 M_\odot \end{aligned} \tag{7.9}$$

for the polynomial potential, whereas for the modified Coleman-Weinberg potential

$$\begin{aligned} M_{CW} &= \frac{3.981 \times 10^{-58} e^{B/2}\tilde{G}A^{3/2}(3+2\beta)^{3/2}\sum_\phi \sigma}{\tilde{I}\tilde{R}^{1/2}(1-2\beta)^{5/4}} \times \\ &\quad \left[1 + \frac{5.232 \times 10^{-19} e^{B/4}A^{1/2}\beta^{9/8}\sigma}{\tilde{I}^{1/2}\tilde{R}^{1/4}(1-2\beta)^{5/8}}\right]^2 M_\odot. \end{aligned} \tag{7.10}$$

7.2.4 Fitting the Shell Thickness

The present thickness of the shells is, from (6.71),

$$\Delta R_0 = R_0 - \alpha\pi G\rho_s(t_0 - t_f)^2 \tag{7.11}$$

where α is a model parameter which we have set equal to unity, G is Newton's constant, t_f is the time of shell formation, ρ_s is the surface density of the shells given by

$$\begin{aligned}\rho_s = \frac{M}{4\pi {r_f}^2} &= \frac{8\pi\Gamma {r_f}^2\sigma^2\Sigma_\phi}{4\pi {r_f}^2} \\ &= 2\Gamma\sigma^2\Sigma_\phi\end{aligned}$$

and the decay rate Γ was given in the previous section for both forms of potential. Now, since in all probability, t_f is no greater than $t_d \approx 10^{13} sec$, we approximate $(t_0 - t_f)^2 \approx {t_0}^2$ and (7.11) becomes

$$\Delta R_0 = R_0 - 2\pi G\Gamma\sigma^2\Sigma_\phi {t_0}^2, \tag{7.12}$$

where Σ_ϕ is defined in (6.67) and t_0 is the present age of the Universe. Thus, for the polynomial potential

$$\Delta R_0 = R_0 - 1.2 \times 10^9 \tilde{G} A^{3/2}(1+\beta)^{3/2}\sigma^3 Mpc \tag{7.13}$$

whereas for the modified Coleman-Weinberg potential

$$\Delta R_0 = R_0 - 1.5 \times 10^8 \tilde{G} A^{3/2}(3+2\beta)^{3/2}\sigma^3 Mpc, \tag{7.14}$$

where all symbols have their previous meanings and where we have converted from natural units to Mpc. It is evident from the above equations that the shell thickness is very insensitive to A and β, the main contribution coming from the σ^3 term. It seems, therefore, that $\tilde{G}$ but most importantly σ would have to be

exceedingly small to account for the observed shell thickness in this way implying a phase transition that occured extremely late. It therefore seems unlikely that we can use the thickness of the shells to determine the potential parameters.

7.3 Results

As mentioned previously, in presenting our results we will consider two possibilities, namely requiring $\tilde{G} = 1$ so that the couplings of the ϕ field to matter are those of the standard model Higgs field, or alternatively $A = 0.1$ as in the Coleman-Weinberg $SU(5)$ GUT. We plot the variation of the potential parameters against the resulting shell parameters and hence obtain the allowed ranges for the potential parameters which agree with observations. Because of the number of parameters involved we have been quite selective on our presentation of results. Since the potential parameters depend on the tunnelling action, and the tunnelling action depends critically on our choice of β, we only give results for a limited number of values of β. In particular we will find that β has to be larger than 0.38 and smaller than 0.44 (otherwise the values of A required become too large or too small) and so we only examine cases where the height of the barrier lies between these limits.

A first restriction on the allowed values of the potential parameters can be set from the time of formation of shells of matter (cf. (7.6)). Restricting t_f to be no later than about $t_d \approx 10^{13} sec$, the time when matter begins to dominate and structure can begin to form, seems a reasonable limit as any structure that evolved from shells of matter that where formed later than this would not have had time to evolve to the present highly condensed state. We start, therefore, in figures (7.1), (7.2), by plotting on log-log axes t_f against A for different values of β, for $\sigma = 250$ and $10^{14} GeV$ respectively, with the polynomial potential. It can

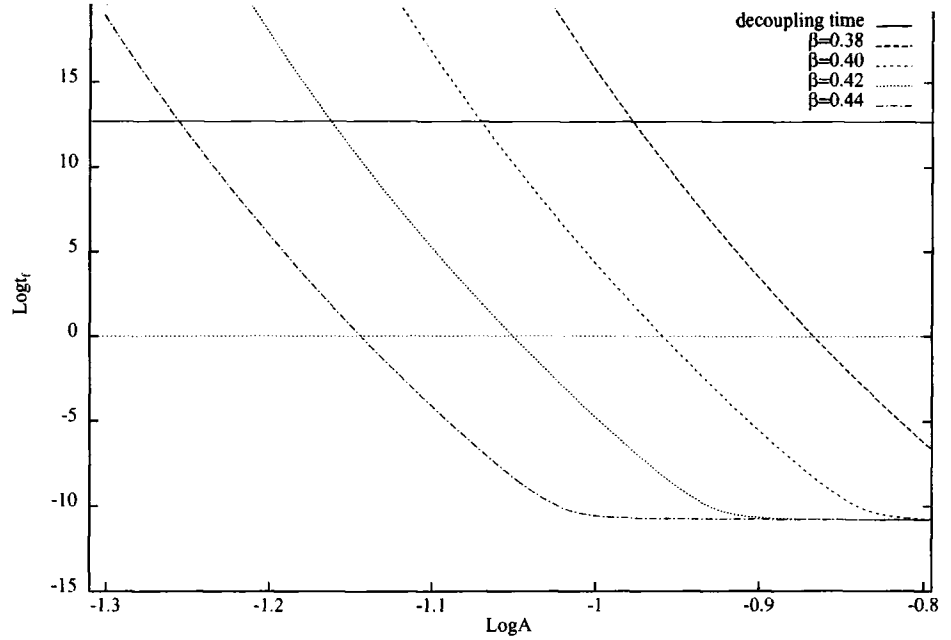

Figure 7.1: Variation of the time of shell formation t_f with A for different values of β, with $\sigma = 250GeV$ for the polynomial potential (with t_f in seconds). The lower limit at $t_{pt} \approx 10^{-10}sec$ results from the fact that shell formation can not happen earlier than the original phase transition.

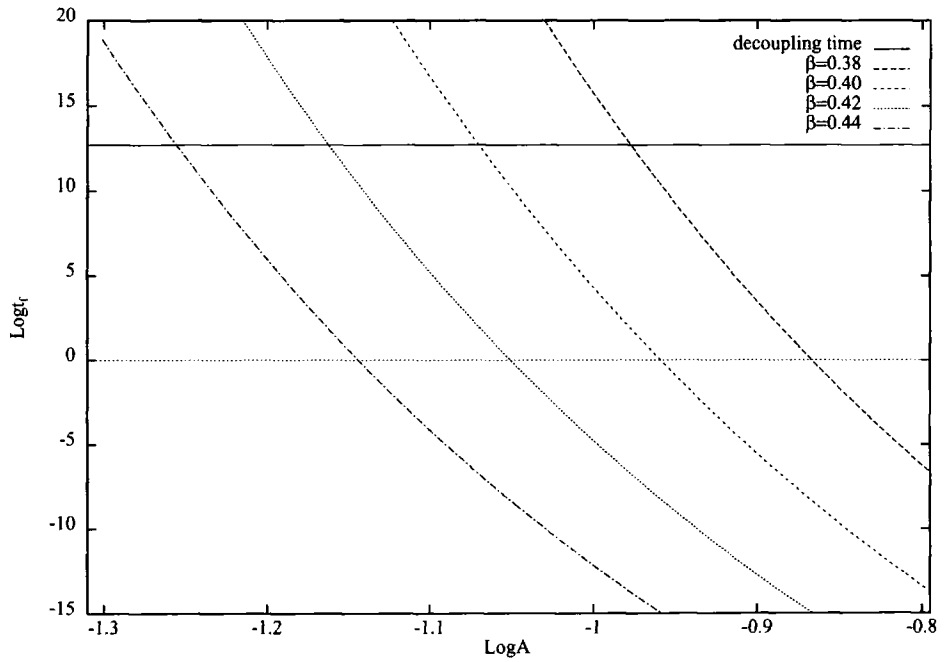

Figure 7.2: Variation of the time of shell formation t_f with A for different values of β, with $\sigma = 10^{14}GeV$ for the polynomial potential (with t_f in seconds). As in figure (7.1), the graphs corresponding to different values of β will converge at a time $t_{pt} \approx 10^{-35}sec$.

be seen that, to obtain $t_f < t_d$, A and β vary inversely to each other in the sense that small values of A require large values of β and *vice versa*. Also, for each value of β we can impose constraints on the allowed values of A. For example, for $\beta = 0.38$ A will have to be larger than about 0.1 whereas for $\beta = 0.44$ we only need $A > 0.06$. Our theoretical prejudice in favour of small values of A enables us here to impose a lower limit on β, that is, for A not to exceed 0.15 we must have $\beta \gtrsim 0.38$. Also, comparing figures (7.1) with (7.2) we see that the huge increase in σ has made essentially no difference to the variation of t_f with A: if we were to superimpose the two graphs the lines corresponding to the same values of β would completely match except for the lower cutoff on t_f which, depends on the value of σ since it gives the time of the phase transition.

In figure (7.3) we plot the variation of t_f with σ for different values of β and for $A = 0.1$. It can be seen that for smaller values of β, t_f is practically independent of σ. However, as β increases the dependence of t_f on σ becomes more apparent and, for $\beta = 0.44$, we see a power law dependence of t_f on σ for small σ. As we said before this is due to the behaviour of equation (7.6) which for certain values of A, β and σ can be approximated by setting the term in brackets equal to one. The results for the modified Coleman-Weinberg potential are very much the same and are shown in figures (7.4) to (7.6).

We next plot (in figures (7.7) and (7.8)) the shell radius against A for different values of β, remembering that the shell radius is independent of σ (see (7.8)). If we allow R_0 to vary with no restrictions whatsoever then, as the graphs show, the variation of R_0 with A and β is quite dramatic owing to the fact that the exponential of the action that appears in (7.8) is proportional to $(A\beta)^{-1}$. If, however, we restrict R_0 to be, say, smaller than $10^5 Mpc$, which is almost certainly the case, a plot of R_0 against A for different β on log-log axes consists of essentially

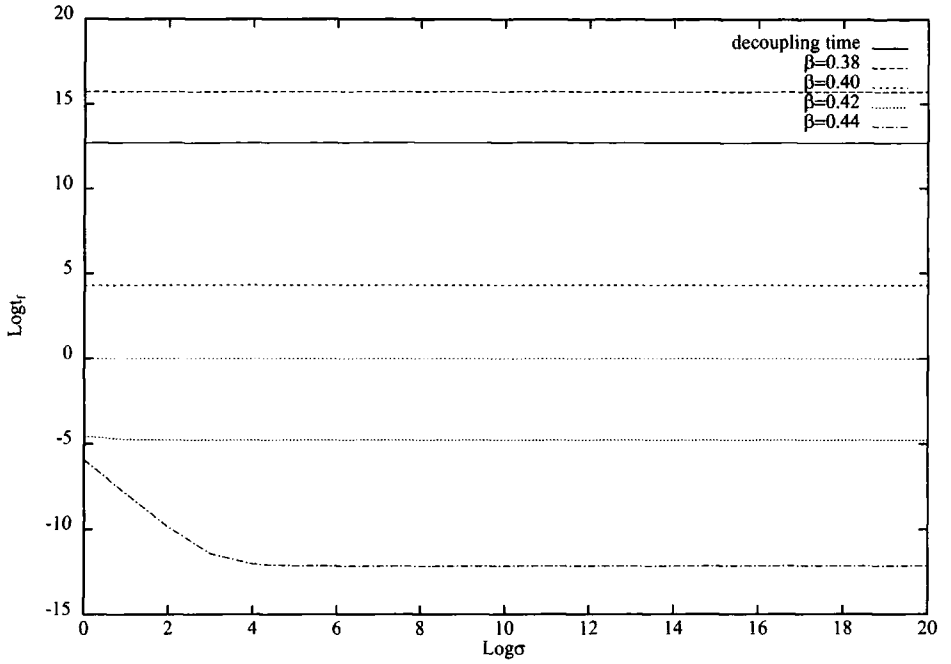

Figure 7.3: Variation of the time of shell formation t_f with σ for different values of β, with $A = 0.1$ for the polynomial potential (with t_f in seconds). t_f is independent of σ except when the tunnelling action is too small (cf. eqn. (7.6)).

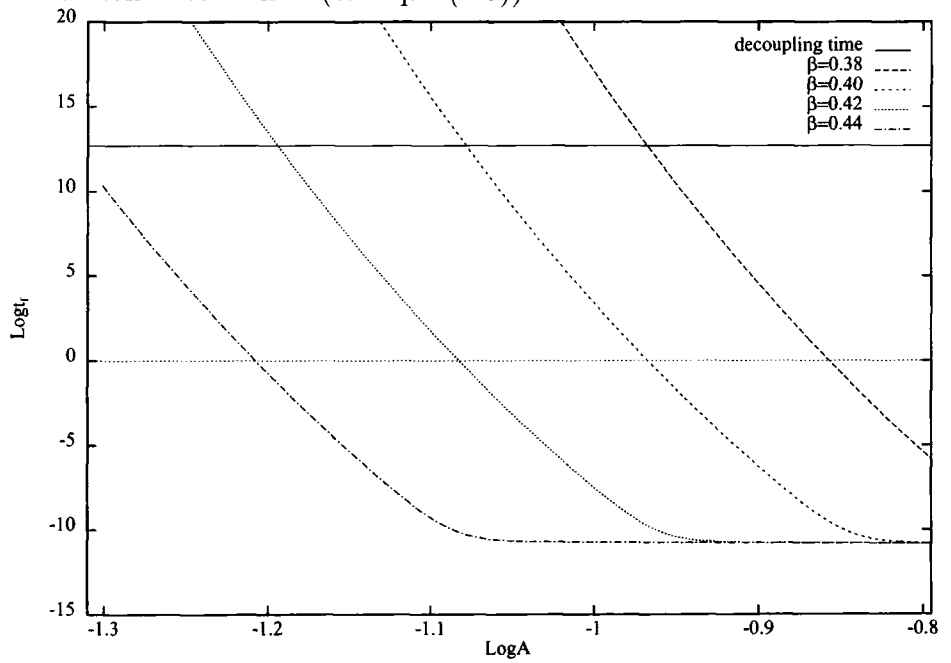

Figure 7.4: Variation of the time of shell formation t_f with A for different values of β, with $\sigma = 250GeV$ for the modified Coleman-Weinberg potential (with t_f in seconds). Compare with figure (7.1).

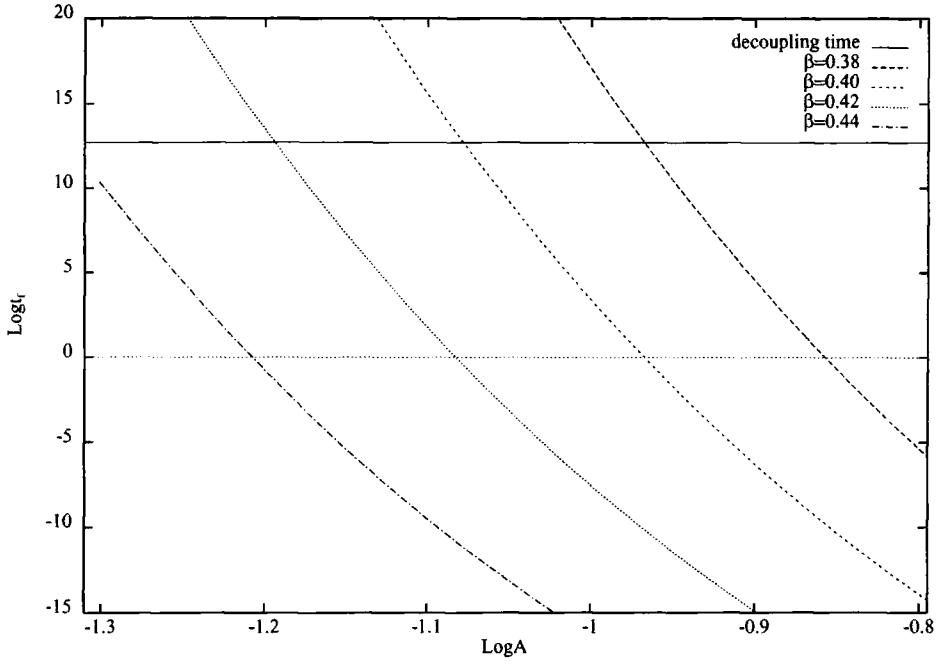

Figure 7.5: Variation of the time of shell formation t_f with A for different values of β, with $\sigma = 10^{14} GeV$ for the modified Coleman-Weinberg potential (with t_f in seconds). Compare with figure (7.2).

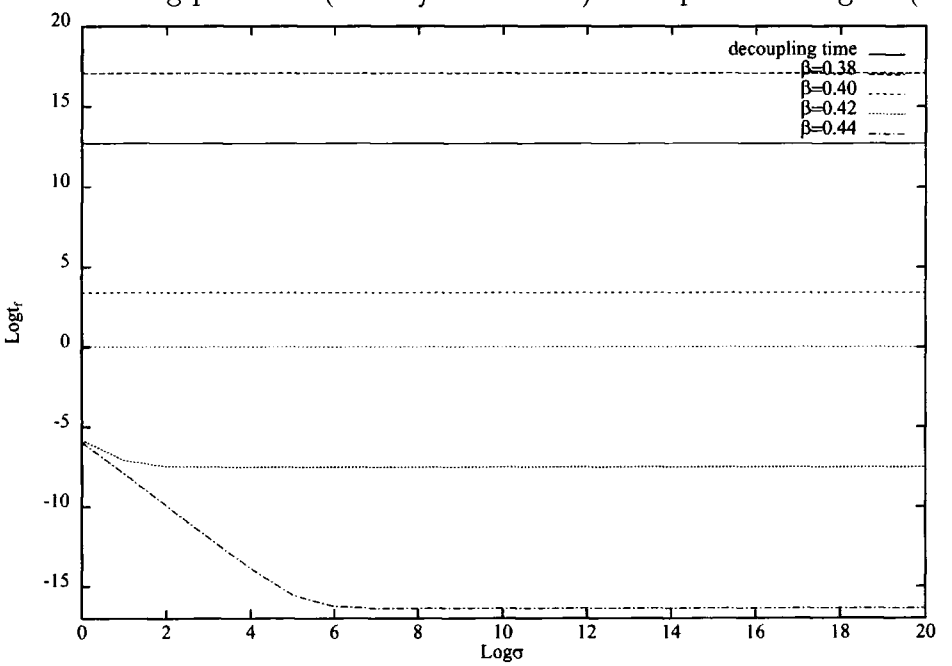

Figure 7.6: Variation of the time of shell formation t_f with σ for different values of β, with $A = 0.1$ for the modified Coleman-Weinberg potential (with t_f in seconds).

straight lines (see figs.(7.9) and (7.10)) indicating an approximate power law dependence of the shell radius on A. If we insist upon values for R_0 lying in a band extending either side of $R_0 = 25Mpc$, to take into account the aforementioned uncertainties in the evaluation of the shell parameters, (cf. section (7.1)), then the corresponding range of allowed values of A for each value of β is considerably reduced. For the polynomial potential with $\beta = 0.38$ we find that $0.108 < A < 0.112$ whereas for $\beta = 0.44$, $0.057 < A < 0.059$ is needed. These graphs show that the smaller the value of β the larger A has to be if the shell radii are to be similar in magnitude to those observed, in accordance with our conclusions concerning the variation of t_f. Large values of A are unacceptable, not only because they would be contradictory to the Weinberg-Salam standard model or GUT theories, but also because perturbation theory would no longer be applicable. Again we conclude that if the predicted shell radii are to match those observed we must have larger values of β near to 0.40 corresponding to flatter potentials with smaller barriers (see, for example, figs. (6.1) and (6.3)).

Next, we plot the shell mass $LogM$ against $Log\sigma$ for both forms of potential and for $\beta = 0.38$ and $\beta = 0.44$ respectively (see figs. (7.11)-(7.14)). Different lines in the graphs correspond to values of A ranging from 0.05 to 0.15 (except those cases which give rise to a shell mass far too big to be depicted on the chosen scales when only smaller values of A are included). It can be seen that again the larger the value of β the smaller A has to be to reproduce the observed shell mass.

The same conclusions can be drawn by examining the next set of figures (figs. (7.15) to (7.18)) which show the variation of the shell mass with A for both forms of potential with σ taking its limiting values. In particular, it is clear that $\beta = 0.38$ is too small, whereas with $\beta = 0.44$ reasonable values of

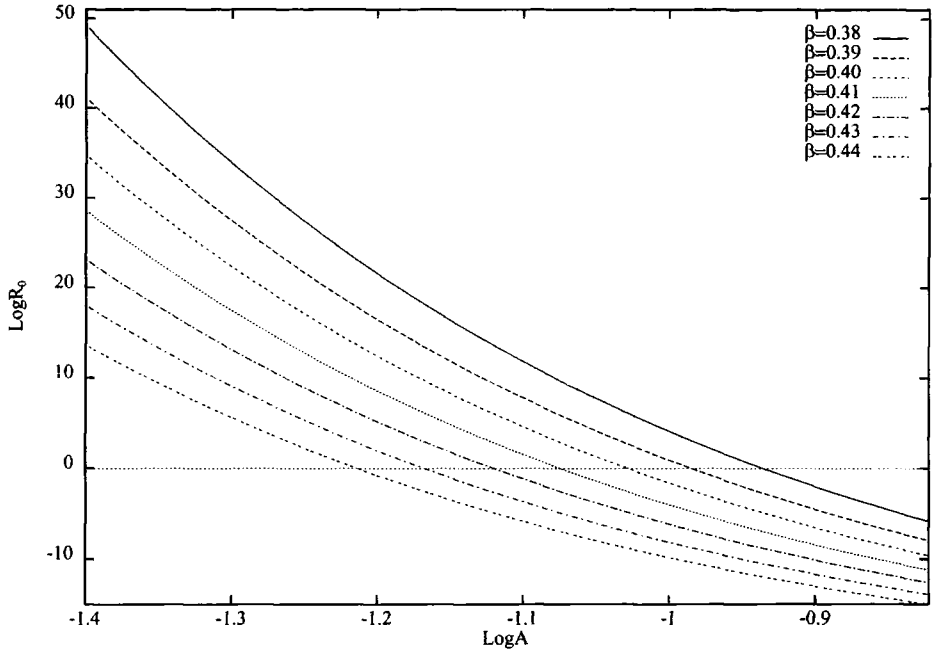

Figure 7.7: Variation of the shell radius R_0 with A for different values of β for the polynomial potential (with R_0 in Mpc).

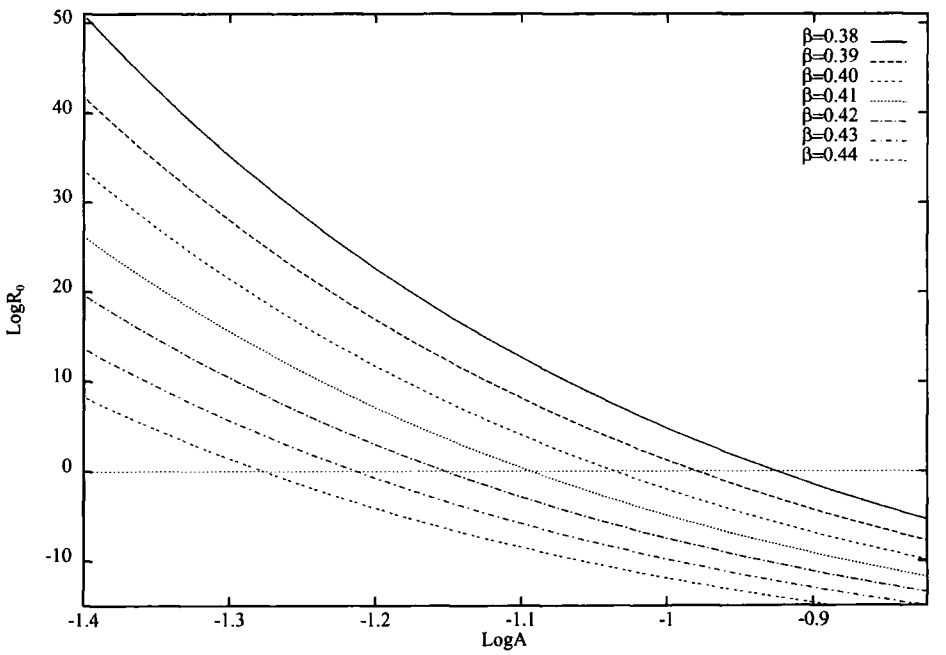

Figure 7.8: Variation of the shell radius R_0 with A for different values of β for the modified Coleman-Weinberg potential (with R_0 in Mpc).

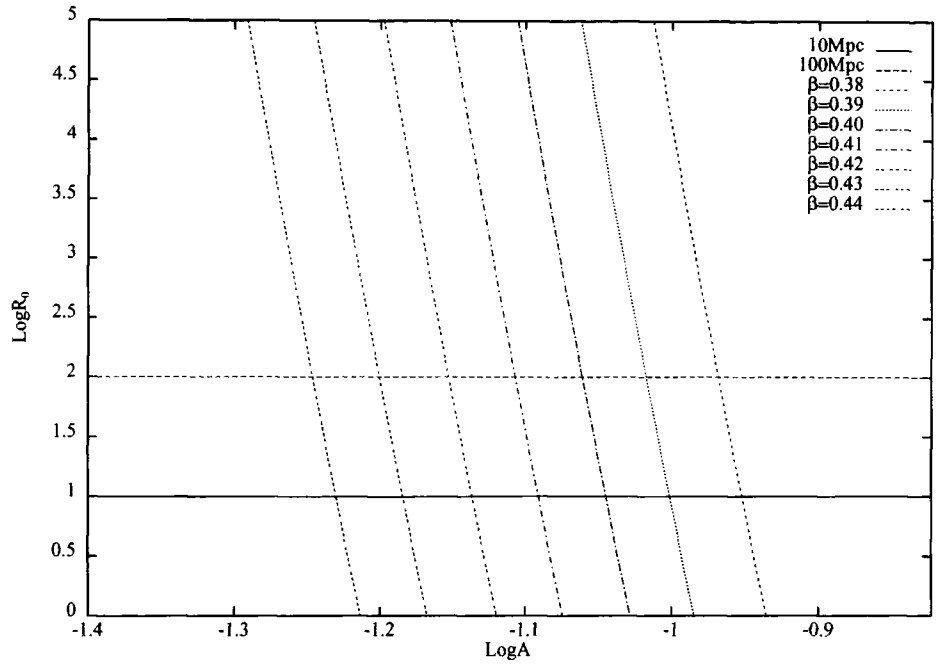

Figure 7.9: Variation of the shell radius R_0 with A for different values of β for the polynomial potential with $0 \leq R_0 \leq 10^5 Mpc$.

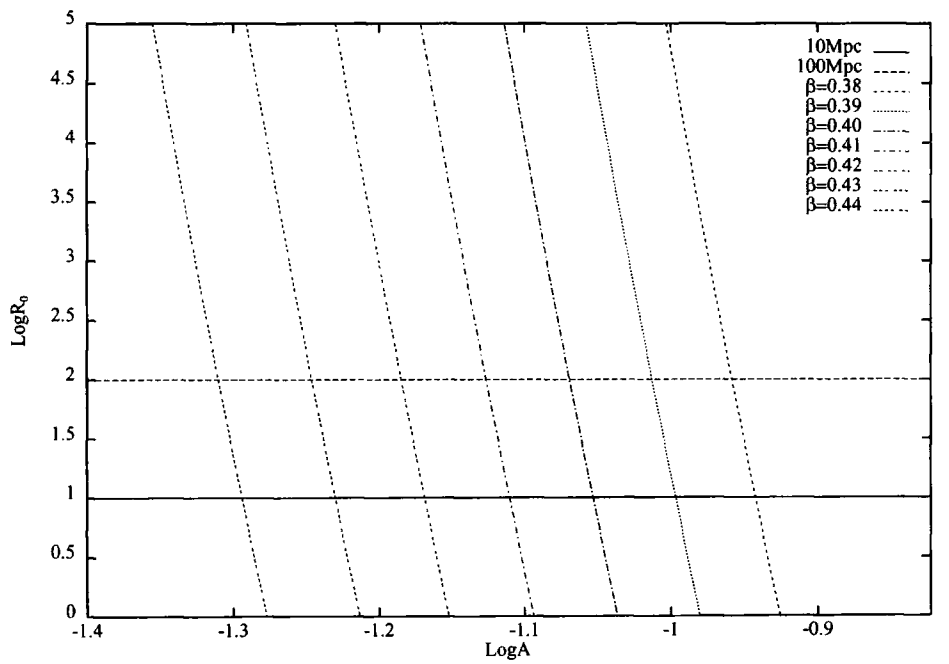

Figure 7.10: Variation of the shell radius R_0 with A for different values of β for the modified Coleman-Weinberg potential with $0 \leq R_0 \leq 10^5 Mpc$.

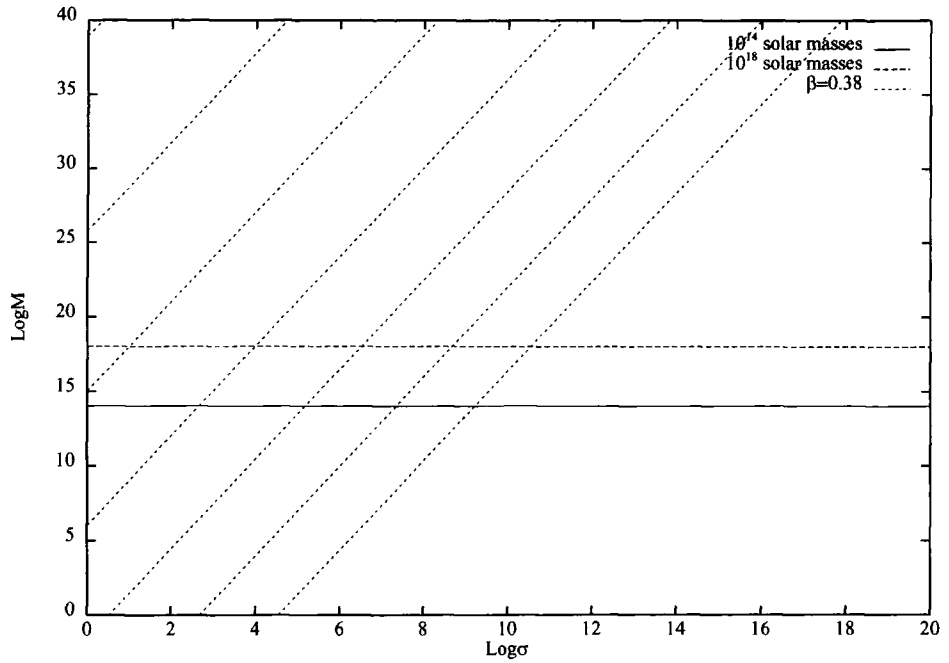

Figure 7.11: Variation of the shell mass M with σ for $A \in [0.10-0.15]$, with $\beta = 0.38$ and $\tilde{G} = 1$ for the polynomial potential, with M in solar masses.

$A \approx 0.06$ for $\sigma = 250GeV$ and $A \approx 0.1$ for $\sigma \approx 10^{14}GeV$ are obtained. The corresponding values for the modified Coleman-Weinberg potential are somewhat smaller ($A \approx 0.05$ and $A \approx 0.08$ respectively).

Next we examine how the shell thickness varies for different A, β and σ for both the polynomial and the modified Coleman-Weinberg potentials. As we mentioned before (cf. section (7.2.4)) small variations of A and β will not affect the result much because σ appears in the cubic power. It turns out that there is no useful solution since, for any sensible value of σ, ΔR_0 is very large, as fig. (7.19) shows for the polynomial potential (results for the modified Coleman-Weinberg potential are almost the same).

Having obtained reasonable results for the shell radius and the shell mass, it is unfortunate that we have failed to do so for the shell thickness as well. The reason is obviously that our model in section (6.9) is too simple for the underlying

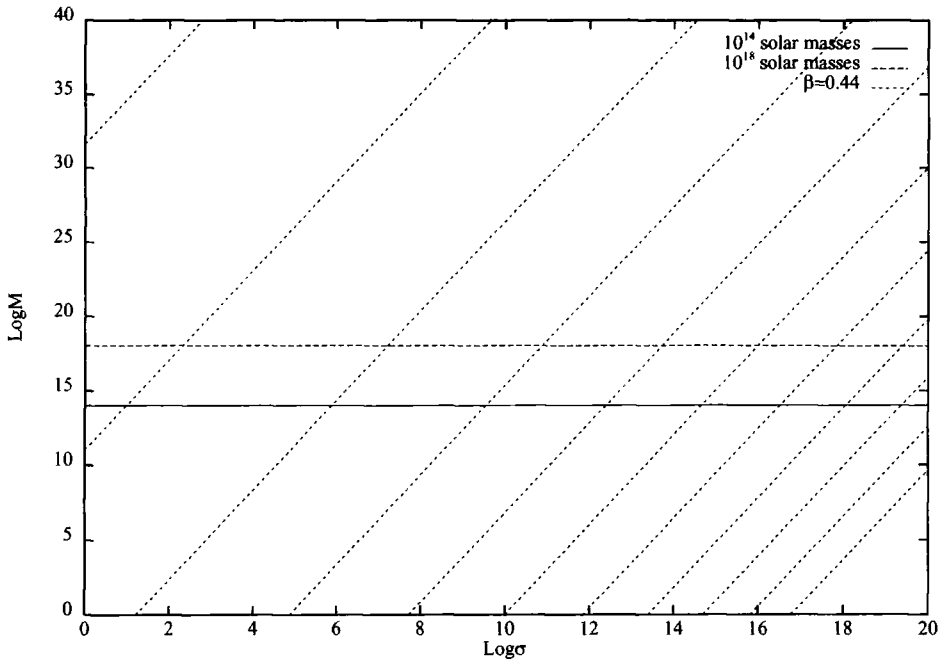

Figure 7.12: Variation of the shell mass M with σ for $A \in [0.05-0.15]$, with $\beta = 0.44$ and $\tilde{G} = 1$ for the polynomial potential, with M in solar masses.

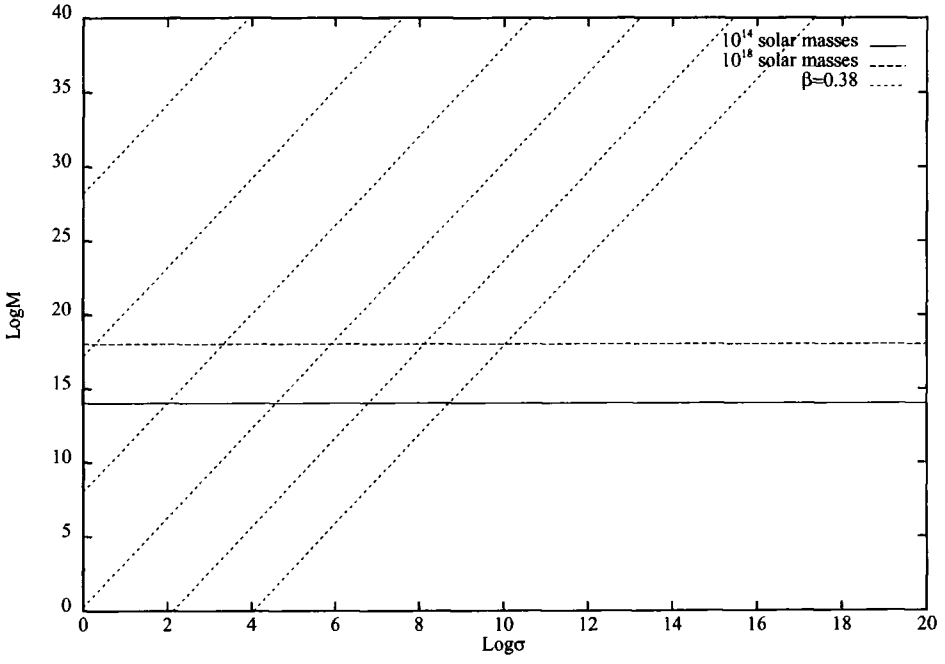

Figure 7.13: Variation of the shell mass M with σ for $A \in [0.10 - 0.15]$, with $\beta = 0.38$ and $\tilde{G} = 1$ for the modified Coleman-Weinberg potential, with M in solar masses.

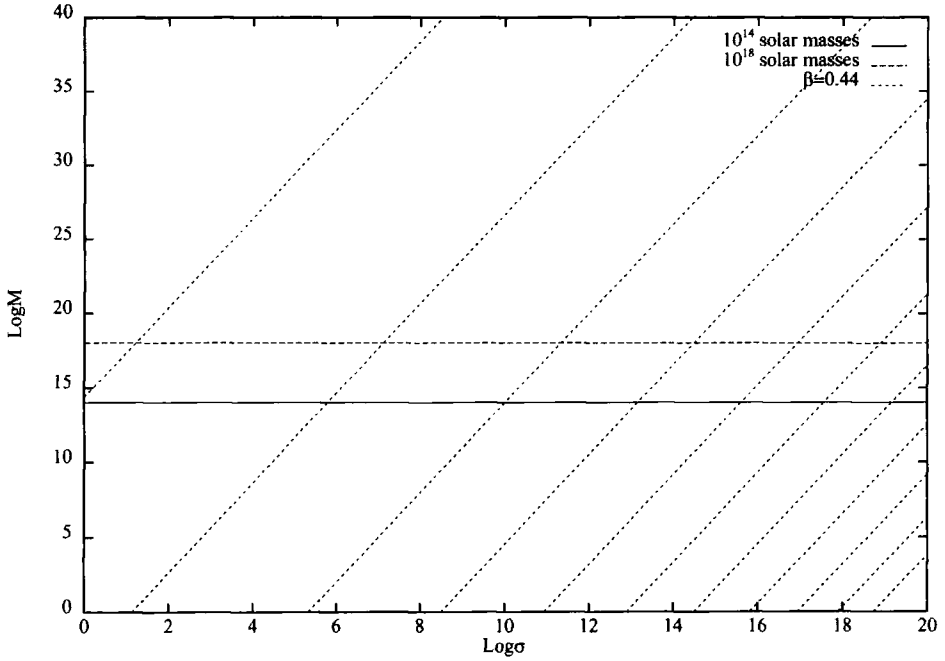

Figure 7.14: Variation of the shell mass M with σ for $A \in [0.05-0.15]$, with $\beta = 0.44$ and $\tilde{G} = 1$ for the the modified Coleman-Weinberg potential, with M in solar masses.

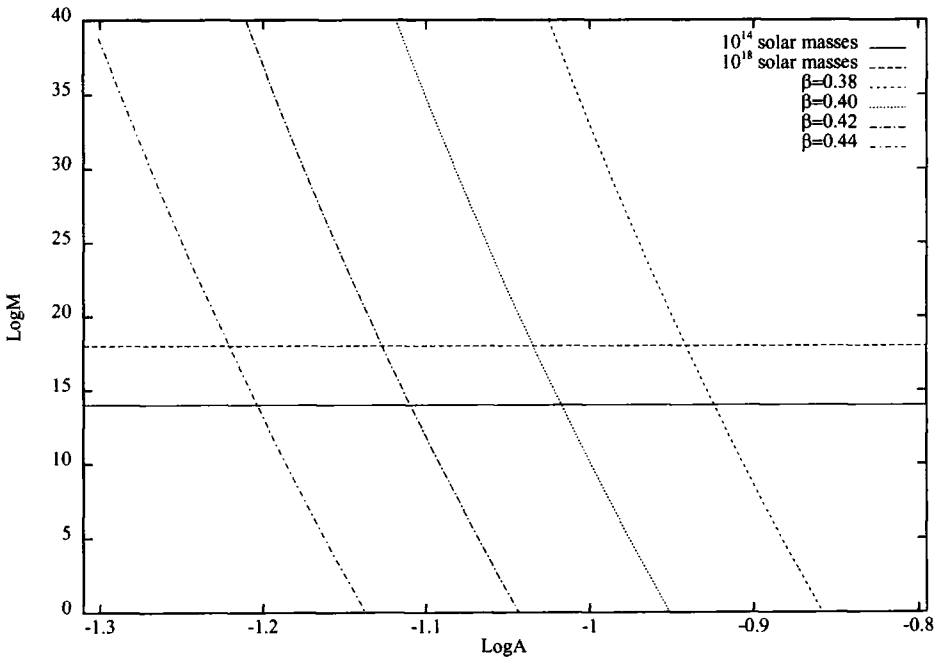

Figure 7.15: Variation of the shell mass M with A for different values of β, with $\sigma = 250GeV$ for the polynomial potential, with M in solar masses.

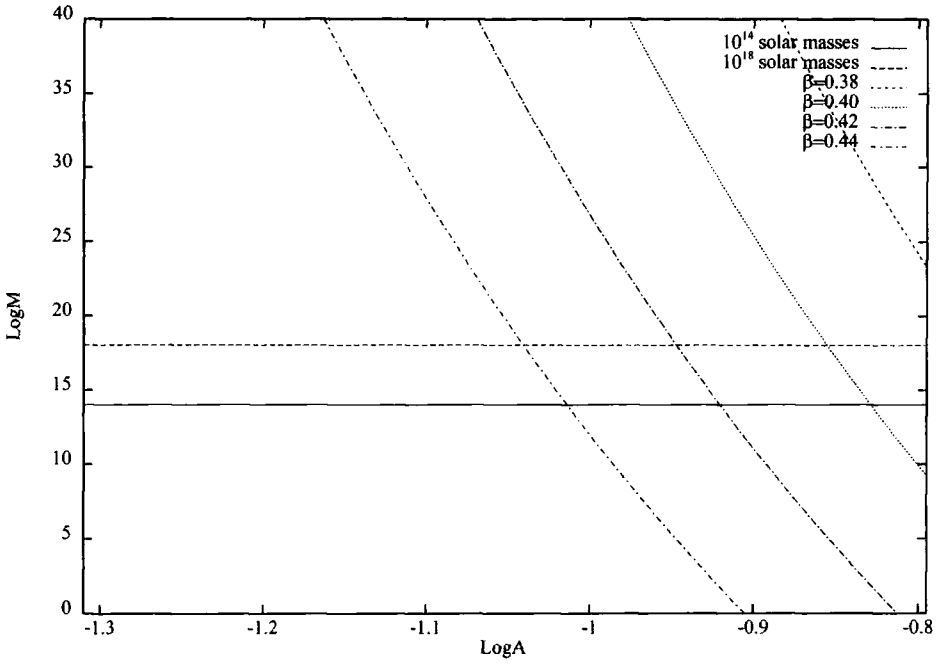

Figure 7.16: Variation of the shell mass M with A for different values of β, with $\sigma = 10^{14} GeV$ for the polynomial potential, with M in solar masses.

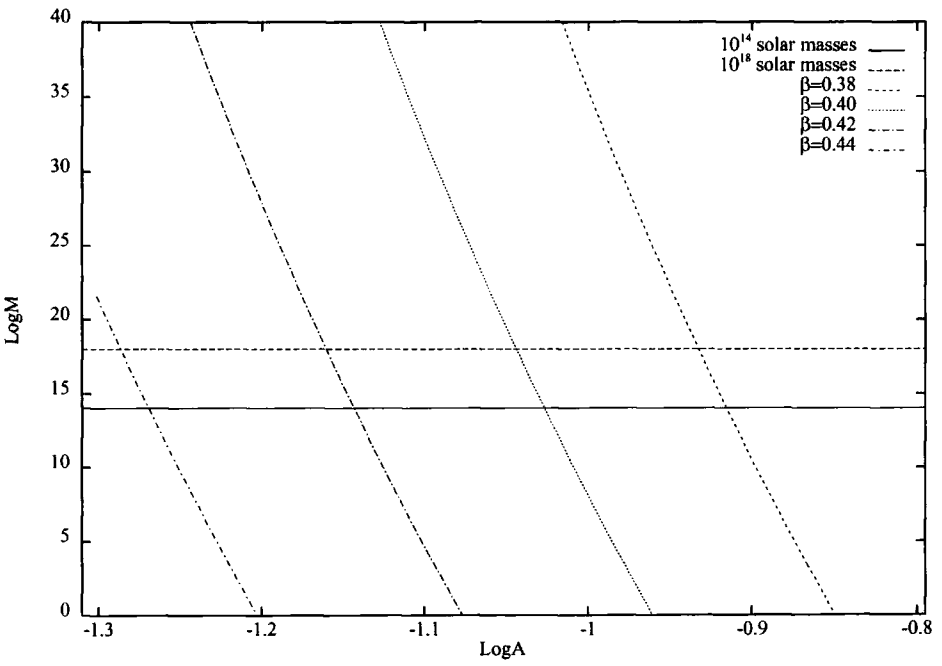

Figure 7.17: Variation of the shell mass M with A for different values of β, with $\sigma = 250 GeV$ for the modified Coleman-Weinberg potential, with M in solar masses.

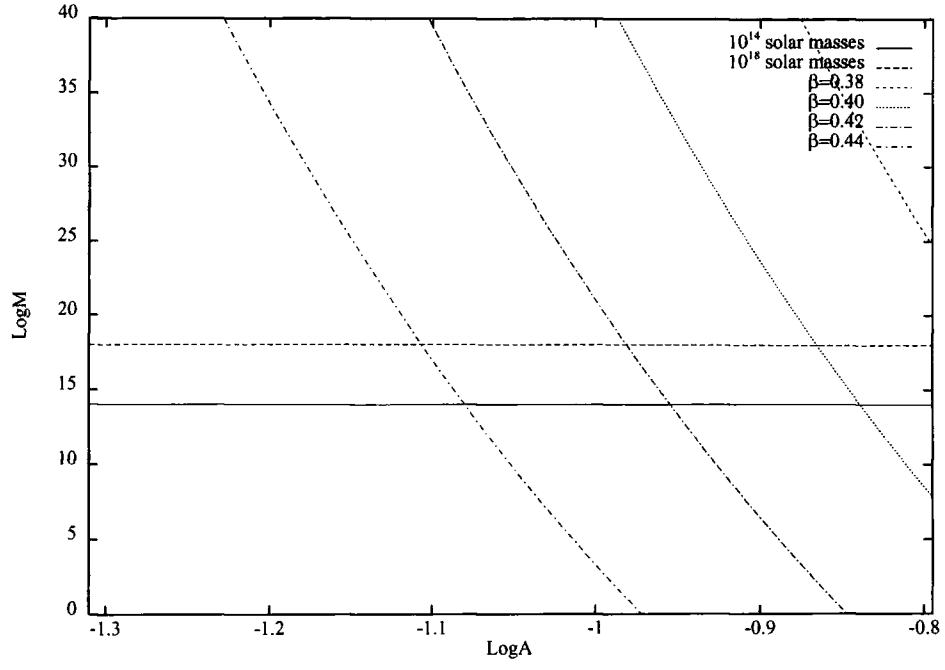

Figure 7.18: Variation of the shell mass M with A for different values of β, with $\sigma = 10^{14} GeV$ for the modified Coleman-Weinberg potential, with M in solar masses.

physics of the problem to be explored properly. Ignoring any internal motions within the shell, we can estimate the time it would take for the shell to collapse completely (i.e $\Delta R_0 \longrightarrow 0$) as follows. From (7.11) with $\Delta R_0 = 0$ we obtain

$$t = t_f + \sqrt{\frac{R_0}{\pi G \rho_s}},$$

where the surface density of the shell is

$$\rho_s \sim \tilde{G}\sigma^3.$$

Thus, for $\tilde{G} = 1$ and $R_0 = 25 Mpc$ it follows that

$$t = t_f + \frac{5 \times 10^{14}}{\sigma^3} sec$$

with σ measured in GeV units. Since $t_f \ll t_0$, it follows that for any reasonable value of σ, the shells will have completely collapsed already. This means that the observed thickness must be the result of the internal dynamics of the shells not

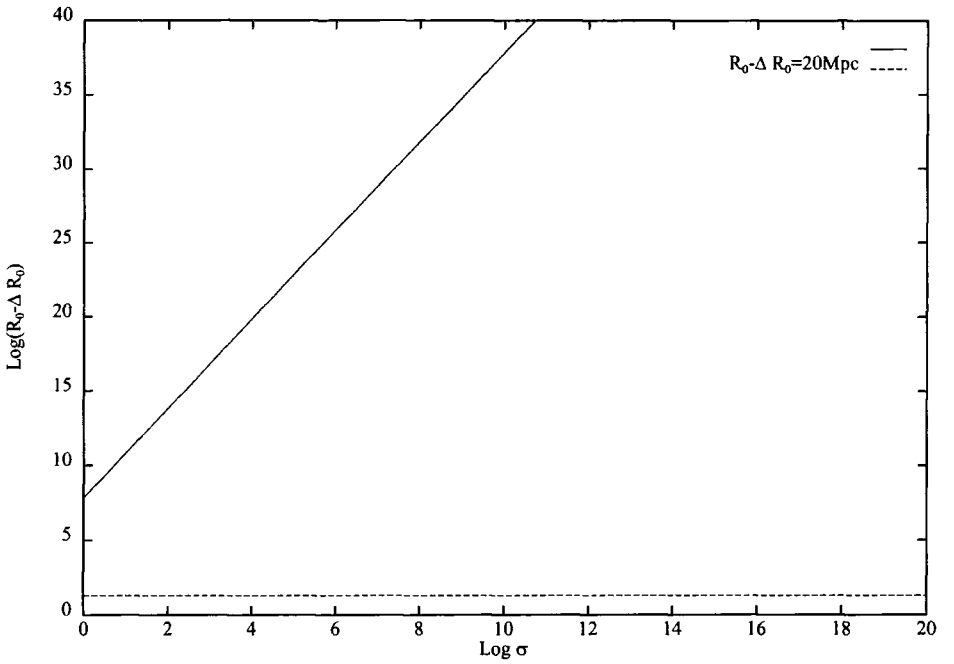

Figure 7.19: Variation of $\Delta R_0 - R_0$ with σ for the polynomial potential, with $\tilde{G} = 1$ and $\beta = 0.4$. The observed value $\Delta R_0 - R_0 \approx 20 Mpc$ is not obtained for any reasonable value of σ.

their formation and so, contrary to our hopes of determining the three potential parameters by fitting our computed shell parameters to observations, we are only able to determine two, namely the height of the barrier separating the two ground states and the coupling A. Finally, we show in figs. (7.20)-(7.23) the corresponding solutions if the coupling of the scalar field to matter $\tilde{G}$ is allowed to vary, for both potentials, setting this time $A = 0.1$ as in the Coleman-Weinberg $SU(5)$ GUT theory. Since the shell radius does not depend on $\tilde{G}$ we only plot the variation of the shell mass.

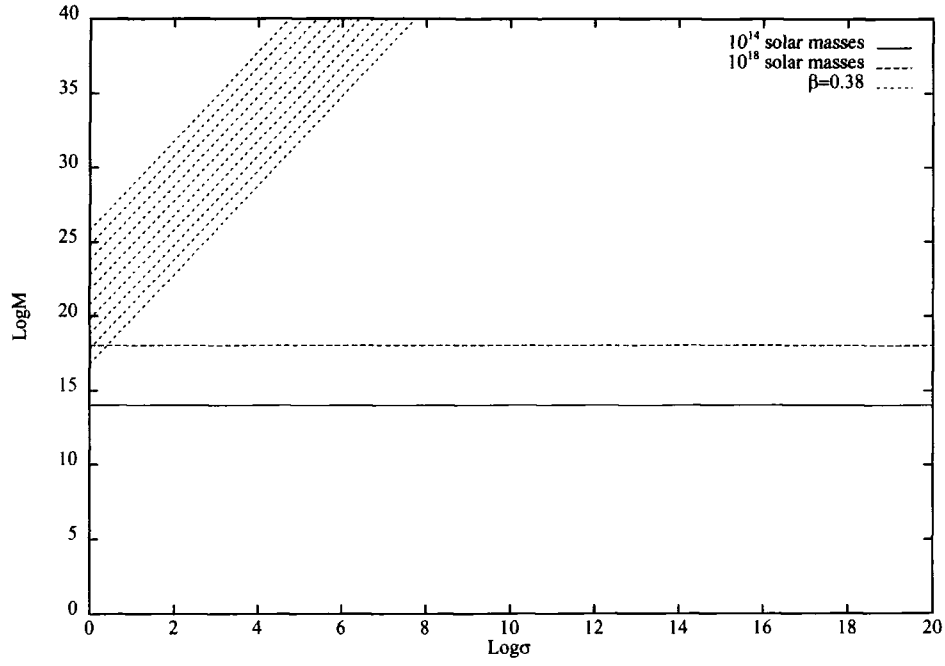

Figure 7.20: Variation of the shell mass M with σ for different values of $\tilde{G}$, with $A = 0.1$ and $\beta = 0.38$ for the polynomial potential, where M is in solar masses. In this and in the following figures $\tilde{G}$ is reduced from 1 (the line furthest to the left) to 10^{-9} in steps of 10^{-1}.

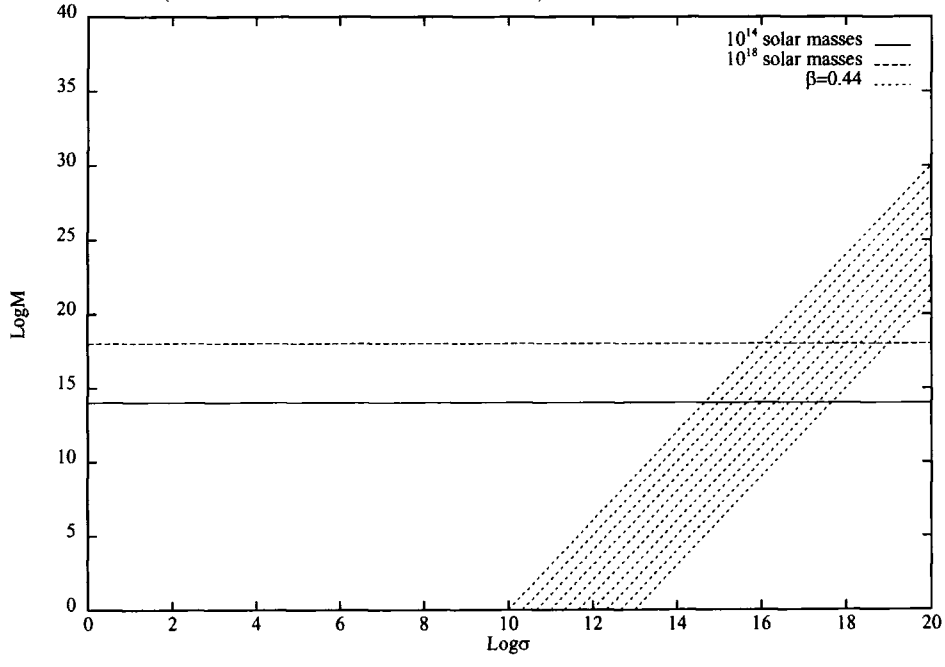

Figure 7.21: Variation of the shell mass M with σ for different values of $\tilde{G}$, with $A = 0.1$ and $\beta = 0.44$ for the polynomial potential, with M in solar masses.

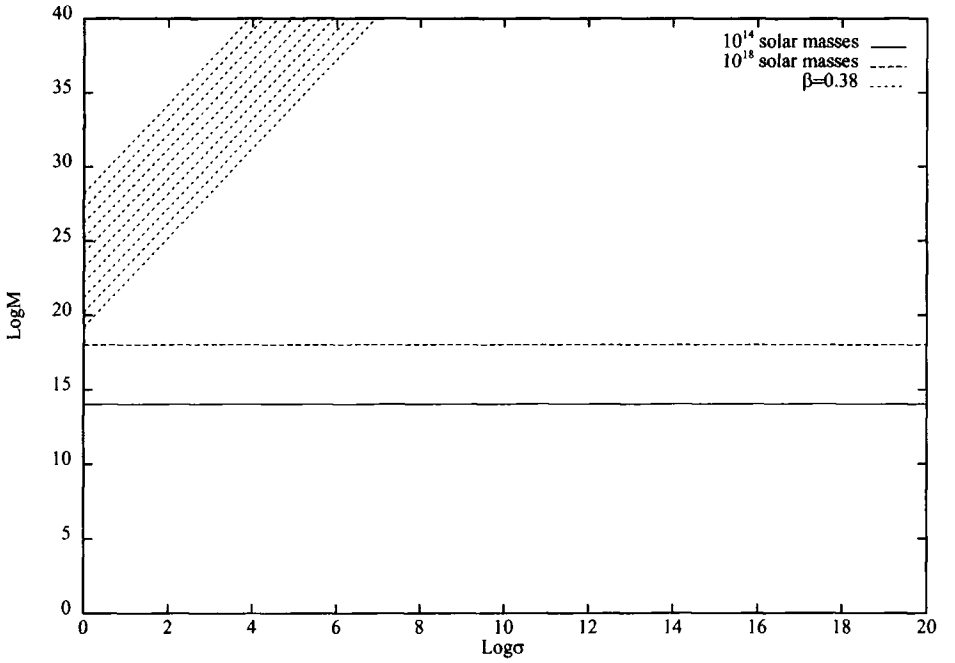

Figure 7.22: Variation of the shell mass M with σ for different values of $\tilde{G}$, with $A = 0.1$ and $\beta = 0.38$ for the modified Coleman-Weinberg potential, with M in solar masses.

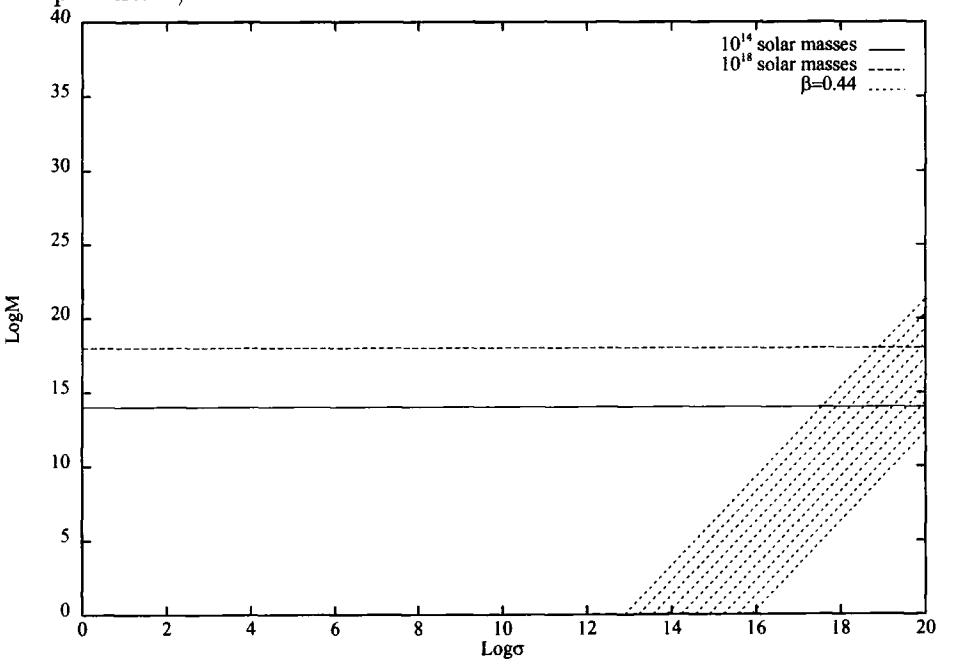

Figure 7.23: Variation of the shell mass M with σ for different values of $\tilde{G}$, with $A = 0.1$ and $\beta = 0.44$ for the modified Coleman-Weinberg potential, with M in solar masses.

7.4 Comments

In presenting our results we have assumed that, if the resulting parameters are to make physical sense, it is necessary to keep

$$0 < A < 0.15$$
$$0 < \beta < \frac{1}{2}$$
$$0 < \sigma < 10^{15}$$
$$\tilde{G} \leq 1$$

The first of these conditions ensures that the coupling constant is small enough to be consistent with expectations from the Weinberg-Salam theory of electroweak SSB or *GUT* theories and is such that perturbation theory will be valid. The second, ensures that there is a barrier separating the false from the true ground state through which the decay of the ϕ-field can proceed by quantum tunnelling. As far as the third condition is concerned we could in principle have $\sigma > 10^{15} GeV$ but then the phase transition would probably occur before the period of inflation and so any resulting structure would be diluted out of sight. The final condition, which is somewhat arbitrary, restricts the coupling of the ϕ-field to matter to be that of the Standard Model or less.

As can be seen from the graphs, our solutions appear to be straight lines, or nearly so, when plotted on log-log axes. Thus, the shell parameters have (approximately) a power law dependence on the potential parameters. By studying the results we can conclude the following:

1. A and β vary inversely to each other in the sense that if the shell parameters are to match those observed we need to combine small values of A with larger values of β and *vice versa.*

2. Because $\tilde{A} = A\beta$ appears in the denominator of the expression for the tunnelling action, small changes in either of these parameters induce very large variations in the computed shell parameters (cf. (6.31) and (7.8)-(7.10)). For example, take fig. (7.17) which shows the variation of the shell mass with A for different values of β. For fixed β (say $\beta = 0.38$) a small change of $\log A$ from -0.9 to -1.0 will produce an increase in the computed shell mass of more than 22 orders of magnitude. This might give the impression that A has to be very accurately specified in order to get the shell mass near its observed value. However, the effect of letting β vary as well is to remove this illusion of accuracy (compare, for example, the lines corresponding to $\beta = 0.38$ and $\beta = 0.40$, which for the same change in $\log A$, correspond to similar values for M).

3. If the time of shell formation is not to be larger than the decoupling time we need $\beta \gtrsim 0.38$ (see figs. (7.1)–(7.6)). Smaller values of β are excluded because in that case A becomes too large.

4. The same conclusion can be derived from the graphs showing the variation of the shell radius and the shell mass with A (see figs. (7.9), (7.10)).

5. Constraints on A can be obtained from the variation of the shell radius with A (see figs. (7.9), (7.10)) by noting that for the polynomial potential

$$\beta = 0.38 \implies 0.108 < A < 0.112$$

$$\beta = 0.44 \implies 0.057 < A < 0.059$$

whereas for the modified Coleman-Weinberg potential

$$\beta = 0.38 \implies 0.110 < A < 0.114$$

$$\beta = 0.44 \implies 0.049 < A < 0.051$$

Thus, for large β the required value A is different for the two potentials even though the shape of the potentials is similar.

6. Constraints on A can also be obtained from the variation of the shell mass with A, but this time the results depend on our choice of σ (see figs. (7.15)-(7.18)). For instance, for $\sigma = 250GeV$ and $\beta = 0.44$ with the polynomial potential, the observed value of M is obtained if $0.060 < A < 0.062$, or with the modified Coleman-Weinberg potential if $0.052 < A < 0.054$. As σ increases the corresponding values of A increase as well and for $\sigma \approx 10^{14}GeV$ we need, for the polynomial potential, $0.092 < A < 0.097$, or for the modified Coleman-Weinberg potential, $0.079 < A < 0.084$. Again, we see that for large β the required value A is different for the two potentials. If we concentrate, however, on smaller values of β in particular $\beta = 0.38$, then for $\sigma = 250GeV$ we need $0.115 < A < 0.120$ with the polynomial potential or, for the modified Coleman-Weinberg potential, $0.117 < A < 0.122$. All of these values are quite acceptable but if σ is increased to $10^{14}GeV$, A becomes far too large.

7. When $\tilde{G} = 1$ there is no restriction on the allowed value of σ which can be as high or as low as we want it, so we can invoke any regime of particle physics that we choose to describe the second phase transition.

8. If, however, we hold A fixed, even if we allow $\tilde{G}$ to vary, we can tighten the range of values for β further. For example, it can be shown that for $\sigma = 250GeV$ only the values $0.38 < \beta < 0.40$ can satisfy the shell mass constraint without having to resort to either very large or exceedingly small values of $\tilde{G}$. As σ increases the required value of β increases as well and for $\sigma = 10^{14}GeV$ it is found that we need $0.42 < \beta < 0.44$ corresponding to a

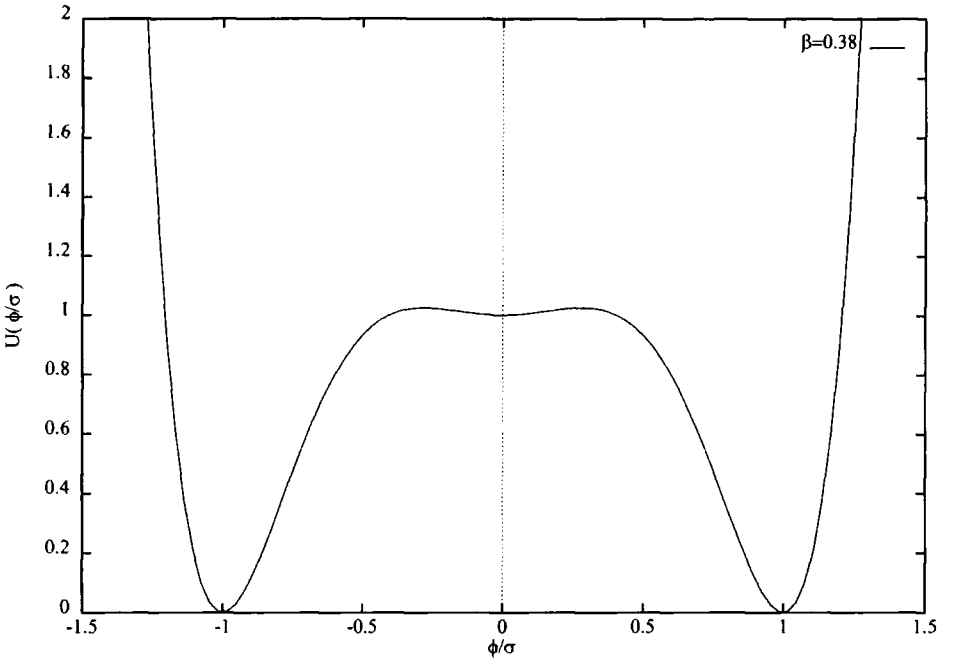

Figure 7.24: The parametrised polynomial potential with $\beta = 0.38$.

very small potential barrier (cf. figs.(7.20)–(7.24) where only the limiting cases corresponding to $\beta = 0.38$ and $\beta = 0.44$ have been plotted).

It is notable that the values for both A and σ are quite reasonable, since with $A = \mathcal{O}(0.1)$ σ can take any values in the range $[0 - 10^{20} GeV]$. The fact that we cannot pinpoint the value of σ reflects the fact that our simple model for the shell thickness has failed (cf. section (6.9) and the end of section (7.3)) and thus instead of determining the three potential parameters we are only able to estimate two, A and β. Hence our approach does nothing to pin down the nature of the particle physics theory that would determine σ.

Combining all the constraints would seem to indicate that the values $A \approx 0.11 - 0.12$ and $\beta \approx 0.38$ are favoured though slightly larger (smaller) values of β coupled with smaller (larger) A are still allowed in accordance with comment (1) above. The polynomial potential with $\beta = 0.38$ is shown in figure (7.24) (the coresponding modified Coleman-Weinberg potential is very similar).

Our results suggest that it may be possible to explain the bubble-like structure of the Universe on large scales by invoking a second phase transition, one which occured after inflation, and which proceeds by quantum tunnelling. Even though we have failed to predict the observed thickness of the shells, we have shown that in this model sensible solutions, giving rise to shells of matter with the observed mass and radius, can be found and that the scalar field coupling can be similar to that of the Higgs field of the Standard Model. However, the required energy scale of the scalar field potential is not determined.

Chapter 8

Summary and Conclusions

In the last chapter we saw how constraints on the parameters which describe the potential $U(\phi)$ of a scalar field ϕ, whose decay leads to the formation of bubbles and consequently to shells of matter, can be obtained by comparing the computed shell parameters with their observed values. Here we will consider further the sort of theory that might give rise to ϕ and will also discuss the implications of our approach for the understanding of cosmology and structure formation. Firstly, however, we present a summary of the preceeding chapters.

8.1 Summary

We started in chapter 1 with an introduction to explain the purpose and aims of this work, followed in chapters 2 and 3 by a discussion of the standard Big Bang model of cosmology and its successes and its failures, and we saw how attempts to solve the latter led naturally to the idea of inflation. In particular we examined how the evolution of a homogeneous and isotropic Universe obeying the Robertson-Walker metric can be described by Friedmann's equations and how the universal expansion was affected by the nature of the energy content of the Universe and in particular whether it is radiation-dominated or matter-dominated. The successes of the Big Bang model were discussed, followed by an

exposition of a number of difficulties (such as, for example, the horizon problem) which could be solved by the inflation of the Universe for some brief period in its early history during which it underwent exponential expansion. We reviewed a number of inflationary models and explained the main mechanisms which have been proposed for the generation of the primaeval density perturbations that led to the formation of structure. In particular we reviewed Guth's original inflationary model and saw how attempts to resolve the graceful exit problem led to the idea of slow-roll inflation. The fact that new inflation was not completely free of problems, as is evident from the fine tuning required to produce structure as we see it, has led in a renewed interest in first order phase transition models such as extended inflation built on the Brans-Dicke theory of gravity. Finally, we saw that, although inflation in general is a very attractive mechanism for solving the problems of the Big Bang model, none of the specific models which have been proposed is completely satisfactory. This should not worry us too much because there is as yet no truly compelling particle physics 'theory of everything' to explain the origin of the scalar field 'inflaton'.

In chapter 4 we started by examining the structure of the Universe from an observational point of view and saw how recent observations have led to the discovery that galaxies appear to be mostly situated on shell-like boundaries surrounding large voids which contain very few galaxies. We then briefly examined the dark matter problem and outlined a number of theories that have attempted to explain the origin of this bubble-like structure. We concluded with a discussion of the inhomogeneites observed in the CMBR and the possibility that this structure may have resulted from a first order phase transition. In particular we saw that CMBR constraints impose severe tests on all cosmological models and presented arguments suggesting that perhaps the best way to account for the

bubbly structure of the Universe might be to invoke a two field inflation model.

We have proposed instead a mechanism of structure formation where the nucleation of bubbles results from a phase transition which occurs *after* the period of inflation. We began to explore this possibility in chapter 5 where, following Coleman's approach, we derived a formula for the decay rate of the bubbles. Then, in chapter 6 we saw how collisions between the expanding bubbles could have led to the creation of shells of matter which might eventually evolve into structures similar to those we observe today. Next we derived equations relating the shell parameters to those of the ϕ-field potential. Since we lack an underlying theory that would predict the potential $U(\phi)$, we instead tried to determine the parameters of the potentials that are required to reproduce the observed shell masses, thicknesses and radii. These results were presented in chapter 7. We now look at some of their implications.

8.2 The Underlying Theory

In the last chapter we found that the structure of the Universe seems to be consistent with our hypothesis that it has resulted from the decay of a scalar field ϕ that has evolved to the true minimum of its potential through barrier penetration, with a coupling A of order 10^{-1}, provided that the height of the barrier is quite small.

We have mentioned in chapter 4 recent work (Amendola *et al* (1996)) in which the nucleation rate of the true vacuum bubbles has been explicitly calculated, taking into account gravitational effects and going beyond the thin wall approximation, both of which increase the nucleation rate Γ. As a result r_{pt} and consequently r_f decrease (cf. (6.74), (6.78)) leading to a reduced shell radius and shell mass (cf. (6.79), (6.72)). This allows for slightly smaller values of A and β

than those we obtained in the previous chapter. However, since we abandoned the thin wall approximation anyway in favour of numerical calculations (cf. section (7.2.1)) and since we anticipate that gravitational corrections to the bubble nucleation rate will be significant only on energy scales comparable to the Planck energy, we do not expect that this improved method of calculation would change our results by much.

We have also seen that, in principle, there are no restrictions on the value of the energy scale of this transition, σ, which could be as low or as high as we like. This uncertainty in the value of σ reflects a major problem suffered in many cosmological models, that we cannot be certain what regime of particle theory has given rise to the observed structure. It may also be partly due to the inadequacy of the model we have employed for studying the shell thickness.

We have had to propose the existence of a new ϕ field just for the purposes of creating shells of matter through bubble collisions. This is obviously unsatisfactory and if our proposal is to be credible it will be necessary for a ϕ field with the properties given above to emerge from some more complete particle physics theory. For instance, since for specific values for A and β, $\sigma \approx 250GeV$ may be favoured, and since for most of our results we have used Standard Model couplings to matter so that $\tilde{G} = 1$, it is just possible that the field responsible for the creation of the shells might be the Higgs field of the Weinberg-Salam theory. This would enable us to constrain the nature of the Higgs from cosmological considerations and in particular by observation of the large scale structure of the Universe! This is reminiscent of the bounds on the masses of the $WIMPS$ derived in chapter 4 from the constraint that the energy density of the Universe should not be too great.

As we saw in section (7.2) for the polynomial and the modified Coleman-

Weinberg potentials respectively,

$$m_H = 2A^{\frac{1}{2}}(1+\beta)^{\frac{1}{2}}\sigma$$

or

$$m_H = A^{\frac{1}{2}}(3+2\beta)^{\frac{1}{2}}\sigma.$$

Setting $\sigma = 246GeV$, as in the Standard Model, and restricting the allowed ranges for A and β as in the last chapter, we could in principle obtain constraints on the Higgs mass for the potentials under consideration. For example, with $0.38 < \beta < 0.44$, for the polynomial potential we obtain

$$\begin{aligned} 0.057 &< A < 0.12 \\ 138GeV &< m_H < 205GeV, \end{aligned}$$

whereas for the modified Coleman-Weinberg potential

$$\begin{aligned} 0.052 &< A < 0.13 \\ 148GeV &< m_H < 243GeV. \end{aligned}$$

If further observations of the shell parameters, or a more accurate determination of the Hubble parameter, rule out $\sigma \approx 250GeV$ we shall have to look for some other theory containing a scalar field with a higher energy scale such as supersymmetry ($SUSY$) for example.

$SUSY$ theories have been introduced mainly in an attempt to reconcile the small mass of the W boson compared with Planck's mass M_P, known as the hierarchy problem. They also try to address the fact that weak interactions in the Standard Model are not natural in the sense that the radiative corrections to physical quantities appear to be larger than the physical value of the quantities themselves. $SUSY$ models attempt to solve these problems by postulating

a fundamental symmetry between bosons and fermions such that every fundamental particle has a supersymmetric partner that obeys the opposite statistics. In this way unwanted divergences are naturally canceled though the number of fundamental particles is doubled. It is expected that $SUSY$ theories will be spontaneously broken since the underlying symmetry between bosons and fermions is obviously now lost. The scale of $SUSY$ breaking, M_S, has been estimated to be in the range $10^3 GeV < M_S < 10^{11} GeV$.

There are of course other theories of particle physics beyond the Standard Model such as composite models in which the Higgs particle is considered to be a composite state of 'techniquarks' bound together by some new kind of interaction, or superstring theories where elementary particles are no longer considered to be points but rather closed vibrating loops which cut out a cylindrical area as they move through space.

In all these models a number of phase transitions are thought to have occured as the underlying symmetries of the theory are successively broken, and it is possible that such phase changes are of first order and procceed by quantum tunnelling. Without a 'Theory of Everything' uncertainty as to the exact nature of these phase changes is likely to remain. They could occur at any scale up to the Planck scale, $10^{19} GeV$.

If our approach is accepted, a more accurate knowledge of the shell parameters will help to determine the parameters of the potential including perhaps the epoch of the second phase transition. It could also have important implications as far as particle physics theories are concerned in the sense that models that fail to reproduce the observed structure could be ruled out. Alternatively, starting from a sensible particle physics theory, the graphs in the last chapter could be used to predict the expected scale of the resulting structure. Larger and deeper

astronomical surveys are clearly vital since a more accurate determination of the shell parameters will reduce the allowed range of the potential parameters and hence tighten the constraints on the scalar particle mass, for example. Of course an important constraint on our proposal comes from the CMBR since the presence of large bubbles at decoupling would destroy its homogeneity.

If Amendola *et al.* are right (see section (4.6)), the only way of producing large scale structure through bubble wall collisions, retaining the successes of the original EI models, while passing the CMBR constraints, is to invoke a two-field inflation model in which the first order phase transition which nucleates the true vacuum bubbles is followed by a period of slow-roll inflation. We might, therefore, want to modify our model by incorporating our potentials into a two-field inflation model. Another way out might be to retain an inflationary model that resolves the graceful exit problem without violating the CMBR constraints, such as, perhaps, a classical EI model which produces a large number of very small bubbles which are then rapidly thermalised after inflation. A subsequent first-order phase transition, such as the electroweak phase transition for example, could then be deployed to produce astrophysically interesting bubbles. The fact that the phase transition we are considering is late (compared to the epoch of inflation) and does not result in accelerated expansion means that very big bubbles such as those produced in the early phases of an inflationary phase transition are not expected to occur and thus our bubble spectrum should be compatible with the CMBR constraints. This, however, remains to be demonstrated in detail. A proper calculation of the bubble spectrum will have to be carried out and were it to be found that our model cannot survive a comparison with the CMBR constrains then a mechanism to suppress the overproduction of large bubbles would have to be devised, perhaps similar to Amendola's two-field inflation.

8.3 Conclusion

We have found that a second phase transition that procceeds by the quantum tunnelling of a scalar field ϕ may explain the bubble–like structure of the Universe on large scales. We have shown that for virtually any value of the energy scale of the SSB, σ, reasonable values of the couplings of $\mathcal{O}(0.1)$ are needed but that the height of the ϕ-field potential barrier separating the two ground states should be quite small. The true nature of the ϕ-field thus remains hidden as it depends on what short of particle theory we want to use. If the Standard Model of electroweak interactions is invoked, we have shown how further observations of the shells of matter might help determine the Higgs mass from astronomical considerations, a fact that highlights the close interplay that now exists between cosmology and particle physics.

Despite the fact that the current concensus concerning structure formation through a phase transition points towards a two field inflation model, we have argued that because our phase transition occurs after inflation the bubble spectrum may still be compatible with the CMBR constraints.

Looking to the future, the next step should be to determine the bubble spectrum in detail and to investigate how the CMBR constrains affect the plausibility or otherwise of our proposal. If it is found that our bubble nucleation scheme interferes with the CMBR too much then a mechanism for supressing the overproduction of large bubbles will have to be devised. That would make an interesting project for the future!

REFERENCES

Adams F. and Freese K., *Phys. Rev. D*, **43**, 353, (1991)

Albrecht A. and Steinhardt P.J., *Phys. Rev. Lett.* **48**, 1220, (1982)

Amendola L. and Occhionero F., *Ap. J.*, **413**, 39, (1993)

Amendola L., Baccigalupi C. and Occhionero F., *Phys. Rev. D*, **54**, 4760, (1996)

Amendola L., *et al.*, *Phys. Rev. D*, **54**, 7199, (1996)

Baccigalupi C., Amendola L. and Occhionero F., ASTROPH-9611308

Bardeen J., Steinhardt P.J. and Turner M.S., *Phys. Rev. D*, **28**, 679, (1983)

Barrow J.D., *Fundamentals of Cosmic Physics* Vol. **8**, 83, (1983)

Barrow J.D., *Q. Jl. Ast. Soc.* **29**, 101, (1988)

Bernstein J., Brown L.S. and Feinberg G., *Rev. Mod. Phys.* **61**, 25, (1989)

Boesgaard A. and Steigman G., *Astron. Astrophys.* **23**, 319, (1985)

Brandenberger R.H., *Rev. Mod. Phys.* **57**, 1, (1985)

Brans C. and Dicke C.H., *Phys. Rev.* **24**, 925, (1961)

Callan C.G, Coleman S., *Phys. Rev. D* **16**, 1762, (1977)

Coleman S., *Phys. Rev. D* **15**, 2929, (1977)

Coleman S., *Aspects Of Symmetry*, (CUP, Cambridge 1985)

Coleman S., Glaser V., Martin A., *Commun. Math. Phys.* **58**, 211, (1978)

Collins P.D.B., Martin A.D. and Squires E.J., *Particle Physics and Cosmology*, (John Willey, 1989)

Davis M. *et al.*, *Ap. J.* **292**, 371, (1985)

Davis M. *et al.*, *Ap. J.* **327**, 507, (1988)

Doroshkevich A., *et al.*, **1995** *To be submitted to MNRAS.*

Efstathiou G., Sutherland W.J. and Maddox S.J., *Nature* **348**, 705, (1990)

Geller M.J. and Huchra J.D., *Physical Cosmology*, ed. by Blanchard A. *et al.* (Edditions Frontieres, 1991)

Gregory P.C and Condon J.J, *Ap. J. Phys.* **75**, 1011, (1991)

Guth A. H., *Phys. Rev. D* **23**, 347, (1981)

Guth A. H. and Weinberg E., *Nucl. Phys.* **B212**, 321, (1983)

Halzen F. and Martin A.D., *Quarks and Leptons*, (Wiley, New York, 1984)

Hawking S.W. and Moss I.J., *Phys, Lett.* **110B**, 35, (1983)

Hoyle F. and Tayler R.J., *Nature* **203**, 1108, (1964)

Kleinert H., *Path Integrals In Quantum Mechanics, Statistics And Polymer Physics*, (World Scientific (1990))

Kibble T.W.B., *J. Phys.*, **A9**, 1387, (1976)

Kolb E.W, *Physica Scripta* **T36**, 199, (1991)

Kolb E.W and Turner M.S, *The Early Universe*, (Addison-Wesley, 1990)

La D., *Phys. Lett. B* **265**, 232, (1991)

La D. and Steinhardt P.J., *Phys. Rev. Lett.* **62**, 376, (1989a)

La D. and Steinhardt P.J., *Phys. Lett. B* **220**, 375, (1989b)

La D., Steinhardt P.J. and Bertschinger E.W., *Phys. Lett. B* **231**, 231, (1989)

de Laparent V., Geller M.J. and Huchra J.P, *Ap. J.* **302**, L1, (1986)

Liddle A.R. and Wand D., *Mon. Not. R. astr. Soc.* **253**, 637, (1991)

Linde A. D., *Phys. Lett.* **108B**, 389, (1983)

Linde A. D., *Particle Physics and Inflationary Cosmology*, (Harwood Academic Press, Chur, Switzerland, 1990)

Linde A. D., *Observational Tests of Cosmological Inflation*, (Kluwer Academic

Publishers, Netherlands 1991)

Mandl F. and Shaw G., *Quantum Field Theory* (Wiley, New York 1984)

Occhionero F. and Amendola L., *Phys. Rev. D* **50**, 4846, (1994)

Ostriker J.P. and Cowie L.L., *Ap. J.* **243**, L127, (1981)

Ostriker J.P. *et al.*, *Phys. Lett.* **B180**, 231, (1986)

Peebles P.J.E., *Origin and Evolution of Galaxies*, (Reidel, Dordrecht, 1983)

Peebles P.J.E., *Ap. J.* **285**, L45, (1984)

Peebles P.J.E., *Principles Of Physical Cosmology*, (Princeton University press, 1993)

Polyacov A. M., *JETP Lett.* **20**, 194, (1974)

Reasenberg R.D., *et al.*, *Ap. J* **234**, L219, (1979)

Ryder L., *Quantum Field Theory*, (CUP, Cambridge 1992)

Sachs R.K. and Wolfe A.M., *Ap. J.* **147**, 73 (1967)

Smoot G.F. *et al.*, *Ap. J.* **371**, L1, (1991)

Smoot G.F. *et al.*, *Ap. J. Lett.* **396**, L1, (1992)

Smoot G.F., *Clas. Q. Grav.* **Vol 10**, S3, (1993)

Steinhardt P.J., *Int. J. Mod. Phys. A* **Vol 10**, 1091, (1995)

Strauss M.A., *et al.*, *Ap. J.* **385**, 421, (1992)

't Hooft G., *Nucl. Phys.* **B79**, 276, (1974)

Turner M.S., Weinberg E.J. and Widrow L.M., *Phys. Rev. D* **46**, 2384, (1992)

Vainstein A.I., *et al.*, *Sov. Phys. Usp.* **25(4)**, 195, (1982)

Vilenkin A., *Phys. Rep.* **121**, 263, (1985)

Vilenkin A. and Shellard E.P.S., *Cosmic Strings And Other Topological Defects*, (Cambridge University Press, 1994)

Vogeley M.S., Geller M.J. and Huchra J.P., *Ap. J* **382**, 44, (1991)

Weinberg E.J., *Phys. Rev. D* **40**, 3950, (1989)

Weinberg S., *Gravitation And Cosmology*, (John Willey, 1972)

White S.D.M. *et al.*, *Ap. J. Lett.* **274**, L1, (1983)